The Miocene Carbonate crash: Shifts in carbonate preservation and contribution
of calcareous plankton

Dissertation zur Erlangung des Doktorgrades der Naturwissenschaften
(Dr. rer. nat.) am Fachbereich Geowissenschaften
Universität Bremen (Deutschland)

Dissertation submitted for the Doctoral Degree in Natural Sciences
(Dr. rer. nat.) at the Department of Geosciences
University of Bremen (Germany)

vorgelegt von/ by

Inga Preiß-Daimler

Bremen
im Juli 2011

Erklärung

Hiermit erkläre ich, dass ich:

- die vorliegende Arbeit ohne unerlaubte fremde Hilfe angefertigt habe.
- keine anderen, als die von mir angegebenen Quellen und Hilfsmittel benutzt habe.
- die den benutzten Werken wörtlich oder inhaltlich entnommenen Stellen als solche kenntlich gemacht habe.

_____

Inga Preiß-Daimler

Abstract

This thesis documents sedimentary changes in the middle to late Miocene of the Atlantic and Pacific Ocean basins. This time interval known as the "carbonate crash interval" (12-9Ma) displays a severe perturbation of the carbonate system in the framework of the major Cenozoic cooling accompanied by changes in circulation mode, global nutrient shifts, plankton size changes and stratification of the ocean basins. These developments led to modern patterns of biogenic sediment distribution and ecological niches. The main goal of this work was to investigate control mechanisms on Carbonate-Crash-events (CC-events) and to find hints to major discrepancies concerning timing and strength of these events.

For this purpose carbonate preservation proxies and carbonate budgets were investigated and evaluated in the Atlantic at the Ceará Rise in a depth transect (ODP sites 926, 927 and 928). The data show that the dissolution occurred in a broad zone between the foraminiferal lysocline at 3300 m depth and the carbonate compensation depth (CCD) at about 4000 m water depth. Detailed mass losses of coccoliths and foraminifer carbonate were calculated among sites. Dissolution is evident throughout the record however preservation seems to increase in correspondence to Northern Component water formation (precursor of North Atlantic Deep water). Productivity decreases of calcareous plankton productivity here (centered at about 9.5 Ma) seem to be as well a factor controlling CC-events during the late Miocene. Furthermore the evaluation of preservation proxies from the coarse calcareous silt fraction (CSmean and CS percent) showed that the fragmentation of foraminifera is probably a more suitable indicator of carbonate dissolution. CSmean and CSpercent did not reproduce the depth dependant carbonate dissolution, which was evident in all other parameters (carbonate content, coarse fraction content, foraminiferal fragmentation). The comparison of Ceará Rise coarse fraction records to Caribbean Site 999 showed in contrast to earlier results preservation in phase.

The contrasting results obtained from comparison of Ceará Rise records with the Caribbean led to a revision concerning CC-events especially in key locations of the Pacific and Indian Ocean. The productivity decreases in the beginning of the CC-can be assigned to a shift from La Niña-like to El Niño-like conditions, imprinted in the sediments off Baja California and in the Eastern Equatorial Pacific (EEP). Own data from the SE – Pacific (ODP Site 1237) in offshore Peru/Chile provided evidence for enhanced dissolution starting at about 10.5 to 10.3 Ma.. This trend is possibly indicating the influx of corrosive southern sourced waters coupled to better carbonate preservation in the Atlantic. Hence significant basin to basin fractionation is evident. The end of the CC is characterized by a change to better preservation at the same time in the low latitude Caribbean, the Pacific and the Indian Ocean at about 9.5 Ma at similar

water depths (~3000 m). Nannofossil productivity decreases were at least important in the Atlantic in the late phase of the CC.

Restructuring of plankton communities driven by the paleoceanographic revolution during the CC-events may have resulted quite often in productivity decreases, which however are confirmed only by few case studies. Budgeting of calcareous nannoplankton seems desirable. Especially during carbonate crash events bigger nannofossils the discoaster nannoliths comprise an important part of the sediments, in order to budget these nannoltihs 3-d models of 11 Neogene discoaster morphologies as well as *Sphenolithus* nannoliths based on morphometric measurements were set up and applied in a test studie on samples of Ceará Rise ranging from 8.6 to 3.3 Ma to. The significance of carbonate contribution exceeds by far their abundance. A rather abrupt abundance decrease of discoaster nannoliths was found in low latitude sediments of ODP sites from the Indian Ocean and the equatorial Pacific associated with the "small" *Reticulofenestra umbilicus-* interval (starting at 8.85 Ma). This event is associated with rising MAR in these key locations initiating the transition from the "carbonate draught" period of the CC-events to the period of the "biogenic bloom".

Kurzfassung

Diese Arbeit dokumentiert sedimentologische Veränderungen im Übergang vom mittleren zum späten Miozän im Atlantic und Pacific. Dieses Zeitintervall, das „ Karbonat – Crash-Intervall" (12-9 Ma), ist gekennzeichnet durch Störungen des Karbonatsystems, begleitet von Änderungen in den Zirkulationsmustern, der globalen Nährstoff-Verteilung, Planktongrößen und Schichtung der Ozeanbecken im Rahmen des allgemeinen Abkühlungstrends im Känozoikum. Diese Entwicklungen führten zu den heutigen Mustern in der Verteilung biogener Sedimente und ökologischer Nischen. Das Hauptziel dieser Arbeit war es die Kontrollmechanismen der „Karbonat-Crashs" (CC) zu untersuchen, sowie Hinweise auf Diskrepanzen bezüglich des zeitlichen Auftretens und der Intensität dieser Ereignisse zu finden.

Zu diesem Zweck wurden Karbonat-Erhaltungsproxies und Karbonatbudgets im Atlantik am Ceará Rise Tiefentransekt (ODP Bohrungen, 926, 927 und 928) erhoben und evaluiert. Die Daten zeigen, dass Karbonatlösung während des miozänen CC in einer breiten Zone zwischen Foraminiferenlysokline bei 3300 m Wassertiefe und Karbonatkompensationstiefe (CCD) bei ca. 4000 m stattfand. Detaillierte Massenverluste von Coccolithen- und Foraminiferenkarbonat zwischen den Bohrungen wurden berechnet. Lösung zeigt sich im gesamten Zeitintervall, aber die Erhaltung scheint sich im Gleichtakt mit der Bildung von nördlichem Tiefenwasser (Vorläufer von Nordatlantischem Tiefenwasser) zu verbessern. Einbrüche in der Produktivität von kalkigem Plankton (bei etwa 9.5 Ma) scheinen ebenfalls ein Einflussfaktor der CC-Ereignisse im späten Miozän zu sein. Desweiteren zeigte die Evaluierung der Erhaltungsproxies des kalkigen Grobsilts (Grobsilt mean und Grobsilt %), dass die Fragmentierung der Foraminiferen wahrscheinliche ein geeigneter Anzeiger für Karbonatlösung ist. Mean und Prozentanteil des Grobsilts zeigten keine tiefenabhängige Lösung an, die in allen anderen Parametern offenkundig (Karbonatgehalt, Grobfraktionsanteil, Fragmentierung der Foraminiferen) war. Der Vergleich von Sandgehalten der Bohrungen vom Ceará Rise (926) und der Karibik (Bohrung 999) ergaben im Gegensatz zu frührern Ergebnissen gleichschwingende Lösungsrekords.

Die widersprüchlichen Ergebnisse aus dem Vergleich von Ceará Rise und der Karibik führten zu einer Revision bezüglich der CC-Ereignisse, insbesondere in Schlüsselbohrungen im Pazifik und Indik. Die Produktivitätseinbrüche zu Beginn des CC können auf den Wechsel von La-Niña ähnlichen Bedingungen zu El Niño ähnlichen Bedingungen, die sich in Sedimenten vor Baja Kalifornien und im ostäquatorialen Pazifik abzeichnen, erklärt werden. Eigene Daten aus dem südöstlichen Pazifik, (Bohrung 1237) vor Peru, liefern Hinweise auf zunehmende Lösung ab 10,5 bis 10,3 Millionen Jahren. Diese Tendenz ist

möglicherweise auf den Zustrom von korrosivem südlichen Tiefenwasser zurückzuführen und ist an einen Trend zu besserer Erhaltung im Atlantik gekoppelt. Daher wird erhebliche Becken-zu-Becken-Fraktionierung angenommen. Das Ende des CC-Intervalls ist gekennzeichnet durch gleichzeitige Änderungen zu besserer Erhaltung (bei 9,5 Millionen Jahren) in niederen Breiten in der Karibik, dem Pazifik und dem Indischen Ozean und bei ähnlichen Wassertiefen (~3000m). Die Produktionseinbrüche des kalkigen Planktons waren mindestens in der späten Phase der CC-Ereignisse im Atlantik von Bedeutung.

Restrukturierungen in der Plankton Gemeinschaft, gesteuert durch die paläozeanographischen Umwälzungen während der CC-Ereignisse, resultierten wahrscheinlich oft in Produktivitätseinbrüchen, die aber nur in wenigen Fällen belegt sind. Eine Budgetierung des kalkigen Nannoplanktons scheint wünschenswert. Insbesondere während der CC-Ereignisse bildeten größere Nannofossilien, die sogenannten Discoaster–Nannolithe den größten Teil des Sediments. Um den Anteil dieser Nannofossilien einschätzen zu können wurden 11 drei-dimensionale Modelle von Neogenen Discoaster-Nannolithen erstellt und an einer Teststudie an Proben vom Ceará Rise von 8,6 bis 3,3 Millionen Jahre zur Karbonat-Budgetierung angewendet. Die Discoaster-Nannolithe tragen in diesem Intervall nur einen geringen Prozentsatz zu den gesamten Nannofossilien bei, ihr Massenbeitrag zum Gesamtkarbonat ist hingegen bedeutend. Ein abrupter Häufigkeitsrückgang der Discoaster-Nannolithe wurde in niederen Breiten in ODP Bohrungen des West-Pazifiks, der Karibik und des Indischen Ozeans in Verbindung mit dem Beginn des *Reticulofenestra* paracme Intervalls (bei 8.85 Millionen Jahre) festgestellt. Dieses Ereignis steht in Verbindung mit zunehmenden Massenakkumulationsraten von Karbonat, die einen Übergang von der „Karbonat-Dürre-Periode" der CC-Ereignisse zu der fruchtbaren Periode des „Biogenic Bloom" in diesen Schlüsselregionen kennzeichnen.

Table of contents

Chapter 1 - Introduction

1.1 The framework of global cooling in the middle to late Miocene

Ice and cooling

Understanding past climates means to understand different heartbeats and pulses of the climate. Today our climate is governed by both poles caped with ice. We understand ourselves to live in an ice age, which is currently intermitted by a warm phase. The ice caps responded to changes of the earth orbital parameters (Imbrie et al., 1993). The leading period in these cycles of waxing and waning of ice is the 100kyr cycle, which corresponds to variations in the shape of the path of the earth around the sun (eccentricity). From 3 to 1Ma the rhythm of the climate followed the 41kyr cycle, which was in accordance with obliquity cycles (axial tilt). Why eccentricity variations, which are weaker than other orbital changes (Milankovitch cycles) designated our climate the past one million year is not completely understood and many questions arose (e.g. Maslin, 2005). Answers to these questions involve complex feedback mechanisms in ice dynamics, precipitation, ocean circulation and the carbon cycle.

During the Middle Miocene a similar border of climate heartbeat was crossed. The middle Miocene was a time period of cooling with the establishment of constant ice caps on Antarctica and first smaller dimensioned ice shields in Greenland (St John and Krissek, 2002, Zachos et al., 2001) leading the way to a change to the bipolar state. The expansion of Antarctic ice shields is documented (together with temperature changes) in the $\delta^{18}O$ record and appears in Miocene records as Mi-Events (Miller et al., 1991) which however, can often not be traced in the record and then fails as a stratigraphic tool (Anderson and Jansen, 2003; Westerhold et al., 2005), which it is for the younger glacial interglacial cycles.

A major cooling step centered at 13.9 Ma is accompanied by a change from obliquity to eccentricity driven $\delta^{18}O$ variations (Holbourne et al., 2005)., similar to the aforementioned Pleistocene revolution. Evidence from Mg/Ca – temperatures points to a higher proportion of ice effect in the $\delta^{18}O$ record (Lear et al., 2003). Explanations involving atmospheric pCO_2 as thresholds of boundary conditions are unfortunately not corroborated sufficiently by data compilations, because proxy records are at low resolution (see Fig. 1.1, Pagani et al. 1999, Pearson and Palmer 2000). These explanations involve e.g. the silicate weathering and the expansion of C4 plants, which due to more effective photosynthesis could have drawn down the atmospheric pCO_2 (Cerling

et al., 1997). A coupling between climate and *pCO₂* proxy records might be implicated as long term trends of *pCO₂* show a close correlation (Tripati et al., 2009).

The ocean is a huge reservoir of CO_2 which is 60times bigger than the atmosphere, thus small changes in the ocean can account for vast changes in the smaller atmospheric reservoir. (Berger, 1991). The understanding of past changes is crucial for scenarios in the future and understanding of feedback mechanisms. Especially the Cenozoic offers therefore a huge archive of ocean sediments, formed in mostly warmer climates than today.

Fig. 1.1: Reconstructions of middle to late Miocene atmospheric pCO₂ (Pagani et al., 1999; Tripati et al., 2009; Pearson and Palmer, 2000).

Ocean circulation and Gateway configurations

The establishment of the modern pattern of circulation is believed to be in the middle to late Miocene. This means that the thermohaline circulation with a dominant North Atlantic source was initiated. This further means that the southern sourced carbonate corrosive deep waters were replaced step by step by fresher deep water from the North. The changing circulation is the central subject in the interplay of dissolution, preservation and nutrient availability governing the carbonate crash interval (12-9 Ma). The most common tracer for these water masses is the ratio of stable carbon isotopes ($\delta^{13}C$), which can be used as a tracer of the "age" of a deep water (e.g. Kroopnick et al., 1985). Freshly formed North Atlantic deep water (NADW) has the most positive signature, because it evolves from low nutrient delta $\delta^{13}C$ surface waters and flows in southward direction towards the Southern Ocean. On its way it mixes with southern sourced waters (Antarctic Bottom Water -AABW and Antarctic Intermediate Water -AAIW) with a more depleted signature, indicating as well higher nutrient concentrations and greater potential to dissolve carbonates. The most depleted values can be found in the North Pacific, where water traveled from South to North until it takes up some of the remineralized carbon produced in the surface waters.

In order to calculate the Northern Component water (NCW-here used as ancient equivalent to NADW) percentage the use of mixing calculations between different basin endmember δ^{13}C according to Oppo and Fairbanks (1987) is reasonable by assuming that δ^{13}C differences developed in the same way as today. The gradients among ocean basins became significant at the beginning of the CC-events about 12 Ma (see Fig 1.2 - Poore et al., 2006) suggesting no earlier significant deep water formation. Complications in the modern analogue assumption involve e.g. deep water pathways, especially the closure of the Central American Seaway (CAS) and changing productivity patterns, erosion of terrestrial soils and organic matter from shelves (Bickert et al., 2004) which could have influenced gradients.
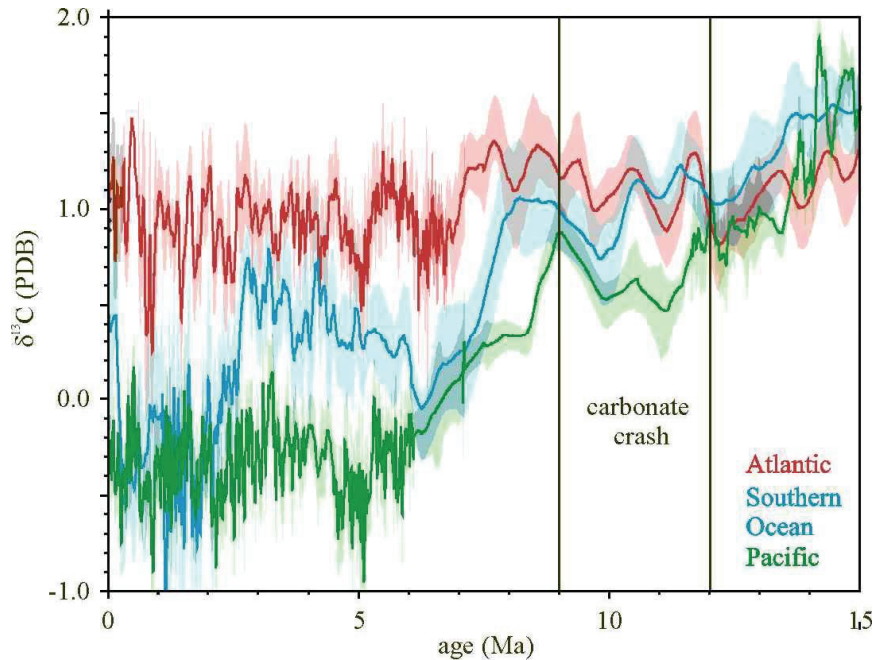
Fig. 1.2: Carbon stable isotope composition of endmembers of deep water in the Atlantic (red), Southern Ocean (blue) and Pacific (green) after Poore et al. (2006).

The closing of the CAS is believed to have had a great impact on deep water formation in the North Atlantic. The new gateway configuration would have led to a strengthened western boundary current and would enhance temperature and salinity of source waters for deep water formation. A convergence of Southern Ocean (Site 1088) and North Atlantic δ^{13}C signatures at about 6-6.6 Ma (Billups, 2002) was attributed to the establishment of this pattern. Other results based on salinity gradients between Pacific and Caribbean place this pattern at 4.6 Ma (Haug and Tiedemann, 1996; Haug et al., 2001). One modeling study suggests, however, significant NADW formation in a

setting with an open CAS (Nisancioglu et al., 2003). Heinze and Crowley (1997) investigated the sedimentary response for a restricted exchange through the CAS. A shoaling of the lysocline could have happened in the North Indian Ocean and in the Eastern Equatorial Pacific (stretching into the North Pacific) accommodated by elevated opal sedimentation compared to the control run (Heinze and Crowley, 1997). However, sedimentary data contrasts with modeling results. At about the time of the final closure (3.2 to 2.7 Ma) of the CAS the carbonate compensation depth was deepening in the EEP (Farrell and Prell, 1991) according to carbonate wt.% data.

The role of the Greenland Scotland Ridge (GSR) which moved vertically due to the activity of the mantle plume underneath is assumed to control the spill-over of NCW (Wright et al., 1992; Wright and Miller, 1996; Poore et al., 2006). However, recent modeling of the Atlantic circulation showed that the $\delta^{13}C$ pattern might not be influenced by GSR movements (Butzin et al., 2011). Their experiments showed furthermore that the formation of deep water might have been located in the Labrador Sea which is in accordance with ε_{Nd} from the Walvis Ridge depth transect, that suggests the onset of deep convection in the Labrador sea as early as 10.6 to 7.3Ma (Kastanja and Henrich, 2007; Thomas and Via, 2007) or 12 Ma (Muiños et al., 2008). The development of the emergence of the Indonesian Seaway is another example of a process that is difficult to trace in its timing. The passage for deep water might have been already restricted in the late Oligocene at about 25 Ma ago and closed in the early Miocene (Kuhnt et al., 2004). Consequences of this and further shoaling of the passage might have been as severe as the shoaling of the CAS involving heat and moisture transport to high latitudes, a permanent El Niño-like state (Molnar and Cane, 2002; Molnar and Cane, 2007) as well as the establishment of the West Pacific Warm Pool and equatorial Pacific circulation (e.g. Nathan and Leckie, 2009). The application of the ENSO-concept to the Miocene climate change is most recently debated in (Von der Heydt and Dijkstra, 2011).

1.2 Carbonate cycle and budget

The main questions addressed in this study are concerning the burial and dissolution of calcareous shells of plankton as part of the global carbonate system in the time interval of the CC-events. The removal of carbonate from the oceans in form of calcite or aragonite in planktonic organisms is an efficient way to remove Ca^{2+} and CO_3^{2-} for longer timescales through burial in sediments. However

at the same time carbonate is produced there is a net release of CO_2 to the surface water and thus atmosphere, through equilibria reaction:

(Eq. 1.1) $CO_2 + H_2O + CO_3^{2-} <=> 2HCO_3^-$
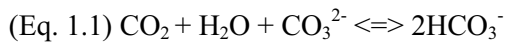
Thus the uptake of bicarbonate through formation of biogenic carbonate drives the equilibrium to the left and carbonate dissolution (release of bicarbonate) drives it to the right. In a simple model this carbonate production (P) together with dissolution (D) can be regarded as balancing mechanisms to maintain a steady state between burial (B) and input of Ca^{2+} and CO_3^{2-} ions through weathering and via rivers (R) (Broecker and Peng, 1987): B=R

So if input increases (R) this results in higher productivity balancing in order to produce higher burial (B). And the other way round, if input decreases dissolution acts to balance for ions. This mechanism is know as "carbonate compensation" and operates on a short (several kyrs) timescale as e.g. at glacial/interglacial changes (Archer et al., 2000). Also sea level highstands and the flooding of shelves influences the location of carbonate formation and its preservation potential (basin-to-shelf fractionation, Berger 1970) as well as the general saturation in carbonate of the ocean (Walker et al., 2002). Other mechanisms maybe more important on longer timescales as the silicate rock weathering, that provides the ions in order to account for the loss through carbonate burial mostly (Caldeira and Berner, 1999). It is a negative feedback mechanism, because the weathering is in turn controlled by the temperature and CO_2 concentration in the atmosphere and stabilizing the climate on scales of hundreds of kyrs to millions of years (Berner and Caldeira, 1997). The ultimate recycling of carbonate sediments is driven by subduction of oceanic plates and decarbonation resulting in CO_2 release to the atmosphere. This can be understood as the opposite of silicate weathering and is relevant within tectonic timescales (Ridgewell and Zeebe, 2005). Also the "shelf to basin fractionation" was considered to influence the location of carbonate deposition. This concept is based on the hypothesis that during sea level lowstands, deposition might preferably take place in the pelagic enviroments, however this was not corroborated by studies concerning carbonate budget analysis (Milliman, 1993).

Studies of the purpose to budget today's ocean carbonate production resulted in considerable descrepanicies. The unresolved questions are pointing to the role of carbonates from shelf environments, and state that only the input of rivers can reasonably be estimated. The dissolution processes are still hardly understood and still are not much further progressed. It is still counter intuitive that carbonate dissolves in a supersatured environment, which is called supralysoclinal

dissolution, however the evidence is compelling and arose especially clear from sediment trap data and alkalinity considerations (Millimann et al., 1999, Chung et al., 2003).

Chapter 2 - Methods and Material

In this thesis a suit of sedimentological carbonate proxies are applied and evaluated. The standard procedure of sample preparation is illustrated in Fig 2.1. The goal was to gain data that can be used for *carbonate budget* analysis and *carbonate preservation* studies.

The interpretation of preservation proxies regarding circulation hypothesis are based on a modern analogue. The deep water formed in the North Atlantic is less corrosive to calcareaous shells of plankton than its southern sourced "aged" counterpart and also intermediate waters might show these differences. Following this classical assumption these water masses can be traced in a critical depth (where these water masses meet) by dissolution proxies based on the visual preservation of calcareous plankton remains.

Carbonate budget calculation means determination of the contribution of the two main calcareous plankton groups - coccoliths and shells of foraminifera. The size distributions' overlap of these groups is located in the calcareous silt fraction as described below. Another approach of a budget calculation is to calculate the mass of a shape (e.g. coccolith shield) and then infer to the mass it contributes to the sample from shapes abundances in a representative split of a sample.

Carbonate measurements where conducted on bulk samples using a Leco CS infrared combustion analyzer. The principal of the measurement is the infrared light absorption through Carbon-monoxides stemming from the combustion of the sample. Two sample for each carbonate content were measured. The difference between the total carbon (TC) and the total organic carbon (TOC) multiplied by the ratio of the molecular weight of carbonate to carbon (8.33) results in the carbonate content of a sample. The quality of the measurements is maintained through usage of multiple Carbon standards and their calibration.

2.1 Silt grain size measurements with the Sedigraph – carbonate preservation and budget

A suit of proxies can be derived from the distribution of grain sizes. The choice of method will rely on the purpose and grain sizes. For hydrodynamic reconstructions (e.g. paleo flow intensities) e.g. a sedigraph might be preferred, because it "translates" from particle's settling behavior into a size of an equivalent sphere with the same hydrodynamic properties and settling velocity as the differently shaped real particle. The settling velocity of spheres in a laminar flow is given by an expression of Stokes law for low Reynolds numbers (Re<<1):

(Eq. 2.1) V=settling velocity = $2/9[(\text{Density}_{sphere} - \text{Density}_{fluid})(\text{radius}_{sphere})2\ g\ ]/\ \text{Viscosity}_{sphere}$

The concentration of the particles of a certain equivalent spherical diameter (ESD) will be measured through the attenuation of x-rays in the suspension. Comparing the attenuation at a certain settling depths to attenuation of a reference liquid ("clear water" with lowest attenuation) let infer to a mass concentration of a certain ESD. The statistic features of the cumulative grain size distributions were obtained through classical moments-statistics according to Krumbein (1936) with own developed auxiliary routines using Matlab.

All silt measurements were prepared by removing the clay through repeated settling in Atterberg tubes at 2µm ESD using this law. However, the "true" (maximum) diameters of the remaining silt fraction are bigger, because most of them are platy shaped coccoliths or clay particles, that might have settled not as straight as a sphere would have. Therefore if clay separation is done properly the remaining particles are often bigger than 3-4µm.

Several circumstances can hinder an appropriate measurement of materials, the presence of flocs and clays that build water in between their layers and magnetic material that sticks to the magnetic stirrer of the Sedigraph device, for very high carbonate contents it might be useful to add some Calgon solution already for separating clays. The principal of settling diameters brings another feature in comparison to optical grain size measurements the Sedigraph overestimates smaller particles. A review on methodologic aspects and advice on sample preparation is given by Stein (1985) for comparison of different grain size distribution methods as well as accuracy and precision

Fig. 2.1: Flow chart of sample procedures as applied in this study.

see Coakley and Syvitski (1991) and for proxy applications and evaluations (McCave et al., 1995; Ledbetter, 1984; Frenz et al, 2005; Preiß-Daimler and Henrich, submitted; Weltje and Prins, 2003).

Most of the pelagic (open ocean-far away from the continent) sediments are composed of some terrigenous fractions and biogenic opal and carbonate from foraminifera and coccolithophores. In about 95% of the decalcified samples the terrigenous (non-calcareous opal free fraction) silt constituted less than 5% of the bulk silt. The terrigenous fraction is concentrated in the clay fraction and in the fine silt. Thus it was unfortunately not possible to collect evidence for relative paleoflow speed reconstruction based on the terrigenous part of the non-cohesive silt (10-63µm) known as sortable silt (McCave et al., 1995). However, this in turn allowed for simplifications regarding carbonate budget estimates. Due to the low concentration of terrigenous silt the bulk silt distribution can be regarded as a close approximation of the calcareous silt distribution. The silt grain size distribution follows in nearly all cases a bimodal distribution with a minimum centered at about 8-10µm. This border separates the coarse silt that is mainly made of foraminifera and their fragments from coccoliths and other nannoliths in the fine silt. The border moves with relative proportions of the coarse and fine silt and with the modes of the endmembers.

Some authors theorized that progressing dissolution and fragmentation of foraminifer will result in a fining of coarse silt and relative to fine silt lower contribution of coarse silt. This process might be further supported, if coccoliths or other nannoliths are more dissolution resistant with respect to foraminifera (pro: Hay, 1970; Honjo, 1976; contra: Paull et al., 1988; Buitenhaus et al., 1996) The proxies used for dissolution are known as CS mean (coarse silt mean) and CS % (percentage of coarse silt fraction) and used in several studies (Gröger et al., 2003; Frenz et al., 2006; Kastanja et al., 2007) using the same Sedigraph devices and sample preparation as used during this study. In this study these proxies and principals are critically evaluated in Chapter 3.

2.2 Biometry and mass estimation on nannofossils for carbonate budgets

The procedure used to prepare samples for SEM investigations follows a protocol of a wet splitting - filtration technique after Andruleit (1996). About 70 mg of the sample was weighed, brought into a buffered suspension, splitted and filtered on a polycarbonate membrane using a vacuum pump. An area of about 0.5 cm^2 was cut out of the dried filter and sputtered with Au/Pd. Assemblage counts were made using a scanning electron microscope (Zeiss DSM 940A) on a known area containing about 500 specimens. Abundance counts and morphometric meassurements where conducted under 3000times magnification.

2.3 Age models and accumulation rates

Age models used can be assigned mostly to the timescale of (Berggren et al., 1995) with small differences. Previous work on the Ceará Rise depth transect offers well dated sediments and a high resolution age models based on orbital tuning (Shackelton and Hall, 1997). Site 1237 offered a very detailed magentostratigraphy in the investigated interval. Site 982 had only few datums and isotopic records were not regarded as being helpful in attempts to gain better age control (Andersson and Jansen, 2003), therefore mass accumulation rates were not reported for this site. The quality of the age model is decisively important for the rating of the accumulation rates, which were calculated as follows:

(Eq. 2.2) $MAR_{component}$=Linear sedimentation rate * dry bulk density*proportion of the component

The DBDs were deviated from Gamma-Ray Attenuation (GRA) core-logging data, which were calibrated by discrete density measurements (ship board gas pycnometer –Method C) by linear interpolation at sample depths. The dry bulk densities were calculated according to the equation of Curry, Shackleton, Richter et al. (1995) with a water density of 1.035 [g/cm^3]:

(Eq. 2.3) DBD [g/cm^3] = (ρ_{GRA} - ρ_{water} * ρ_{grain})/(ρ_{grain} - ρ_{water}).

2.4 Study areas and regional settings

The areas of interest were mostly the Atlantic and the Pacific (Fig. 2.2). In the Atlantic four cores were investigated. The Ceará Rise depth transect offered a well dated sequence of cores in the Western tropical Atlantic in front of the Amazon river. Here the transition zone between NADW and AABW could be studied in cores 926, 927 and 928. The Ceará Rise is located at the western edge of the subtropical Atlantic gyre in an oligotrophic setting. The Amazon drainage system started to operate effectively in the late Miocene after the CC- interval (Hoorn et al., 1991)

The North Atlantic was investigated at Site 982 at the Rockall Plateau. Surface waters here are part of warm the North Atlantic current as part of the Atlantic Meridional Overturning Circulation (AMOC). The temperate currents are an important heat source for western Europe and favor the warm regional climate. The warm waters pass the Iceland Faroer Ridge and consequently cool and sink to form deep waters in the Iceland and Greenland Seas. The relatively shallow Site 982 (1134m water depth and
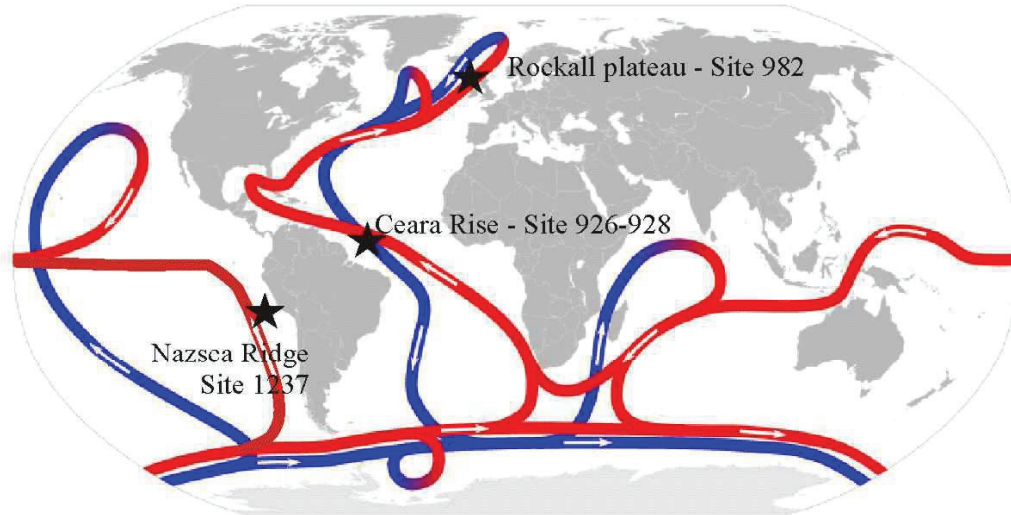
Fig. 2.2: Position of study areas within the global conveyor belt (red-surface currents, blue-deep and bottom currents-modified after Rahmstorf (2006), source: Wikipedia).

57º31'N, 15º52'W) was chosen because it is supposed to reflect the evolution of North Atlantic Intermediate water by which it is bathed today.

The South Pacific Site 1237 is located at water depth of 3212 m water depth off Peru (16°0.42´S, 76°22.69´W) in an upwelling region today, which can be backtracked to some hundred kilometers offshore in the late Miocene. The Andean uplift has also influenced the southeast Pacific throughout the last 10 Ma and acted probably as an atmospheric barrier forcing winds to blow parallel to the coast, favoring even more upwelling. Site 1237 recorded the variability of the Pacific Central Water (PCW) and is therefore ideally situated to test some hypothesis concerning deep water flux during CC events in a meso- to oligotrophic environment.

2.5 Main objectives of the study

The main goal of this study was to trace the Miocene Carbonate crash events in its final phase in the Atlantic and Pacific by using preservation proxies derived from the silt fraction and coarse fration accompanied by mass accumulation rates in order to get insight into carbonate budgets and thus to find evidence, whether carbonate **dissolution, dilution** or **productivity** contributed to the crash events. Furthermore…

1)…how carbonate dissolution effected the different carbonate contributors

2)…to apply and test carbonate preservation proxies based on silt grain size measurements

3)…test hypothesis concerning deep water and surface processes, as:

- NADW initiation

- permanent El-Niño-scenario

- ecologic influences on plankton accumulation

Chapter 3 - The final phase of the Miocene Carbonate Crash in the Atlantic: Assessment of existing models by carbonate accumulation, preservation proxies and shifts in the contribution of calcareous plankton groups

Authors: Inga V. Preiss-Daimler, Rüdiger Henrich
Status: submitted to Marine Geology

Abstract

The Carbonate Crash-events were a widespread phenomenon of carbonate dissolution, dilution and productivity changes throughout the main world's ocean basins in the middle to late Miocene. This study provides data of carbonate preservation proxies as silt grain size parameters, sand content, fragmentation index and mass accumulation rates in sediments of the equatorial Atlantic Ceará Rise depth transect (Site 926, 927 and 928) in the late Miocene from 10.5 to 9.5Ma. A comparison to the modern situation reveals that the calcite lysocline was located at depth of Site 928 (~4000 m) and the foraminiferal lysocline at depth of Site 927 (~3300 m water depth) with a broad transition zone and a trend towards better preservation in the proxy data record. However, silt preservation proxies do not entirely reproduce the depth dependant dissolution. A critical evaluation and comparison to former studies suggest preferring the classical foraminifer fragmentation index. Preservation proxy trends do correspond to North Component Water percentage estimates until 10.2 Ma, afterwards trends are conflicting. Preservation trends of Caribbean and Ceará Rise records were in phase in contrast to former hypothesis that suggested antithetical preservation during Carbonate Crash-events. Furthermore, a detailed comparison of the nannofossil grain sizes shows that a trend towards the finer nannofossil carbonate accompanied sedimentation in various environments of the late Miocene Atlantic Ocean.

3.1. Introduction

The middle to late Miocene transition towards icehouse conditions and its consequences for ocean carbonate budgets and preservation.

The transition from greenhouse to icehouse climate during the middle to late Miocene is in the focus of ongoing paleoceanographic discussions. During this period severe perturbations of the carbonate system occurred changing the distribution pattern of carbonate in the major ocean basins. The main Antarctic ice shields were about to become permanent and a considerable build-up of ice took place in the northern hemisphere (Zachos et al., 2001; Fronval and Jansen, 1996). Huge mountain chains rose and atmospheric pCO_2 reached preindustrial levels (Pagani et al., 1999). In addition, the general

Cenozoic cooling tended to increase temperature gradients between high and low latitudes, in turn enforcing wind systems as well as oceanic mixing and upwelling.

Other prominent changes occurred at oceanic gateways. The closure of the Tethys, the emergence of the Panamanian Isthmus and Indonesian Gateway are thought to have essentially controlled circulation pathways in the middle to late Miocene oceans (Nisancioglu et al., 2003). The rise of the Panamanian Isthmus from bathyal to neritic depths as well as the establishment of the Caribbean loop current (Eberli, 2000), took place in the middle to late Miocene (Coates et al, 2004; Duque-Caro, 1990), influencing the heat transport to northern latitudes. Interestingly, a drastic change of the geochemical properties of deep waters is registered during the same period. $\delta^{13}C$ signatures of deep waters in the three major ocean basins in particular are becoming significantly different, indicating the isolation of basins. A main feature with regard to this aspect is that variations in sill depth of the Greenland-Scotland Ridge might have controlled North Component Water (NCW) formation (Poore et al. 2006; Wright and Miller, 1996), which should also be reflected by shifts in the carbonate preservation patterns in the ocean basins. These changes are manifested in the Miocene Carbonate Crash (CC) events that are best characterised by distinct minima in carbonate accumulation with extreme developments in the equatorial Pacific and the Caribbean where carbonate accumulation dropped to zero (e.g. Lyle et al., 1995; Roth et al. 2000). These events are also recognised in the Ceará Rise record where a long-term shoaling of the lysocline took place from 14 Ma to 11.5 Ma (King et al., 1997). The timing of crash events in the Pacific is from 12 Ma to 9 Ma with the Crash nadir at 10 Ma, while in the Caribbean these events can be recognised from 12 to 9 Ma and from 13.8 to 12 Ma as precursors.

The partial coincidence of events suggests a common cause often explained by changing circulation patterns. The Caribbean CC events are ascribed to the influx of carbonate corrosive AAIW (or its precursor/ancient equivalent) replacing sinking waters in the northern hemisphere in times of re-established NADW formation (Roth et al., 2000). Another hypothesis postulates the influx of corrosive Pacific intermediate waters triggering dissolution in the Caribbean (Newkirk and Martin, 2009).

However, carbonate preservation and accumulation pattern in the Atlantic ocean can often not solely be explained by changing preservation. This is shown at ODP Site 1085 in the Benguela upwelling system, where terrigenous dilution by Orange river sediments and shifts in coccolith production rates are the main causes for low carbonate contents in the middle to late Miocene (Krammer et al., 2006; Kastanja et al., 2006; Diester-Haas et al., 2004). Investigation of plankton sizes led to the conclusion that the middle to late Miocene might take a threshold position in the changing body size of marine plankton. During the last about 10 Ma *C. leptoporus* shows a placolith size decrease (Knappertsbusch, 2000) and coccoliths of the *Reticulofenestra* lineages also appear to become smaller (Young, 1990), while foraminiferal size in subtropical to temperate climates shows a long-term increase since 11-10

Ma (Schmidt et al., 2005). It has been shown that extant coccolithophore lineages follow a long-term morphological trend of decreasing size rooted in the Miocene (Aubry, 2007).

Instead of one explanation for the Carbonate Crash events there are various processes involved pointing to local influences. Shifts in carbonate accumulation and preservation were induced by (1) reorganisation of deep and intermediate water circulation, (2) climatically induced changes of terrigenous supply diluting carbonates, and (3) variations of production rates of the main calcareous marine plankton groups, which in turn may be related to evolutionary size trends and the emergence of new ecological niches. In order to test and assess the various controls suggested a multi-proxy study addressing all these parameters is needed. In this paper we focus on silt and foraminiferal preservation patterns and their changes as well as the role of the different carbonate contributors, arranged by size, concerning budget estimates. A depth transect at Ceará Rise (ODP sites 926, 927 and 928) and ODP Site 982 at the Rockall Plateau was investigated in the time slice 10.5 Ma to 9 Ma covering the nadir of Miocene carbonate crash events in the Pacific and the end of Carbonate crash events in the Caribbean. Preservation proxies like changes of the content of coarse calcareous silt and its mean will be tested in comparison to former studies. Changes in the accumulation of the main carbonate contributors, namely foraminifera and coccoliths, will be addressed and compared to results from ODP Site 1085.

3.2. Study areas

Ceará Rise is an aseismic ridge located 700 km to the north-east of the mouth of the Amazon River, below the oligotrophic subtropical West Atlantic gyre (Fig. 3.1 A). Its sediments are composed of terrigenous clay supplied by fluvial discharge and carbonate from nannofossils and foraminifers. The evolution of today's Amazon drainage system dates back into the Miocene (Hoorn, 1994). In the Pliocene discharge rates approached modern levels testified by significant increase of terrigenous accumulation rates at Ceará Rise. Here it is possible to decipher the imprint of the main deepwater masses from unique, highly resolved Neogene sedimentary sequences. Particularly, the transition from North Atlantic Deep water (NADW) and Antarctic Bottom water (AABW) is well documented along the depth transect of ODP sites at Ceará Rise. Today, the calcite lysocline is located at a water depth of 4500-4600 m

Site 982 (57°30.992'N, 15°52.001'W) is located on the Rockall Plateau within a water depth of 1133 m (Fig. 3.1 A) and bathed in North Atlantic Intermediate water (NAIW). The Site is supposed to document the development of intermediate water circulation in times of Iceland Faroer Ridge subsidence to a depth that allows deep water exchange with the North Atlantic. Results from grain size analysis of Site 982 are included in Results section 4.2.
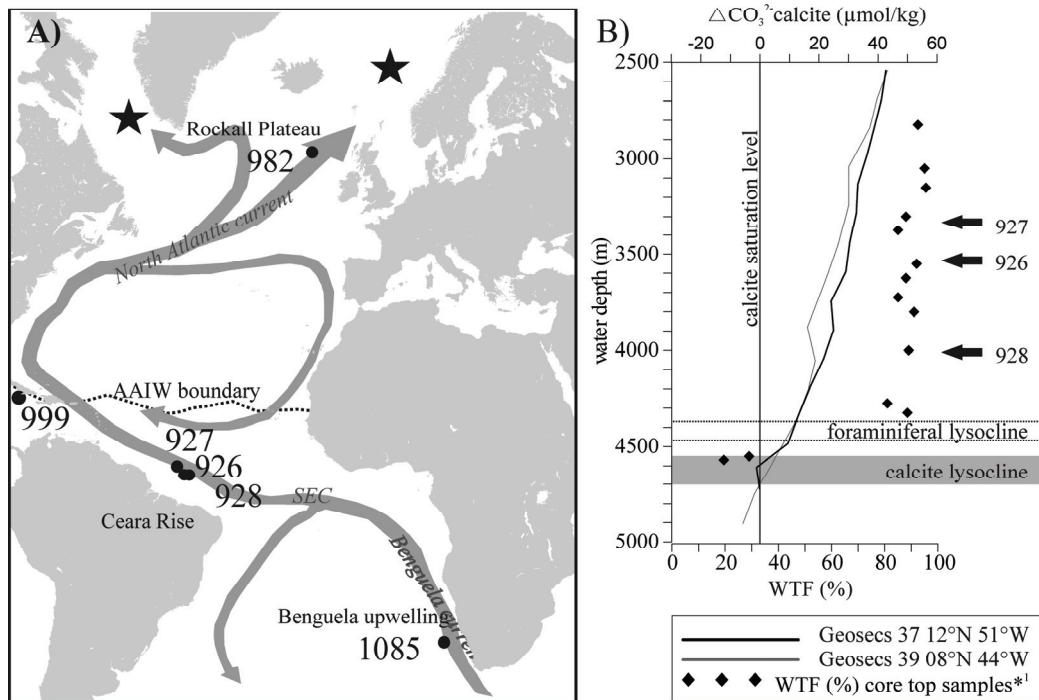
Fig. 3.1: **A)** Map of surface circulation and locations of cores from this study (Rockall Plateau and Ceará Rise) and additional locations (999 and 1085) discussed in the text. The stippled line indicates the northernmost position of Antarctic Intermediate Water (AAIW) according to Talley (1999); stars indicate locations of deep water formation. **B)** Ceará Rise water properties calculated from Geosec stations 37 and 39 (Bainbridge, 1981) indicating a modern calcite lysocline at 4.6km depth and the foraminiferal lysocline indicated by a rapid decrease in whole test foraminifer (WTF (%)) in core top samples (Curry and Cullen, 1995) at 4.4km.

3.3. Methods and Material

We sampled ODP sites 927 (5°28′N, 44°29′W, 3314 m water depth), 926 (3°43'N, 42°54'W, 3533 m) and 928 (5°27'N, 43°45'W, 4011 m) in the interval from 10.5 -9 Ma. Sediments consist of nannofossil oozes with clay and variable contributions of foraminifera. Careful inspection of the sedimentary sections during sampling campaigns showed that the Miocene sections were occasionally affected by sediment instability, comprising contorted bedding, folding and tilting (Curry, Shackleton and Richter et al., 1995). These sections as well as some additional sections suspected of slumping at Site 927 (248.41-257.25 mcd following the original splice) were excluded from further interpretation and

samples from sites 927 and 926 were merged to form a composite record. Samples of 10cc volume were taken every 10ky according to the orbitally tuned age model (Shackleton & Crowhurst, 1997). ODP Site 982 (1145 m water depth) was sampled at a resolution of about 30 ky from 9 - 10.5 Ma. Sediments are nannofossil oozes partly with clay. Paleodepth estimates suggest that Site 982 was 100-150 m shallower than today (Andersson and Jansen, 2003). The shipboard age model from Leg 162 provides the age control (Jansen, 1996). The samples were freeze-dried and split. One portion was wet-sieved at 63 µm under weak spray to prevent the unintentional breakage of foraminifers. The other part was analysed for total Carbon (TC), and, after the removal of carbonate, for total organic Carbon (TOC) by using a LECO CS 200 infrared combustion analyser. Carbonate Content had been calculated after:

(Eq. 3.1) $CaCO_3$ [wt.%] = (TC [wt.%] - TOC [wt.%]) * 8,33

Calibration was carried out by linear regression of multiple standard measurements. Double measurements were taken on extreme values.

3.3.1 Foraminifer preservation index

Splits of the sand fraction from 125-500 µm were analyzed for foraminifer preservation by the counting of at least 300 particles. Standard literature offers various techniques and methods to count a fragmentation index. In order to make the results comparable to various works three categories were chosen for the preservation state according to Berger (1975). A whole test (W) does not show any signs of fragmentation except attacked surfaces or minor borings. A broken test (B) comprises at least half of the specimen and a fragment (F) less than half of the test. An index (WTF) is calculated as percent whole tests:

(Eq. 3.2) WTF (%) = #W + #B / (#W + #B + #F)*100

3.3.2 Silt grain size distributions

Bulk silt samples of Ceará Rise sites did not contain more than 5% terrigenous silt, therefore there was no possibility to gain proxies for paleoflow speeds as e.g. sortable silt (10-63 µm) from the non-cohesive carbonate free part of the distribution (McCave and Hall, 2006). The almost pure calcareous silt samples offer the opportunity to test silt preservation proxies as the proportion of the coarse silt (CS% in the 10-63 µm fraction) and its mean (CSmean). The coarse silt contains juvenile foraminifers and foraminifer fragments that are more susceptible to dissolution than coccoliths in the fraction <10 µm. This is possible because silt grain size distributions show a striking minimum at about 8-10 µm separating the size distributions of foraminifer silt and coarse nannofossil silt. Thus reductions in the amounts and size of particles in the calcareous CS fraction as shown in previous studies (Gröger et al., 2003; Frenz et al., 2005; Frenz et al., 2007; Kastanja et al., 2007).

In order to extract the silt fraction the fine fraction was transferred to Atterberg settling tubes. Subsequently the clay fraction was reduced in the silt fraction by repeated settling (20 to 35 times) in Atterberg tubes with at least 19 hours of settling time. NaCO$_3$-solution (0,003 mol/L) was used as dispersion agent. The dried weights of sand, silt and clay were summed up and are in the following referred to as 100%. Silt grain size distributions were determined by a Micromeritics SediGraph 5100. The SediGraph measures size distributions from 2 - 100 µm according to Stokes' law as Equivalent Spherical Diameter (ESD) accurately. Finer grain sizes tend to behave cohesively and settling diameters coarser than 100 µm requires increasing Reynolds numbers (Gibbs et al., 1971). 0.1% Sodium polyphosphate have been used as a dispersing agent. The statistical parameters were calculated according to the method of moments (Krumbein, 1936). Bulk silt samples were washed carbonate free by repeated HCl (12.5%) treatment and subsequently washed neutral with deionised water. Afterwards they were dried and weighed. Because the bulk silt samples of the study material contain on average not more than 5% terrigenous silt we will refer to bulk silt in the following as calcareous silt. SediGraph cumulative raw data was interpolated at 0.1 φ increments by linear interpolation. In a second step, the interpolated cumulative data has been normalised by subtracting minima and by dividing resulting cumulative maxima. Afterwards the grain size distributions were calculated in the range from 4φ - 9φ (62.5 µm – 1.95 µm). Nannofossils from randomly chosen silt samples of all sites were checked under the Scanning Electron microscope for successful disaggregation, diagenetic overgrowth and state of preservation, which shows only minor etchings and overgrowth in case of Site 928.
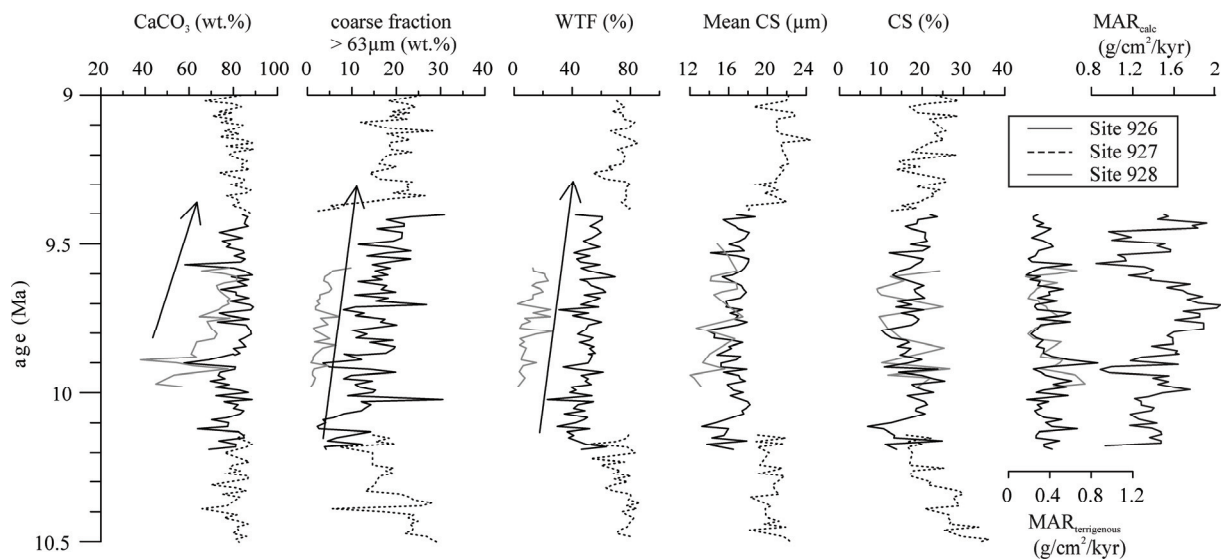
Fig. 3.2: Results from Ceará Rise Depth transect sites 926/927 (black line/dotted lines) and 928 (grey lines) with dissolution proxies from left to right: carbonate content (wt.%), coarse fraction > 63 µm (wt.%), whole test foraminifer index (WTF%), coarse calcareous silt mean (CSmean), content of coarse calcareous silt (CS wt.%), mass accumulation rates of terrigenous (MAR$_{terrigenous}$) and calcareous material (MAR$_{calc}$). Note the overall trend to better preservation at Ceará Rise records and

the offset between both sites in the first three parameters, as well as the missing difference in calcareaous silt preservation proxies (CSmean, CS%) among sites.

3.3.3 Mass accumulation rates and age models

In order to separate influences of dilution and productivity/dissolution changes mass accumulation rates (MAR) provide useful information. The quality of mass accumulation rates strongly depends on the quality of the age model. Orbital tuning methods increase the number of tie points of age models up to a resolution of a precession cycle (~26 kyr). The basic framework of the tuning is mainly tied to biotratigraphy in Miocene sections. Previous work on Site 926 provides high resolution biostratigraphy relying on nannofossil datums (Backmann and Raffi, 1997) calibrated by the orbitally tuned age model (Shackelton and Hall, 1997). The age models of Site 927 and 928 were subsequently established by correlation to Site 926 (King et al., 1997).

Due to grain size analysis it is possible to divide calcareous MARs (MAR$_{calc}$) into the following calcareous components, going from coarsest to finest: foraminiferal carbonate (calcareous silt from 10-63 µm plus foraminifers from the sand fraction >63 µm) (MAR$_{Foraminifera}$), coarse nannoliths (calcareous silt from 2-10 µm) and fine nannoliths (clay raction <2 µm). The border of 2 µm ESD corresponds to grain diameters of 4-5 µm, because of lowered settling velocities of platy-shaped grains.

MAR for calcareous and non-calcareous components (in the following referred as terrigenous owing to the lack of opal) are calculated by multiplying with linear sedimentation rate (LSR), dry bulk densities (DBD) and the proportion of a component:

(Eq. 3.3) MAR $_{component}$ [g/cm^2/kyr]= LSR [cm/kyr]*DBD [g/cm^3]*proportion of component

The DBDs were deviated from Gamma-Ray Attenuation (GRA) core-logging data, calibrated by discrete, density measurements (ship board gas pycnometer) by linear interpolation at sample depths. The dry bulk densities (DBD) were calculated according to the equation of Curry, Shackleton, Richter et al. (1995) with a water density of 1.035 [g/cm^3]:

(Eq. 3.4) DBD [g/cm^3] = $(\rho_{GRA} - \rho_{water} * \rho_{grain})/(\rho_{grain} - \rho_{water})$.

In the Results and Discussion we report additional data from ODP Site 1085 (Kastanja et al. 2005) and Site 999 (Roth et al., 2000). An orbitally tuned age model is also available for Site 1085 (Westerhold et al., 2005), here the biostratigraphy is based on the timescale of Berggren et al. (1995) and assigns ages which are slightly older. Site 999 biostratigraphic datums (Kameo and Bralower, 2000) mainly base on results from Leg 138 (Raffi and Flores, 1995) (see Tab. 1). Thus calculation of mass accumulation rates and comparison of these sites is advantageous due to the high quality age models within a common biostratigraphic framework.

3.4. Results

3.4.1 Records of late Miocene sediments from Ceará Rise depth transect

Carbonate and coarse fraction content

A first hint at variations in the preservation record is given by carbonate and coarse fraction records. Maximum carbonate contents are in the order of 80% and similar at both sites (see Fig. 3.2). However, two minima (i.e. carbonate content 40-50%) occurred at Site 928 at 9.96 Ma and 9.9 Ma. In the same interval there is a minimum in carbonate content of 60% at Site 926 as well. After 9.9 Ma the carbonate content of Site 928 is approaching that of Site 926 until it reaches the same level at 9.7 - 9.6 Ma. Coarse fraction contents are in the order of 5 - 30% at Site 926 but do not exceed 10% at Site 928, indicating significant loss in the sand fraction between sites.

Carbonate preservation proxy –whole test foraminifers (WTF%)

The preservation as indicated by the WTF is moderate at Site 926 and poor at Site 928 (Fig. 3.2). The WTF is in the range of 20 - 60% (Site 926) with higher fluctuations but it does not exceed 30% at Site 928. Both records show a trend towards better preservation throughout the investigated interval in accordance with an increasing trend in the coarse fraction.

Carbonate preservation proxies - CSmean and CS%

CSmean and CS% were used as dissolution proxies in former studies (Gröger et al., 2003; Frenz et al., 2005; Frenz et al., 2006; Kastanja and Henrich, 2007) and are supposed to show a reverse relation to dissolution intensity. The CSmean covers a range of 13-18 µm at both sites. The general trend follows the WTF (%) but is in case of Site 926 interrupted by a reverse gradient from 10.05 - 9.8 Ma. The CSmean trend is nearly identical with the CS% reaching values between 10% and 25% of the silt distribution. The trends of CSmean and CS% values show no significant differences among sites. However, the overall rising trend in CSmean still indicates better preservation.

carbonate contributor	MAR 926	MAR 928	MAR-difference	% loss (referring to 926 MAR$_{total}$)
MAR $_{nannoliths\ 2-10\ µm}$	0.8	0.61	0.19	11.4
MAR $_{nannoliths\ <\ 2\ µm}$	0.26	0.22	0.04	2.4
MAR $_{foraminifer}$	0.6	0.17	0.43	25.9
MAR $_{total\ carbonate}$	1.66	1.00	0.66	39.8

Tab. 3.1: Averaged mass accumulation rates from 926 and 928 over the interval from 9.8-9.6 Ma. The mass loss of foraminifera is 39.8% of 926 average MAR$_{total\ carbonate}$, while nannoliths size classes account for 11.4% and 2.4% of carbonate-loss, respectively.

Accumulation rates at the Ceará Rise depth transect

In order to demonstrate the impact of dissolution on the different carbonate size classes mass accumulation rates (MAR_{calc}) were calculated for the different carbonate contributors. Assuming that both sites (926 and 928) received the same amount of carbonate and non-carbonate in the time frame studied the difference should reflect the amount of dissolution. The total MAR_{calc} of Site 926 has two minima centered at 9.95 Ma and 9.6 Ma reaching 1.2 $g/cm^2/ky$ and framing a maximum at about 9.7 Ma with up to 2 $g/cm^2/ky$. The minima are accompanied by moderate to poor preservation (30-55% WTF) at 9.95 Ma and 50-65% WTF at 9.6 Ma, respectively. The reduction in MAR_{calc} is evident in the MAR of foraminifera and coarse nannofossils, both showing minima at these times, while the fine carbonate (<2µm) is relatively stable in low ranges of 0.2 - 0.4 $g/cm^2/ky$. The trend in carbonate accumulation does not follow the preservation index at Site 926 in the interval from 9.5 - 9.2 Ma (decreasing MAR_{calc} accompanied by increasing preservation). Hence productivity patterns are assumed to modulate carbonate accumulation. The MAR of terrigenous material ($MAR_{terrigenous}$) is in the order of 0.2 -0.6 g cm^2/ky (926 and 928) with minor fluctuations in the record. The terrigenous fraction is almost exclusively present in the <2µm ESD fraction. For comparison of MAR between sites the interval from 9.6 to about 9.8 Ma seems suitable, because it comprises the nannofossil datums of T *D. hamatus* and T. *D. coalitus* at both sites. The average carbonate content of Site 926 is 83% from 9.8 - 9.6 Ma while at Site 928 the content is 75% on average. The difference in MAR_{carb} reflects a loss of about 40% carbonate from which two thirds can be assigned to foraminifer carbonate and one third to nannofossil carbonate (Tab. 3.1). The loss from nannofossil carbonate indicates a higher susceptibility of coarse nannofossil to dissolution compared to clay sized nannofossil.

Nannofossil event	Site 926 age (kyr)[*1]	Site 999 age (kyr)[*2]	Site 1085 age (kyr)[*3]
T *D. hamatus*	9.65	9.36	9.63
T *C. calyculus*	9.65	9.36	
B *D. hamatus*	10.49	10.39	10.70
B *D. brouweri*	10.69		
B *C. calyculus*	10.70	10.70	
T *C. miopelagicus*	10.94	10.39	
B *C. coalitus*	10.79	10.71	
T. *D. kugleri*	11.56	11.50	11.50
Bc *D. kugleri*	11.88	11.74	
B *D. kugleri*	11.91	12.20	
T *C. nitescens*		12.12	

Tab. 3.2: Nannofossil events at sites 926, 999 and 1085.

3.4.2 Contribution of foraminifer and nannofossil carbonate at Sites 926, 1085 and 982 in the late Miocene

Comparison of studies of different sedimentary and oceanic regimes reveals varying contributions of different size classes to the total carbonate. In all cases carbonate from foraminifera has a subordinate status (see Fig. 3.3). At Site 926 about half of the carbonate (0.5-1 $g/cm^2/ky$) is accumulating in the upper end of nannofossil carbonate besides continuously lower contributions of clay sized nannoliths in the order of 0.25 $g/cm^2/ky$ and a slightly more fluctuating and rising foraminifer carbonate (0.4 up to 0.8 $g/cm^2/ky$).

Compared to Site 926 the contribution of coarse nannofossil carbonate is in the same order at Site 1085 but with significantly higher values of clay sized nannofossils ranging from 0.8 up to 3$g/cm^2/ky$ and lower values of foraminiferal MAR (0.1 - 0.5 $g/cm^2/kyr$). Peak accumulation of total carbonate MAR_{calc} at Site 926 occurred at 9.7 Ma while at Site 1085 the maximum is at about 9.8 Ma. The age models of 926 (Shackelton and Hall, 1997) and 1085 (Westerhold et al., 2005) base on orbital tuning both, however, applied timescales provide slightly different datums (see Tab. 3.2 and Discussion). Another observation concerning carbonate accumulation is a rising proportion of fine calcareous nannofossil in relation to the coarse coccoliths at Sites 927, 982 and 1085 (see Fig. 3.4). The change in this ratio is especially pronounced at Site 1085 where values rapidly double from 1.25 - 2.5 $g/cm^2/kyr$ at 10.15 Ma preceding the increase in MAR_{calc} accumulation (compare Fig. 3.3).
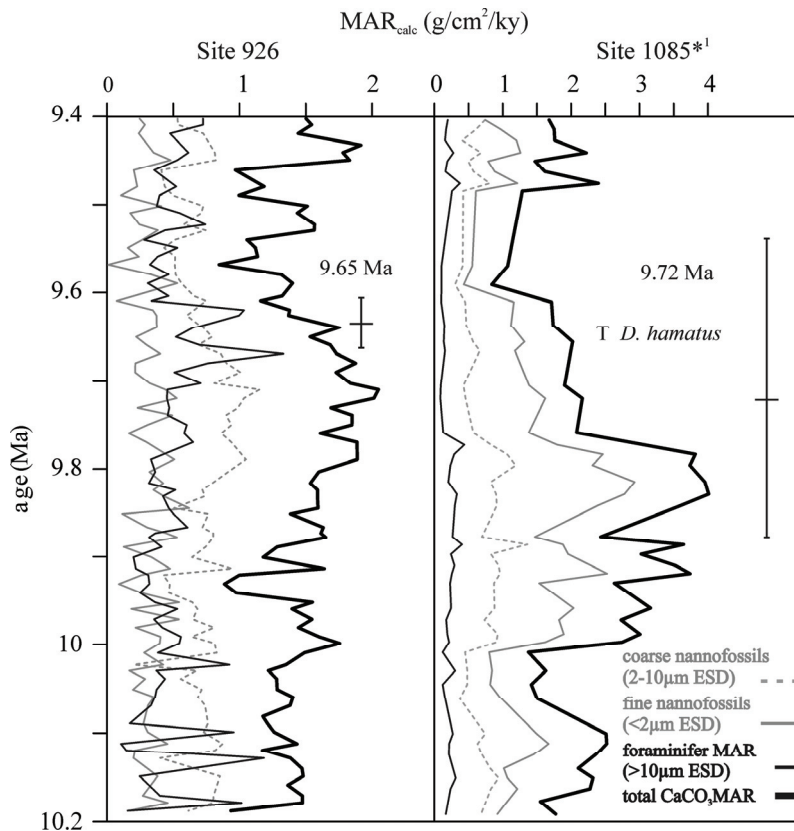
Fig. 3.3: Carbonate mass accumulation rates differentiated by grain size at sites 926 - and Site 1085 – Benguela upwelling (*[1]data from Kastanja et al. 2006): thin black lines-foraminifer carbonate >10 µm, grey lines –nannofossil carbonate <2 µm, dashed grey lines-coarse nannofossils 2-10 µm, thick black line-total carbonate accumulating. The carbonate accumulation at Site 926 is dominated by coarse nannofossils, while at Site 1085 the budget is dominated by clay sized nannoliths. The range of the nannofossil event T *Discoaster hamatus* indicates slightly older ages at Site 1085 compared to Site 926.

3.5. Discussion

We start with testing the reliability of calcareous silt preservation proxies used in previous studies and in this investigation. Then the data from the Ceará Rise depth transect will be assessed and examined for its potential of reconstructing the lysocline during the Miocene. Afterwards the preservation patterns of Ceará Rise and the Caribbean (Site 999) will be discussed in the context of proposed circulation models for the CC-events. Finally, considerations from accumulation rates calculations will be used to estimate the influence of changes in carbonate production patterns trends for the different sites studied.

3.5.1 Consideration of dissolution proxies: comparison of fragmentation index and silt grain size preservation proxies

The difference in preservation between sites 926 and 928 of the depth transect is clearly reflected in the difference between coarse fraction contents and WTF%. The Miocene records of CSmean and CS% lack similarity to WTF% trends and do not appear to reflect preservation differences between
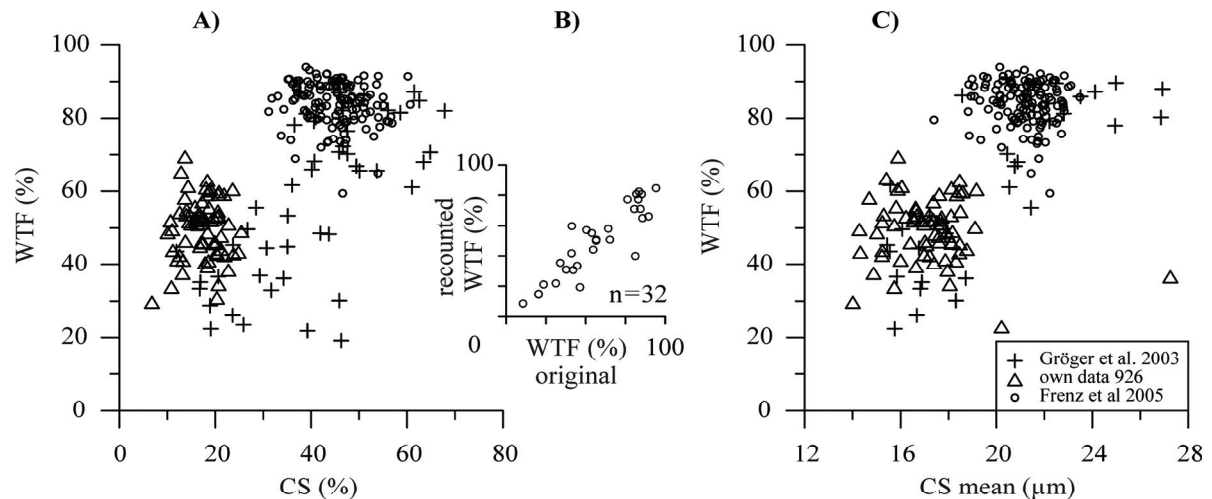

Fig. 3.5: Comparison of calcareous silt preservation proxies and fragmentation index (WTF%) in different time slices from Ceará Rise sites 926 and 927 Miocene (own data - triangles) and Pliocene (Frenz et al., 2005-open circles) and Plio-Pleistocene data (Gröger at al., 2003-crosses). CS% **(A)** and CSmean **(C)** of Pliocene and Miocene time slices do not show a positive correlation to WTF (%). However, for Plio- Pleistocene data (Gröger et al., 2003) both proxies seem to indicate dissolution on a wider range of values reliably. **(B)** The WTF (%) was recounted on sample splits from both studies (n=32, r^2=0,79) indicating good reproducibility among investigators.

sites, thus an evaluation of proxy data seems reasonable. Through recounting of WTF% on samples from the studies of Gröger et al. (2003) und Frenz et al (2005) we can infer good reproducibility among results (r^2=0.79) (Fig. 3.5B) which justifies a comparison. Late Miocene values show a bigger variability in fragmentation than CS% (10-25%- Fig. 3.5 A). The opposite can be seen in the Pliocene record. There the fragmentation is very low and the values of CS% are in the order of 30-60%. As already shown MAR loss of foraminifer exceeds mass loss from coccolith carbonate (Tab. 3.2) among site 926 and 928 in the Miocene. It has been shown that coccoliths are protected through organic coatings (Honjo, 1976) and that they even can be preserved in sediments below CCD level in modern settings (Honjo and Erez, 1978). However, there is sufficient MAR loss in the coarse nannofossil fraction at Site 928 compared to Site 926. Thus progressing dissolution might feed the CS fraction through enrichment of foraminifer fragments and at the same time loss of fragments and coccoliths are

maintaining a balance at a certain stage of dissolution intensity. Also other processes than dissolution could influence the CS distribution and proportion, these could be productivity changes or winnowing of sediments. The Pliocene record, however, offered an offset in size of CSmean between investigated sites 927 and 929 (Frenz et al., 2005) which might be explained by the bigger dissolution difference and strengthens the hypothesis that these proxies are suitable on a wider range of dissolution intensities.

The Miocene record of preservation patterns of the depth transect shows evidence that WTF% is the most feasible proxy in the given range of dissolution intensity, while CSmean and CS% are less appropriate in such low concentrations of coarse silt. It could be argued that WTF% is influenced through productivity of foraminifer species with different susceptibility to dissolution. The investigation of coarse fraction did not give a hint to such argumentation. Therefore, in the following, we will concentrate on differences in the WTF% record and coarse fraction content as an indicator of preservation.

3.5.2 The classical Ceará Rise depth transect and reconstruction of the lysocline during the Miocene

The relative strength of circulation of NADW and AABW controls the modern dissolution horizons at Ceará Rise, causing a relatively strong gradient for foraminiferal fragmentation beginning at 4.3 km (70% WTF) to 4.55 km (<30% WTF) (i.e. foraminiferal lysocline), which is close to the chemical lysocline at 4.6 km (Fig. 3.1). Assuming that values of less than 30% WTF indicate the chemical lysocline, as inferred from core top samples (see Fig. 3.1), Site 928 could be placed within this dissolution horizon or even below in the Miocene. Site 926 shows values that indicate a position between foraminiferal and calcite lysocline. Thus dissolution of foraminifera in the Miocene must have occurred in a much broader zone with the chemical lysocline located at 4000m water depth, elevated by about 600 m and the foraminiferal lysocline at or right below Site 927 (3314 m water depth). These findings are in accordance with results of CCD reconstructions placing the Atlantic CCD of the late Miocene at about 4000 m (Berger, 1972; Van Andel, 1977; Hsü and Wright, 1985; Berger and Wefer, 1996).

3.5.3 Carbonate Crash events Productivity and Circulation hypothesis – a comparison to the Caribbean

The investigated periods are situated at the end of the carbonate crash events in the Caribbean. The proposed model by Roth et al. (2000) calls the influx of corrosive AAIW (see modern northern boundary of AAIW in Fig. 3.1) precursors in response to enhanced Northern Component Water (NCW) production responsible for dissolution events in the Caribbean. This causality would induce opposite preservation conditions in the Caribbean and at Ceará Rise. This is not supported by preservation data from Ceará Rise (see Fig. 6). Comparing the coarse fraction contents, which respond to dissolution more directly in comparison to $CaCO_3$ (wt%) or MAR_{calc}, we find a similarity between Ceará Rise Site 926 and Caribbean Site 999 coarse fraction trends, suggesting dissolution in phase. The coarse fraction records show minima centered at 11.2 Ma and 10.3 Ma and 10.1 Ma. Afterwards both records show an increasing trend in general. The rebound of MAR_{calc} at 10.2 - 10 Ma at Site 999
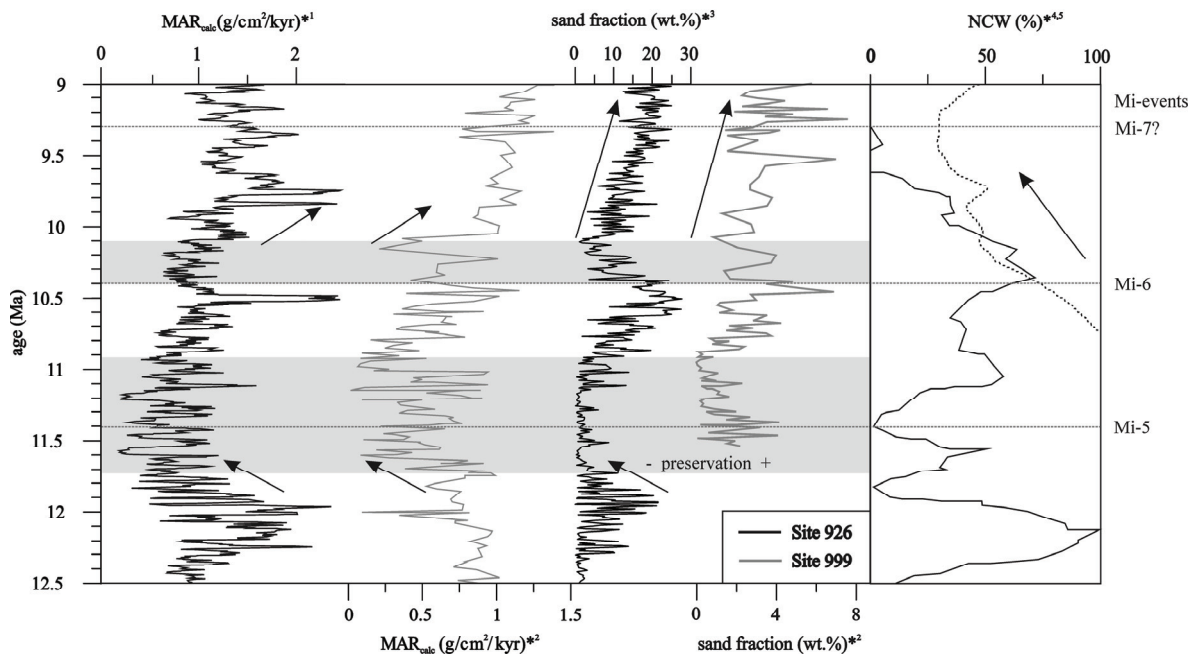
Fig. 3.6: Compiled data from the Caribbean and Ceara Rise. From left to right: Ceara Rise Site 926 – MAR_{calc} (black line)[1] Caribbean Site 999 –MAR_{calc} (grey line)[2],926 -coarse fraction (black line)[3]; NCW (%) estimate (black line[4], dashed line[5]). Sand fraction records of both sites show a similar trend. Some features of NCW (%) reconstructions are similar to sand fraction content trends (here interpreted as dissolution indicator) until about 10Ma. Data from King et al. (1997)[1], Roth et al. (2000)[2], Shackleton and Crowhurst (1997)[3], Wright and Miller (1996)[4], Poore et al. (2006)[5]. Mi-events after Turco (2001) with ages updated to timescale of Berggren et al. (1995).

finds an equivalent increase in MAR_{calc} at 926.

The coarse fraction records of the Caribbean and Ceará Rise generally coincide to NCW reconstructions (see Fig. 3.6).

There is a low in coarse fraction at about 10.4 Ma, a time when also NCW is decreasing, and a maximum in coarse fraction is registered at 10.5 Ma when the NCW% estimate is ranging at 50 - 80%. The similar trends suggest that during times of NCW production the carbonate preservation increases and during times of reduced NCW production the dominance of Southern Component Water (SCW) promoted dissolution. Nevertheless, the increasing preservation since 10.1 Ma is not accompanied by increasing NCW% estimates. The circulation reconstructions even suggest a decreasing trend in the contribution of NCW from the Norwegian Greenland Sea from 10.5 - 9 Ma with a reduced flow, or shut-down of flow, of NCW from 9.7 - 8.8 Ma (Wright et al., 1992; Wright and Miller, 1996; Billups, 2002; Poore et al., 2006). Reconstructions of the relative strength of NCW rely on the difference in benthic $\delta^{13}C$ among ocean basins. Gradients between the Southern ocean and the North Atlantic are still small until about 9 Ma. Therefore small changes produce extreme values in NCW% estimates and its errors. Thus an increase in NCW% between 10 Ma and 9 Ma would still be possible within error estimates. Besides the Norwegian Greenland Sea an alternative source of NCW could have been the Labrador Sea. Thomas and Via (2007) found evidence for the onset of deep convection in the Labrador Sea by results from neodymium isotopes from the Walvis Ridge depth transect. They argue that downwelling started at about 10.6 - 7.3 Ma and that this water mass was denser than today, taking the position of modern lower NADW currently formed in the Norwegian Greenland Sea. This would have caused increasing preservation as well and would fit the scenario at Ceará Rise. The relative strength of the antagonistic water mass to NCW, which is SCW, would possibly be enhanced during times of cooling as represented by Mi-events (see Fig. 3.6) recognized as excursions in $\delta^{18}O$ records of the Mediterranean (Turco et al., 2002). Mi5 e.g. is accompanied by decreased NCW and low coarse fraction contents, which implies the dominance of corrosive SCW. However, Mi events appear problematic as a stratigraphic tool and cannot be correlated among sites (Westerhold et al., 2005; Andersson and Jansen, 2003).

Productivity decreases of coccolithophores were found to be influencing carbonate budgets in the Benguela region (Kastanja et al, 2006; Krammer et al., 2006) in the interval from 10.4 - 10.1 Ma and 9.6 - 9.0 Ma. The interval from 9.7 - 9.5 Ma at Site 926 is also a period of decreasing MAR_{calc} accompanied by increasing preservation. The record of MAR among site 1085 and 926 is quite similar but seems to contain a 100ky difference. This difference is also reflected by the last occurrence datum of D. *hamatus* (see Tab 3.1 and Fig. 3.3). If this date would be synchronous the accumulation patterns of site 1085 and 926 would be in phase. Than it could be speculated that during an upwelling situation in the Benguela region Ceará Rise might have also profited from higher nutrient concentrations advecting northward via the Benguela Current and the South Equatorial Current to the sites (see surface currents Fig. 3.1) (Gardner Hays, 1976). This could imply a shift of the subtropical high pressure zone (Mix and Morey, 1996).

3.5.4 Trends in nannoplankton carbonate sizes and mass accumulation

Sites 1085, 982 and Site 927 ratios of fine and coarse nannofossils show a subtle trend towards fine nannofossils in the investigated interval. These sites display mostly good carbonate preservation. Thus we intend to interpret changing ratios of the groups as due to varying contributions. The observed changes in size of nannoplankton carbonate could be a result of changes in the assemblages towards smaller species or due to changes in size of coccoliths as observed in this interval e. g. in parallel decreases of coccolith size in taxa of *Calcidiscus* (Knappertsbusch, 2000) and *Reticulofenestra* (Young, 1990). However, at Site 1085 the comparison of ESD from sedigraph measurements (Kastanja et al., 2006) and assemblage counts (Krammer et al., 2006) is possible. Here the dominating species of the genus *Reticulofenestra*, underwent an interesting change in abundance and size patterns. At about 10.3-10.2 Ma the accumulation of large species (*R. pseudoumbilicus* large (>7µm) and medium (5-7µm)) declined followed by a period of increasing accumulation of the small species (*R. minuta* and *R. haqii*, <5µm) from 10.2-10 Ma (Krammer et al., 2006). The assemblage change seems to be well reflected by the ratios of fine to coarse nannofossil from grain size measurements of Kastanja et al. (2006) (Fig. 3.3). Interestingly, the change in the ratio appears before the dramatic increase in MAR$_{calc}$ at Site 1085 (compare Fig. 3.3 and 3.4). This could suggest a time of adaption leading to a period of enhanced nannofossil productivity in combination with an upwelling situation.

3.6. Conclusions

The investigation of preservation proxies, mass accumulation rates and calcareous grain sizes from the investigated Atlantic sites and comparison to sites 999 in the Caribbean and 1085 in the Benguela upwelling region led to the following conclusions:

1. The Ceará Rise depth transect shows a shallow foraminiferal lysocline at about depth of Site 927 (~3300m) and a calcite lysocline at 4000m according to foraminiferal preservation data in the late Miocene. Differences in MAR$_{calc}$ of foraminifera and coccoliths among sites indicate mass losses of two thirds in the foraminifer carbonate and one third in the coccoliths with pronounced mass loss in the coarse nannofossil fraction.

2. A classical fragmentation index shows the proposed differences in preservation state while the calcareous silt preservation proxies partly failed to reproduce the depth dependant dissolution at the transect.

3. The carbonate accumulation patterns and coarse fraction trends at Ceará Rise and the Caribbean are in phase and do correspond to proposed NCW% estimates until 10.1 Ma implicating better preservation during enhanced NCW formation. Productivity at least partly influenced changes in the MAR$_{calc}$ at Ceará Rise from 9.5 to 9.2 Ma. The carbonate preservation had been increasing in the Caribbean and at Ceará Rise since ~10.1 Ma.

4. Increasing contribution of fine nannofossil carbonate is evident at sites 927, 982 and 1085 and the ratio of fine to coarse nannofossils decreases from south to north among sites. The change in the ratio of fine to coarse nannofossil carbonate at Site 1085 can probably be related to a coccolith size change in the dominating genus *Reticulofenestra*, however, remains elusive at the other sites.

Acknowledgement

Chapter 4 - Perturbations in the marine Carbonate System during the Miocene: The middle to late Miocene Carbonate Crash- A critical review

Authors: Inga Preiß-Daimler, Rüdiger Henrich, Timo Köhnsen

Abstract

This paper intends to review and assess the middle to late Miocene Carbonate Crash events (CC-events) in the low to mid latitudes of the Pacific, Indian, Caribbean and Atlantic Ocean as part of the global paleoceanographic reorganisations in the Miocene between 12 and 9 Ma with emphasis on preservation records (semi-qualitative estimates on nannofossil and foraminifera, coarse fraction records, fragmentation index, benthos/plankton ratios) and their relation to mass accumulation rates. In the Eastern Pacific the accumulation changes in carbonate and opal offshore California, off Peru and in the Eastern Equatorial Pacific probably reflect an El-Niño-like state of low productivity which marks the beginning of the CC-crash (11.5 Ma) followed by decreased preservation and influx of corrosive bottom waters (10.3 to 10.1 Ma) at about the same time when carbonate preservation in the Atlantic is considerably increasing suggesting basin-to-basin fractionation as the controlling factor.The low latitude Indian Ocean, the Pacific and the Caribbean are all characterised by a similar timing of preservation increase starting at about 9.6 to 9.4 Ma, while the carbonate accumulation rates of these regions show drastic changes with different timing of events. The Atlantic preservation pattern shows an earlier increase starting at 11.5 and increasing from 10.1 Ma on. The shallow Indian Ocean is characterised by low carbonate accumulation throughout and increasing preservation since 9.4 Ma (Mascarene plateau). At the same time the preservation in the Caribbean is increasing, succeeding the increase in carbonate accumulation at 10 Ma. In contrast to postulated preservation anticorellations of the Caribbean and Atlantic records are rather similar. The carbonate preservation in the Caribbean was enhanced through North Atlantic deep water formation. The shoaling of the Central American Isthmus (CAS) might have helped to enhance preservation after 9.4 Ma. Lowered productivity of nannoplankton in the Atlantic (9.4 Ma at Benguela upwelling Site 1085 and Ceará Rise Site 926) additionally contributed to low mass accumulation rates during the late CC-interval.

4.1. Introduction

The Miocene CC-events include several sharp drops in carbonate concentration and/or accumulation occurring in various parts of the oceans, e.g. equatorial Pacific and Indian Ocean (Lyle et al., 1995; Farrell et al., 1995; Peterson et al., 1992), the Caribbean Sea (Roth et al., 2000), the equatorial Atlantic

(King et al., 1997; Murray and Peterson, 1997), the South Atlantic (Diester-Haass et al., 2004; Krammer et al. 2006; Kastanja et al., 2007) and Southern Ocean (Diester-Haass and Nees, 2004) at the middle to late Miocene (12 - 9 Ma). Hence, CC-events obviously are a phenomenon on a global scale. However, timing, duration and number of the different drop events are not consistent, and possible causes are discussed controversially. Postulations of potential mechanisms include changes in deep water circulation, shoaling of the CCD, shifts in shallow to deep carbonate fractionation, terrigenous dilution, productivity changes and evolutionary trends and adaptations of the main calcareous plankton groups.

During the middle to late Miocene major reorganisations on land and in the oceans induced prominent shifts in the global climate system. This includes important changes of plate tectonic settings, e.g. the closure of the Indonesian Seaway (IS) (Lee and Lawer, 1995) and uplift of the Central American Seaway (CAS- Marshall, 1988; Collins et al., 1996; Haug and Tiedemann, 1998). The subsidence of the Greenland-Scotland Ridge is associated with secular variations in its bathymetry induced by variations in temperature and buoyancy of the Iceland mantle plume (Wright and Miller, 1996; Poore et al., 2006), opening and widening of the Frame Strait (Thiede and Myhre, 1996), as well as the uplift of high mountain ranges, in particular the Himalaya and Tibet Plateau as well as the Andes (Benjamin et al., 1987). This, in turn, strongly influenced continental weathering and induced the formation of new huge fluvial drainage systems like the Amazon (Hoorn et al., 1995). During the Miocene strong changes in high-latitude climates are observed. A gradual warming during the early to middle Miocene (24 Ma to 15 Ma) is followed by rapid cooling during the middle Miocene. Contemporaneously the ice shield on Antarctica expanded considerably (Warnke et al., 1992; Flower and Kennett, 1994) and the first small-dimensioned ice sheets were initiated in the Northern Hemisphere (Larsen et al., 1994; Fronval and Jansen, 1996; Thiede et al., 1998).

The asymmetric cooling resulted in more vigorous trade winds in the southern hemisphere and displacement of the Inter Tropical Convergence Zone (ITCZ) to the north (Hovan, 1994; Rea, 1994). The global climate cooled stepwise as e.g. recorded in benthic foraminiferal $\delta^{18}O$ values. The Mi-events (Miller et al., 1987; Zachos et al., 2001; Westerhold et al., 2005) recording increases in ice volume and/or deep water cooling, however these are not always traceable among sites (Andersson and Jansen, 2005). This was connected with major reorganisations of surface and deep water circulation, in particular, the initiation of modern low latitude upwelling systems in the Atlantic (Diester-Haass et al., 2004; Krammer et al., 2006; Kastanja et al., 2006) and Pacific (Lyle et al., 2000). Wright et al. (1992) and Wright and Miller (1996) place the initiation of North Component Water (NCW), a precursor to the modern North Atlantic Deep Water (NADW) and a primary component of deep-water convection, in the late early Miocene. More recently, Poore et al. (2006) stated that based on composite Atlantic and Pacific and Southern Ocean $\delta^{13}C$ benthic foraminifer records there is no

evidence of significant NCW overflow over the Greenland-Scotland Ridge before 12 Ma, which is consistent with evidence from Cd/Ca ratios (Delaney, 1990).

The change in circulation mode also induced a shift in nutrient distribution which is e.g. manifested in the middle Miocene silica switch which shifts the formation of opal dominated sediments from the North Atlantic to the North Pacific between 15 and 10 Ma (Keller and Barron, 1985; Cortese et al. 2004). The response of planktonic organisms in these changing oceanic environments is poorly understood. Schmidt et al. (2006) found a shift in size of mid to low latitude foraminifera assemblages through the Cenozoic with extreme development towards bigger sizes in the late Miocene. Also coccolithophores are suspected to react to oceanographic revolutions, showing extraordinary size trends in the late Miocene (*Reticulofenestra*, Young et al., 1990; *Calcidicus leptoporus*,
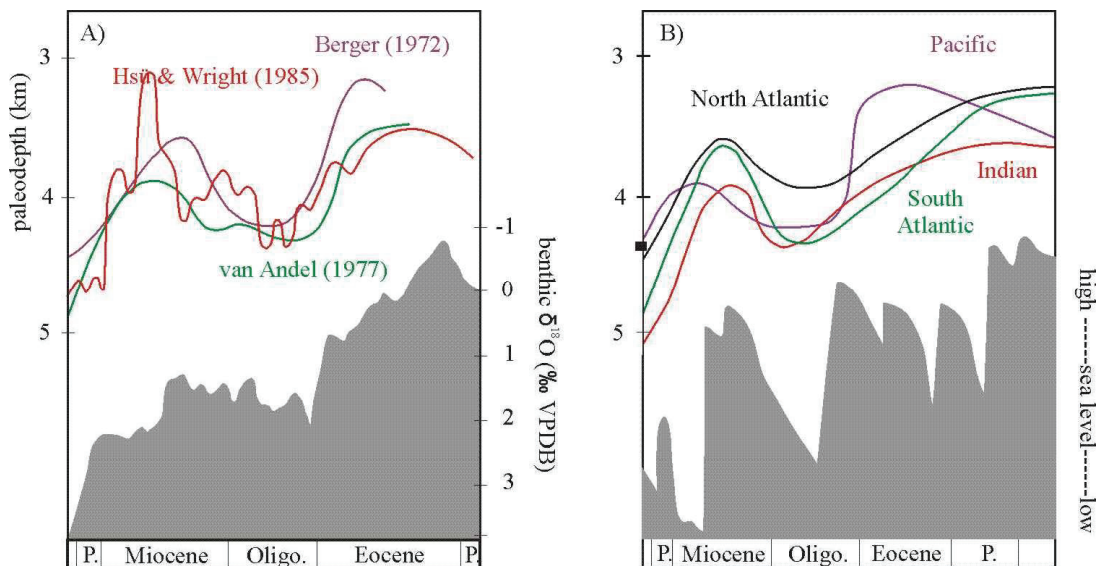
Fig. 4.1. A) CCD reconstructions of the South Atlantic from different authors. B) Compiled CCD reconstructions for the mains oceans after Wefer and Berger (1996).

Knappertsbusch, 2000).

Carbonate accumulation patterns are crucial to understand circulation patterns and climate change. They are supposed to reflect a balance of productivity and preservation on the sea floor. Global budgets should display a steady state of riverine influx and burial rate of $CaCO_3$ (Broecker and Peng, 1987). Because of the similarity of eustatic sea level changes and fluctuations of the calcite-compensation depth (CCD - Bramlette,1976) over the path of the Cenozoic, changes in CCD were associated with shelf-to-basin fractionation. The underlying assumption is that during high sea level, carbonate accumulation would preferably take place on shelves rather than the open ocean (Berger, 1970).In order to trace CCD changes classical work approaches use certain wt%-carbonate values or MAR_{CaCO_3}-values for defining a CCD boundary. Roth et al. (2000) uses the $0.1 g/cm^2/ky$ carbonate

flux to reconstruct CCD changes in the deep Pacific throughout the middle to late Miocene CC-events. Wefer and Berger (1996) or van Andel (1979) used the 20 wt.%-CaCO$_3$ as the level of the CCD (see Fig. 4.1 A). A closer look at preservation proxies might reveal discrepancies between certain value CCD reconstructions and their relation to carbonate productivity levels or dissolution intensities. Therefore, in this study we want to review the carbonate crash events from ODP cores of low to mid latitudes with emphasis on available carbonate preservation proxy data. The review is supplemented by own data contribution of material from ODP Site 1237 in the SE-Pacific offshore Peru.

4.2. Strategies to detect carbonate crash mechanisms: discrimination between dilution, productivity and dissolution

Due to the technical advance of coring deep ocean floor sediments with hydraulic piston corers e.g. during legs of the Ocean drilling program (ODP), there is the possibility to investigate a huge archive of well dated continuous sedimentary successions spanning the middle to late Miocene. A first look at a pelagic carbonate rich sedimentary sequence can give a hint to carbonate variations expressed as cyclic gradational variations in sediment color, where darker color bands represent carbonate decreases. This method is failing in sediments with very high carbonate contents, where even severe dissolution or productivity decreases do not produce low carbonate contents, hence no color bands. A strong dilution signal e.g. through a change in the ratio of opal to carbonate sedimentation or terrigenous input could then produce low carbonate contents. Besides the observation of carbonate contents which can be lowered due to dilution, dissolution, decreased productivity or changing ratio of opal/calcite in the rain rate, mass accumulation rates (MAR) give a measure of the component burial per surface and time and are calculated as follows:

(Eq. 4.1) MARcomponent (g/cm^2 kyr)= p * LSR(cm/kyr) * DBD (g/cm^3)

  p=roportion of the component
  LSR=linear sedimentation rate
  DBD=dry bulk density

In ODP records often GRAPE data (Gamma ray attenuation porosity evaluator) and discrete density measurements are used to calculate DBDs. Routinely the MAR are reported for 1 Ma increments accounting for low resolution age models. Additionally, values from composite sections have to be corrected by a growth factor to account for core expansions and disturbances (e.g. Hagelberg et al. 1992).

MARs can help to find an answer whether the observed change is due to dilution or productivity/dissolution changes. The quality of this data is depending on the quality of the age model and the ablated sedimentation rates. The highest resolution is gained by orbitally tuned age models.

This method interprets the sediment composition as sedimentary response to orbital cycles and is based on high resolution data of density, color and magnetic susceptibility or geochemical measurements in the framework of classical magneto- and biostratigraphy. However, sedimentation rates might be handled with care if there are special burial circumstances involved as e.g. the rapid sedimentation of diatom mats which are laminated sediments that can form thick and spatial widespread deposits (Kemp et al., 1995). These sediments are rather interpreted as results of complex surface water processes than deep water dissolution phases. Additionally, redepositional events like e.g. turbidites and slumps or phases of no deposition (hiatus) disturb the premise of slow and steady pelagic sedimentation, supposed to form an even veneer on the ocean floor topography. Under discussion is also the process of sediment focusing and lateral advection. Attempts to correct for this are e.g. the correction of MAR by ^{230}Th normalisation (Bacon, 1984; Francois, 2004) or assuming a constant rain rate from extra-terrestrial ^{3}He (Marcantonio et al., 1996; Kienast et al., 2007).

However, MARs are the key data to observe CC-events. If decreasing accumulation rates of carbonate (MAR$_{calc}$) are accompanied by e.g. steady and low terrigenous accumulation dilution can be excluded as a main factor. What remains then is the question, whether MAR$_{calc}$ minima are due to lowered productivity or dissolution. Depending on the (paleo-) water depth of the observation one will make a first hypothesis based on the fact that at greater depth calcite will be dissolved more easily and at shallower depth productivity will be the most important factor. Lowered carbonate supply tends to increase the possibility of dissolution as well and will be balanced by a rising CCD. However, especially under high productivity conditions dissolution above the lysocline contributes significantly to overall dissolution (Archer, 1991). Here the rain ratio of organic carbon to $CaCO_3$ is an indicator for high productivity. Elevated proportions of organic carbon are often associated with high rates of opal accumulating (Treguer et al., 1995). The accumulation of opal in the form of diatom frustules might favour the preservation of carbonates. No evidence for enhanced dissolution of foraminifera was observed within diatom mats (Pearce et al., 1995) which might be attributed to the fast settling velocities and/or the strong meshwork that suppresses benthic activity. The release of silica in pore waters might as well act against carbonate dissolution (Wise, 1977). A higher proportion of benthic organisms can also point to higher productivity of surface waters, but might be an evidence of dissolution as well (e.g. Dittert et al., 1999; Diester-Haass et al., 2002). In many cases it is reasonable to investigate multiple proxies as e.g sand content and the classical planktonic foraminiferal fragmentation:

(Eq. 4.2) fragmentation % = #fragments /(# whole tests + # fragments) * 100

investigated on splits of the sand fraction (Peterson and Prell, 1985, Conan et al., 2002). The validity of these methods is restricted to dissolution above the CCD. Nannofossil based dissolution indices might help to find clues for dissolution intensities, despite the high potential of ecological control on

abundance patterns. The application of these preservation proxies might be even better under strong dissolution conditions and for application to closely spaced intersite comparison e.g. at a depth transect (Gibbs et al., 2004). The absence of foraminifera or a strongly reduced taphonomic assemblage in dissolved sediments often inhibits the investigation and/or interpretation of stable isotopes on benthos and plantktonic faunas which are standard proxies for circulation, productivity and climate, however here also the less well understood nannofossils might fill the gap in reflection of surface water processes in future research.

The investigations of MAR_{calc} at depth transects is especially meaningful in CCD reconstructions because site to site differences reveal the loss of carbonate from one site to another and other processes influencing carbonate MAR_{calc} besides dissolution. In case of Walvis Ridge depth transect e.g. winnowing, reworking and down-slope re-suspension seem to alter wt% of carbonate even in that way to produce reversed gradients (Zachos et al., 2004). Accordingly higher carbonate contents are found in the deeper site in comparison to shallower ones. Another example for a depressed carbonate depth gradient is the Ontong Java plateau (Berger et al., 1993).

For the following comparison we have chosen several cores from low to mid latitudes of the world's main ocean representing key locations of the CC-events (see Tab. 4.1 and Fig. 4.2). The MAR were recalculated following the above described method. Carbonate and coarse fraction data from ODP Site 1237 in the SE-Pacific represents the only new data on the middle to late Miocene. Component analysis on these samples was applied to representative splits of the $> 63\mu m$ fraction with at least 300 particles counted. The fragmentation index here is the ratio of whole tests (shells comprising at least
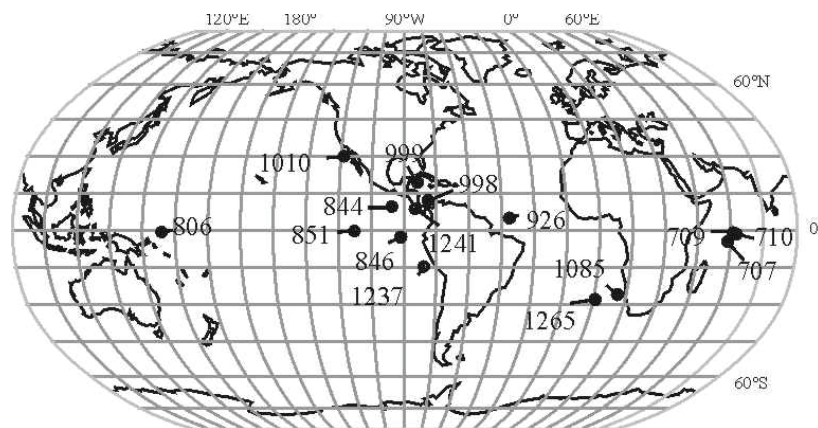
Fig. 4.2: Locations of ODP sites of CC-events reviewed. New data from Site 1237 in the SE- Pacific.

half of a whole planktonic foraminifera test) divided by the sum of whole tests and fragments.

The colour bars in the figures represent preservation data of planktonic foraminifera from the Site reports in the Initial reports of the ODP volumes.

The framework of comparison of different data sets and calculations of MAR_{calc} is given by the age model.

4.3 Age control

The comparison of the cores from the eastern Pacific (Leg 138, Leg 202), Atlantic Leg 154 and Leg 1085 and the Caribbean Leg 165 is advantageous because they are based on the same biostratigraphy using bioevents dated by Flores and Raffi (1995) from Leg 138. Age control of Leg 138 records is provided by biostratigraphy over the whole record, astronomical tuning of GRAPE density down to 10 Ma and magnetostratigraphy in the interval younger than 13.25 Ma (Shackleton et al., 1995). The astronomical tuning of Ceará Rise Site 926 based on correlation of magnetic susceptibility maxima to northern hemisphere insolation minima. The orbital solution of records and was compared to high resolution biostratigraphy from 5 to 14 Ma (Backmann and Raffi, 1997). Age models from Indian Ocean Leg 115 were updated to the common standard of Berggren et al. (1995) timescale. An updated age model was also used for Site 806 from the Ontong Java Plateau (Nathan and Leckie, 2009). Age models of the eastern Pacific Site 1010 along Baja California (Forniaciari, 2000) and Site 1241 in the EEP did not provide magnetostratigraphic control, however displayed the low latitude standard zonation of calcareous nannofossil. At Site 1237 off Peru magnetostratigraphy could be applied giving excellent age control with all chrons and subchrons according to GPTS between 8.4 Ma and 12.4 Ma (Chron 4r and Chron 5Ar, Cande and Kent, 1995). This scale is in good accordance with calcareous nannofossil datums.

Region	ODP-Site	Depth	Data source[X] –(^nannofossil preservation, *foraminifer preservation,'coarse fraction)	Data source –(°CaCO3-MAR/*Opal.-MAR)	Age model/biostratigraphy – source (*updated to Berggren et al. 1995)
East Pacific					
equatorial.	844	3415	^ Farrell et al. (1995)[1];" Vincent & Tourmarkine (1995)[2]	°* Farrell et al. (1995)[1]	Shackleton et al. (1995); Raffi &Flores (1995)
equatorial.	846	3296	"	"	"
equatorial.	850	3786	"	"	"
equatorial.	1241	2027	*Mix et al. (2003)[3]	°* Mix et al. (2003)[3] inc. non-	Mix et al. (2003)
California	1010	3464	*Lyle et al. (1997)[4]	°Lyle et al. (2003)[5],*Janecek	Fornaciari (2000)
Peru	1237	3212	*'This study	°This study	Mix et al.. (2003)
West Pacific					
	806	2521	*Nathan & Leckie (2009)[7]	°Berger et al. (1991)[8]	Nathan & Leckie (2009)
Atlantic					
equatorial.	926	3598	Preiß-Daimler & Henrich - subm.;' Shackleton & Crowhurst (1997)[10]	Preiß-Daimler & Henrich- subm.; °King et al.. (1997)[11]	Shackleton & Crowhurst (1997);Backmann &Raffi (1997)
Benguela upwelling	1085	1713	Benthos/Plankton –ratio Diester-Haass et al. (2004)[12]	°Kastanja et al. (2006)[13]	Westerhold et al. (2005)
Caribbean					
	999	2828	'Roth et al.. (2000)[13], ^Kameo &Sato (2000)[14], ε Nd(t)-Newkirk and Martin (2009)[15]	°Roth et al.. (2000)[13]	Kameo & Bralower (2000)
	998	3180	"	"	"
Indian Ocean					
Mascarene	707	1541	-	°Backmann et al. (1988)[17]	Rio et al. (1990)
Mascarene	709	3038	'Vincent & Toumarkine (1990)[16]	"	"
Mascarene	710	3812	"	"	"

Tab. 4.1: List of locations, core data sources and age model sources.

4.4 The Carbonate Crash events: Timing and mechanisms

In the following chapter compiled data of MAR as well as preservation proxies during the CC-interval, used methods and theories about trigger mechanisms will be summarized for each ocean basin. Existing theories concerning the CC-events in the deep (>3000m water depth) EEP from Leg 138 will be complemented by regional examples in order to relate NE and SE Pacific records to a picture of the entire Eastern Pacific. Results from Leg 202 deliver insight into intermediate water processes in the EEP (Site 1241) and own results of a deep water record off Peru (Site 1237) reflect processes in the SE Pacific. Additionally, sedimentary processes from the upwelling region along the California margin (Leg 167- Site 1010) provide valuable information about paleoceanography in the NE Pacific. Especially proxy data from the Caribbean (Sites 998,999) as a key area of the CC-events will be critically reviewed and reinterpreted. The Atlantic is represented by western equatorial Ceará Rise (Site 926) and Benguela upwelling (Site 1085). Sites of the depth transect of the Mascarene plateau (707,709,710) stand here exemplarily for the low latitude Indian Ocean.

The emphasis in our reviewing observations is on the available estimates of preservation of calcareous fossils along with MAR of the main biogenic components (opal and carbonate). The data and sources are listed in Tab. 4.1 (numbers in Figs. 4.3 to 4.7 refer to Tab. 4.1).

4.4.1 The Pacific carbonate crash events

The modern equatorial Pacific surface productivity is characterised by an asymmetry between the east and the west. The Western Pacific Warm water pool (WPWP) forms a stable water mass with a deep thermocline well recorded in isotopes and foraminiferal fauna (Ravelo et al., 2006). Here carbonate accumulation is moderate while in the East Equatorial Pacific (EEP) accumulation of carbonates is influenced by upwelling intensity and an asymmetric lysocline, which is generally shallow in the east and a deep lysocline east of the East Pacific Ridge (EPR). Upwelling waters in the EEP are sourced from the Equatorial Undercurrent (EUC), which has its orign in the west Pacific and combines waters of both hemispheres (e.g. Dugdale et al., 2002; Goodmann et al., 2006). The eastern boundary currents (Humboldt and California current) form the prerequisite for coastal upwelling along the western boundaries of the two Americas. Oceanic productivity is furthermore distinctly influenced by the ENSO phenomenon (El Niño -Southern Oscillation). A strong El Niño event leads to the breakdown of plankton productivity of upwelling regions in the eastern Pacific. These modern patterns might have their roots in the Miocene influenced through gateway configurations. The emergence of the Indonesian seaway (IS) blocks the westward flow of warm waters to the Indian Ocean and allows warm waters to pile up to form the WPWP. More generally speaking the strength of circulation is driven be the trade winds and boundary currents along the continents, a slackening of these currents would tend to reduce the amount of upwelling waters and result in a deeper thermocline in the EP. Thus the questions concerning the Miocene carbonate accumulation in the equatorial Pacific are: Can

we find the oceanographic patterns compared to today's features? How relevant are these surface processes in comparison to deep water circulation changes?

The Eastern Equatorial Pacific

One of the first studies reporting unusually low carbonate contents during the Late Miocene (i.e. between 9.6 and 9.2 Ma) is by Vincent (1981) on the section of DSDP Site 310 on the Hess Rise and in the northern central Pacific. ODP Leg 138 recovered excellent cores from the EEP. Changes in MAR_{calc} first followed a stepwise decline in various sites of the EEP from 11.2 to 9.5 Ma, with pronounced changes in the Guatemala basin (see Fig. 4.3 Site 844) and Peru basin (Fig. 4.3 Site 846) east of the EPR. This interval is as well characterized by shifts in dominance of carbonate vs. opal in sediments indicating changing surface water ecology as well as deep circulation. At 9.5 Ma MAR_{calc} dropped to zero reaching the carbonate crash nadir at 9.5 Ma. Evidence from nannofossil preservation (Farrell et al., 1995) and MAR_{calc} point to a rapid rise of the local CCD of about 800 m to water depth of about 3400-3200 m at 10 Ma (Lyle et al 1995). After this brief dissolution event the carbonate accumulation did not recover but the preservation as indicated by nannofossil and foraminifer preservation did from 8.9 Ma on (Farrell et al., 1995). West of the EPR in the Central Pacific basin the MAR_{calc} also shows minima centered at 9.5 Ma. Here changes are less clear influenced through dissolution indicated by better nannofossil preservation and no obvious change to higher opal/carbonate ratios like in the Guatemala basin.

Another characteristic feature of sediments is the occurrence of laminated diatom mat deposits in the near equator sites (sites 849-851) of the Central Pacific basin at the beginning and at the end of the CC (see Fig. 4.3 as indicated by stars). These sediments probably were formed as rapid fallouts of equatorial frontal zones developed during La Niña-like events (Kemp et al., 1995). The compact structure of diatom mats furthermore prohibited bioturbation and thus laminae appear well preserved. However the diatom abundance was reduced during the crash nadir and radiolaria dominated the opal instead.

Lyle et al. (1995) concluded that the restriction of carbonate saturated deep water flow from the Atlantic to the Pacific through the emerging CAS would trigger the dissolution in the EEP. As an alternative scenario deep water formation in the North Atlantic would result in basin to basin fractionation, and displacement of corrosive SCW towards the Pacific in turn triggering enhanced dissolution in the deep EEP. However the comparing of timing of these events did not lead to a consistent picture (Farrell et al., 1995) concerning NADW production.
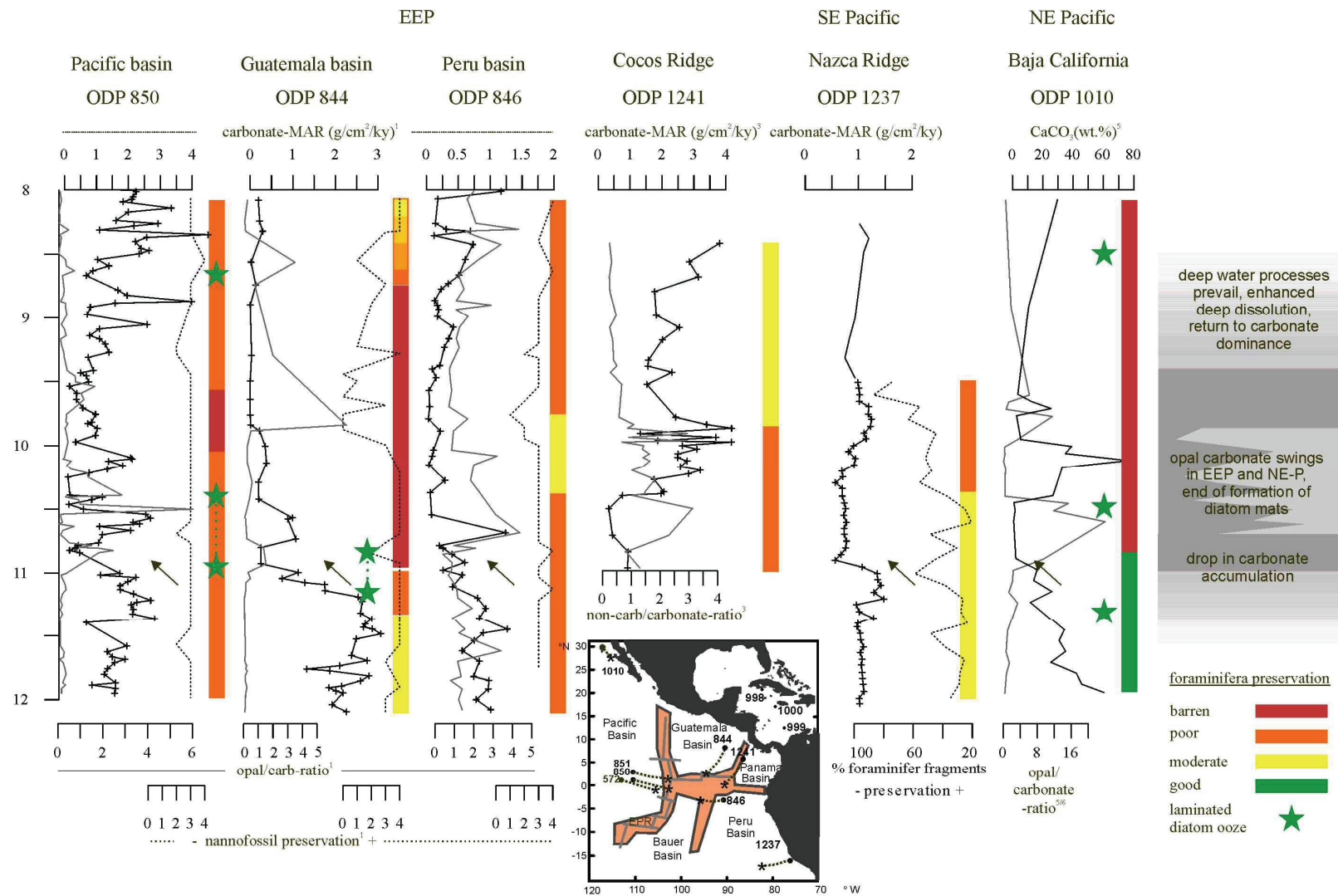
Fig. 4.3: The phases of the Eastern Pacific CC-events can be roughly divided into three phases. First a drop in carbonate accumulation at 11.5 to 10.8 Ma. Afterwards opal and carbonate accumulate in alternating phases ("swings") and the deep water signal of dissolution sets in at about 10.3 to 10.Ma. For data reference see Tab. 4.1.

The West equatorial Pacific (Site 806)

The restriction of the flow of waters through the IS and the CAS is believed to have had a major impact on the circulation system and thus the distribution of temperature and nutrients in surface and near surface waters in the Pacific. The development of the West Pacific Warm Pool (WPWP), the Equatorial Countercurrent system and alternating hydrographic features similar to modern El Niño and La Niña patterns are placed within the middle to late Miocene (Kennett et al., 1985; Kemp, 1995; Li et al., 2006; Nathan and Leckie, 2009; Jiang et al., 2007). These models stress the productivity component in the highly dynamic equatorial system and represent an accomplishment to the models solely based on circulation-dissolution explanations.

Li et al. (2006) place the establishment of the WPWP in the South China Sea at 10 Ma as evidenced by increased abundance of mixed layer foraminifera and the decline of deeper living foraminifera i.e. the extinction of *Globoquadrina dehiscens*. Similar results in the equatorial region place the initiation of the WPWP at 8 Ma (Kennett et al., 1985).

Nathan and Leckie (2009) found evidence for the development of a Proto-WPWP at 11.6 to 9.6 Ma based on foraminifer faunal analyses and stable isotope gradients of mixed layer and thermocline species at Site 806 (2520 m water depth) on the Ontong Java Plateau (see Fig. 4.4).

Thus the establishment of a modern like circulation pattern influenced by the closure of the IS and the arising possibility of piling up warm waters in the west Pacific could have occurred that early. The authors state that the equatorial undercurrent would have been strengthened by the evolution of a WPWP like today bringing nutrient enriched subsurface waters to the EEP. If the carbonate crash events in the EEP were related to the emergence of this circulation pattern one would find El Niño condition during a weak WPWP and better stratification in the west pacific surface waters. Due to their model the dissolution of carbonates through corrosive deep waters during the carbonate crash event was delayed in the early phase (at about 11.5 Ma) through high productivity in a La Niña like phase in the EEP, which would explain the offset in CC-events between the Caribbean and Pacific.

With regard to this hypothesis and a change from La Niña to El Niño conditions at about 10 to 9 Ma the question arises if these shifts are imprinted in the productivity along eastern boundary currents in other regions of the Eastern Pacific as found during modern El Niño events (e.g. Chavez et al., 2002; Takesue et al., 2004). In the following these questions will be addressed to cores from the California upwelling and from the SE Pacific.

The California upwelling (Site 1010)

The California upwelling system was investigated during Leg 167. Sediments of Site 1010 (offshore) and 1021 (coastal upwelling) recorded a major drop in opal contents starting at 11.5 Ma while at the same time MAR_{calc} dropped (Lyle et al., 2000). Despite the probable beginning of NADW circulation which would have enhanced silica availability in general in the Pacific, certain intervals favoured

offshore and others coastal sedimentation of opal. The coastal to offshore opal fractionation was enhanced through low temperature gradients among latitudes damping the strength of the California current accompanied by a deep nutricline (Cortese et al., 2004). According to this mechanism, the time interval from 12-11.5 Ma can be interpreted in terms of increased strength in current intensity favouring offshore opal sedimentation, while a slackening of the currents occurred from 11.5 to 10 Ma inducing coastal fractionation. This trend is associated with a general decreasing trend in opal concentration reaching its minimum at 10 Ma at both sites (shown for Site 1010, see Fig. 4.3). Interestingly, here as well laminated diatom rich sediments appear in similar intervals in comparison to the EEP (see Fig. 4.3). The preservation of planktonic foraminifera is poor except an interval below 148 mbsf (approximately 11.5 Ma), where they appear well preserved within diatom rich sediments and species composition indicates an upwelling sequence (Lyle et al., 1997). The enhanced preservation of foraminifera is probably a result of rapid burial through particle loading. These results strengthen the hypothesis of a general decreasing productivity trend as it can be associated with an El Niño phase influencing both opal and MAR_{calc} at Site 1010 at the same time when carbonate
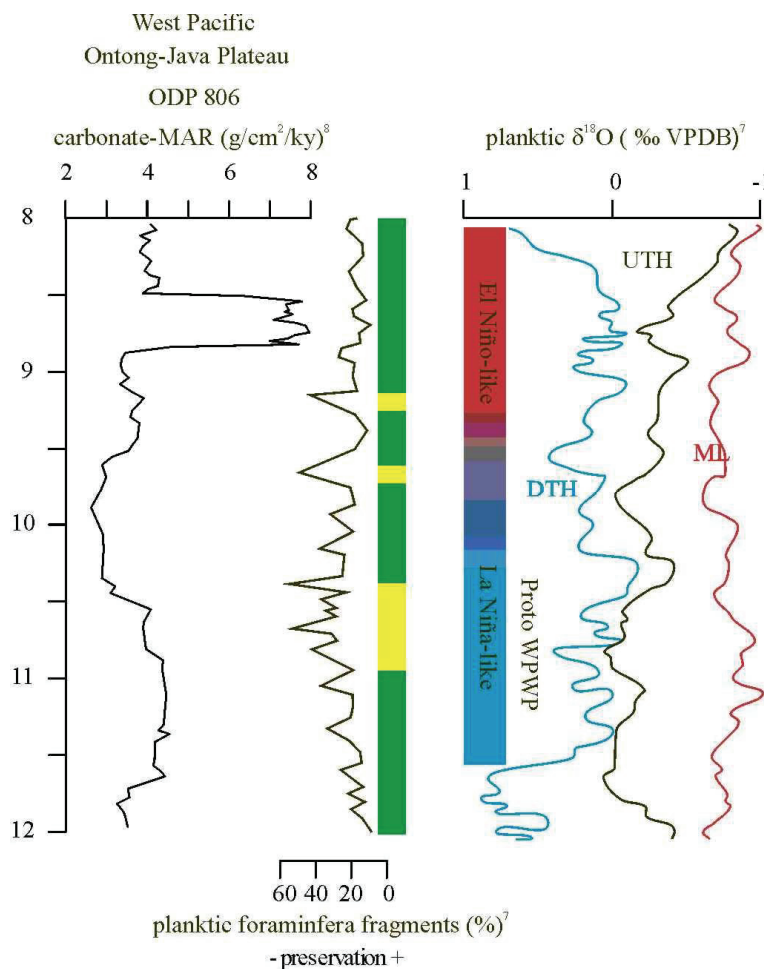

Fig. 4.4: Data after Nathan and Leckie (2009) showing the Ontong-Java plateau Site 806. Oxygen stable isotope records of deep dwelling foraminifera (DTH), a foraminifera record from the upper thermocline level (UTH) and a mixed layer record (ML). The convergence of DTH and UTH representatives is interpreted as the first occurrence of a stable WPWP. The planktonic foraminifera preservation is preferably good, with lower values at about 10.5 to 9.5 Ma.

accumulation dropped in the EEP.

The intermediate EEP (Site 1241) and the South East Pacific (Site 1237)

Leg 202 offers two sites to test some hypothesis concerning the influence of deep and surface water processes during the CC-events in the EP. Site 1241 is positioned at 2040 m water depth above the lysocline on the Coccos Ridge in the EEP and displays the shallowest sedimentary record in comparison to the deep sites of Leg 138 (all deeper than 3000m water depth). The calcareous microfossil tests show evidence of strong dissolution during the oldest part of recovered sediments (the period from 11-10 Ma), when opal and TOC concentrations were relatively high as well as MAR$_{calc}$ (see Fig. 4.3). After 10 Ma tests of foraminifera and nannofossil show moderate preservation associated with increasing carbonate content but a drop in MAR$_{calc}$ as the site moves away from the high productivity equatorial belt. The strong dissolution event ends here at the time when the rapid drop in MAR$_{calc}$ occurs in the Guatemala and Peru basin. Here the preservation of foraminifera is not supported by the sedimentation of diatom rich layers like in Site 1010. In this shallower site might have been a higher probability of organic matter to arrive the sea floor building a benthic fluff layer in which dissolution of foraminifera might be accelerated in comparison to deeper sites (de Villiers, 2005). In the deeper sites of the EP therefore the presence of diatoms might simply enhance the preservation probability by rapid settling of aggregates and particle clusters, which also in their extreme form of diatom mats hinder bioturbation and support rapid burial as positive factors in preservation of calcareous shells.

Thus dissolution at Site 1241 was likely the result of organic matter degradation; however after 10 Ma the MAR$_{calc}$ record shows a minimum at about 9.5 Ma contemporaneous with the nadir of EEP CC-events, suggesting a general low in carbonate productivity followed by an increase afterwards.

Site 1237 (Naszca Ridge, 3212 m water depth) is bathed by Antarctic-Circumpolar–Deep water and was moving more or less along the latitude during the last 10 Ma coming closer to the modern high productivity belt of the Peru/Chile upwelling (Mix et al., 2003). The MAR$_{calc}$ record experienced a first drop at about 11 Ma and stayed low until it recovers from 10.2 to 9.8 Ma, followed by a second slight decrease. The preservation of planktonic foraminifera was preferably good until 10.3 Ma, and then a decreasing trend in the WTF together with enrichment of non-calcareous coarse fraction components (e.g. sponge spicules, radiolarians, ash) points to intensification of dissolution. Thus according to findings at Site 1237 the decreasing MAR$_{calc}$ might be assigned to generally lowered productivity until 10.3 Ma. Because during this period decreasing MAR$_{calc}$ are not clearly accompanied by decreased carbonate preservation. These findings support the hypothesis of productivity decreases in the early phase of the Miocene CC-events and point to intensification of deep water corrosiveness increasing at about 10.3 to 10 Ma.
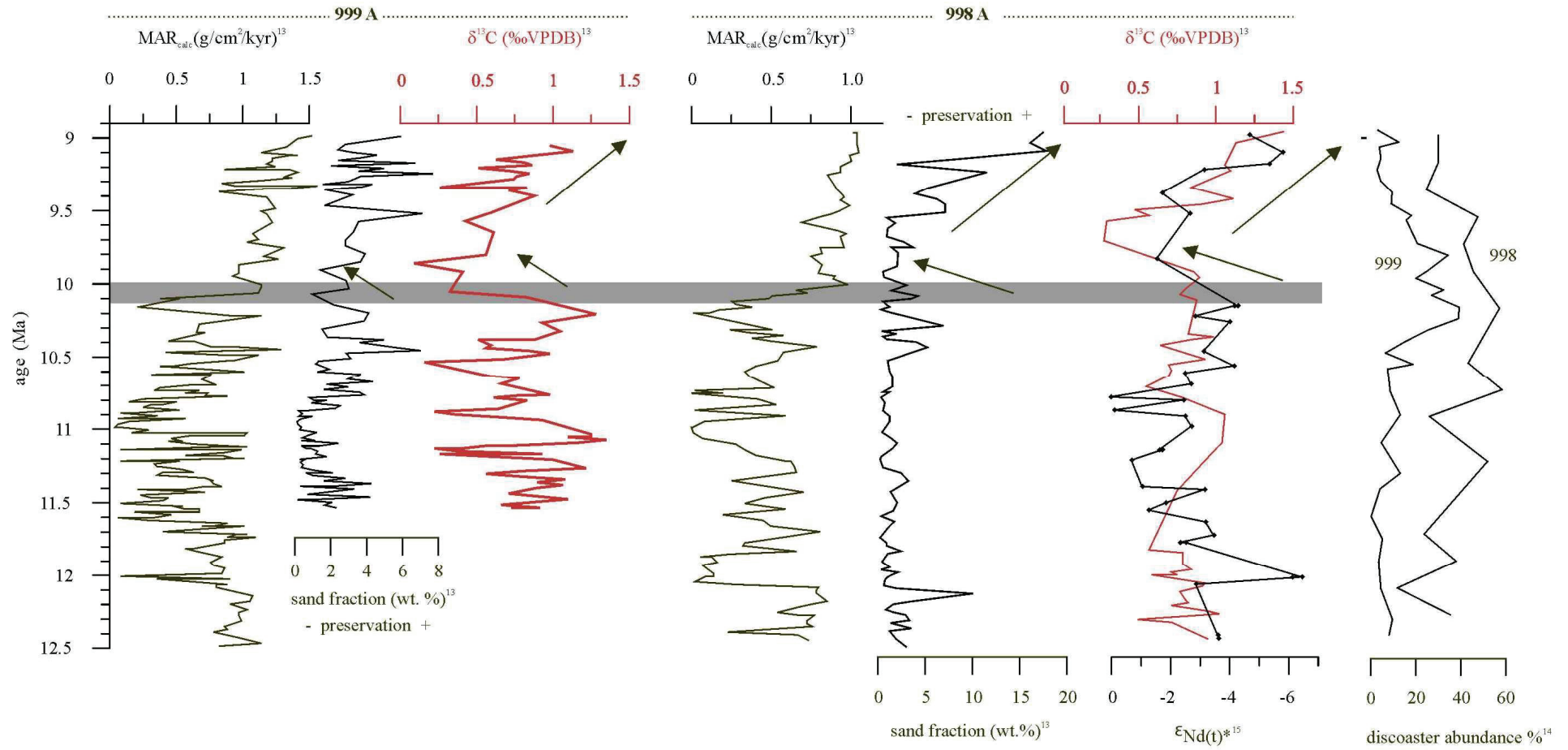
Fig. 4.5: Caribbean records show that the preservation is increasing after 9.5 Ma. However, this development is in conflict with already enhanced MAR.

4.4.2. The Caribbean

The Caribbean basin is characterised by influx of carbonate corrosive waters entering the Caribbean as a mixture of mainly AAIW and upper NADW (e.g. de Menocal et al., 1992; Haug and Tiedemann, 1998). The loop current is an important part in the global thermohaline circulation as surface waters gain salinity through evaporation, which is believed to have enhanced deep water formation in the North Atlantic (e.g. Haug et al., 2001).

Roth et al. (2000) modified the alternative model of Lyle et al. (1995) calling the influx of corrosive SCW responsible for dissolution in the equatorial Pacific. The tectonic situation in the Caribbean (emergence of the CAS and opening of intrabasinal seaways like the Pedro Channel) could have allowed for a strengthening of the Caribbean Current and establishment of the loop current. Based upon the observation of different coccolith assemblages present on either side of the CAS during an interval from 10.7 to 9.4 Ma, the Pacific-Atlantic connection might have been weakened (Kameo and Sato, 2000). At the same time the establishment of surface water connection among sites 999 and 998 and the possible initiation of the loop current was postulated based on similar assemblages.

According to Roth et al. (2000) the changing circulation at the middle to late Miocene transition is well recorded in the contrasting carbonate preservation pattern observed in the Caribbean basins, the EEP, and the western equatorial Atlantic. Roth et al. (2000) suggested in analogy to the theory of glacial/interglacial preservation cycles (Haddad and Droxler, 1996) that North Atlantic Intermediate Water (NAIW) flowed over shallow to intermediate depth sills on the Atlantic side of the Caribbean Basin during times of enhanced carbonate preservation (i.e. comparably to glacial circulation in the Quaternary), while corrosive southern sourced intermediate water (ancient equivalent to AAIW) overflowed the sills during intervals of carbonate dissolution (i.e. comparably to interglacial circulation in the Quaternary). This would furthermore induce that during times of enhanced NCW formation the preservation becomes worse in the Caribbean (corrosive intermediate SCW), better in the deep Atlantic (NCW replacing SCW) and also worse in the EEP (displacement of SCW towards this region). This configuration was based on the correlation between carbonate MAR minima (compare Fig. 5 to 6 for NCW reconstructions) and periods of more intense Northern Component Water (NCW) production (Wright and Miller, 1996) and associated with a closed deep water exchange between the Atlantic and the Pacific.

Recent studies by Newkirk and Martin (2009) comparing carbonate mass accumulation rate patterns and new evidence from Nd isotopes from fossil fish teeth and debris at Sites 998 and 999 in the Caribbean and Sites 846 and 1241 in the eastern equatorial Pacific support the assumption that waters sourced from the Pacific dominated flow into the Caribbean during the Miocene Caribbean CC-events. A gradual decrease in carbonate MAR_{calc} s and an associated increase in ε_{Nd} values at Site 999 prior to the Caribbean crash (Fig. 4.5) provide evidence for the introduction of a more corrosive Pacific intermediate water mass into the Caribbean as the CAS shoaled to critical depths for west to east flow.

During the Caribbean carbonate crash (12–9 Ma), highly variable ε_{Nd} values and MAR$_{calc}$ record pulses of corrosive Pacific waters that filled the deep Caribbean. These pulses of Pacific through-flow correlate well with NCW production, suggesting that NCW production could occur with an open CAS and that flow patterns in the Caribbean region are linked to global circulation patterns. After the Caribbean carbonate crash, ε_{Nd} values gradually shifted to less radiogenic values, indicating a reduction in the amount of Pacific water flowing into the Caribbean coincident with the shoaling of the Isthmus of Panama.

The comparison of preservation records (sand fraction) with carbonate accumulation of sites 999 and 998 suggests that the carbonate preservation is persistently worse, while the MAR$_{calc}$ already recovered at 10 Ma. The sand fraction contents of Site 999 and 998 remains low until 9.4 Ma. This trend is in accordance with lower values of benthic delta 13C at both sites and ε_{Nd} trends from Site 998 indicating phases of dominance of corrosive waters from probably Pacific origin and a trend to better preservation afterwards.

Another interesting pattern is the high abundance of discoaster nannoliths during the carbonate crash at sites 998 and 999 (Kameo and Sato, 2000). Originally interpreted as an ecologic signal they could also display enrichment because of dissolution (Gibbs et al., 2004). Then they would be another preservation proxy pointing to the CC-end at 9.4 Ma. This would have the consequence that the establishment of the loop current cannot be inferred from assemblages. The meaning of such high abundances as an ecologic signal might point alternatively to an interval of low plankton productivity (Chepstow-Lusty et al., 1991; Flores et al., 1995).

The complete closure of the Isthmus might not necessarily be a precondition to enhance carbonate preservation in the deep Caribbean basin. The comparison (Preiß-Daimler and Henrich, submitted) of the carbonate mass accumulation and preservation patterns of the Caribbean sites and those of the western equatorial Atlantic (i.e. Ceará Rise) (Fig. 4.4) reveals that the anti-correlation postulated by Roth et al. (2000) for these two contrasting regions is not evident from the records (see Fig. 4.5). Instead the records of Site 999 and 926 seem to be in phase, however much worse carbonate preservation was prevailing at Site 999 compared to the deeper Site 926 indicating the presence of more corrosive bottom waters. The similar phase trends in the preservation records might suggest that the NADW formation did not trigger a return flow and influx of corrosive waters but seem to weaken/replace/dilute the flux of corrosive waters into the Caribbean. Modelling results showed that NCW formation is possible with an open CAS (Nisancioglu, 2003). However, NCW% estimates and preservation records from the Caribbean and Ceará Rise differ in this important interval as discussed in the next section. A simulation for a restricted exchange through the CAS predicts a drastic shoaling of the lysocline in the EEP (Heinze and Crowley, 1997). However, at about the time of final closure (3 Ma) of the CAS the carbonate compensation depth was deepening in the EEP rather than shoaling (Farrell and Prell, 1991) according to sedimentary data.

4.4.3. The Atlantic

The middle to late Miocene Atlantic is characterised by the fade of opal (Cortese et al., 2004) and the onset of significant deep water formation in the North as well as initiated upwelling off Southwest Africa (Siesser, 1980).

Krammer et al. (2006) and Kastanja et al. (2006) studying the Miocene records of ODP Sites 1085 and 1087 on the continental margin off Namibia found severe reductions in carbonate contents and carbonate accumulation rates. These were related rather to reduction of coccolith productivity than caused by dissolution. Kastanja et al. (2006) showed that a first major drop in $CaCO_3$ concentration between 10.4 Ma and 10.1 Ma was related mainly to changes in calcareous nannoplankton production, while another drop between 9.6 Ma and 9 Ma is thought to have been triggered by a combination of production changes of calcareous nannoplankton and dilution, the latter, presumably occurring in response to high shelf supply in this region during global lowering of sea level (Diester-Haass et al. 2004, Kastanja et al. 2006 -Fig.4.7). Benthic plankton ratios at Site 1085 are increasing from about 9.4 Ma which is attributed to enhanced dissolution due to supply from the shelf (Diester-Haass et al 2004) and possibly aridification with first major dust supply at 9.6 Ma (Roters and Henrich, 2010).

Miocene South Atlantic sediment on the Walvis Ridge displays short-term dissolution events that were closely related to variations in NCW circulation in the deep circulation loop of the South Atlantic (Kastanja and Henrich, 2007). Kastanja and Henrich (2007) registered overall good to moderate preservation in the Miocene sections evidencing persistent NCW supply to this southern location. However some decreases of preservation at, 11.6, and 10.4 Ma were found to coincide with Miocene glacial events (Mi-events), suggesting a increase of SCW influence during these intervals, which occurred as a response to the intensification of Antarctic ice sheet development. At 10.4 Ma a change to overall better preservation points to a weakening of SCW that occurred as a response to the strengthening of NCW.

The western equatorial Atlantic (Ceará Rise, ODP Leg 154) sedimentation patterns are as well influenced by increasing preservation and distinct lows in carbonate accumulation occurring at 11.8 to 11 Ma and 10.4 to 10.1 Ma at Site 926 (King et al., 1997, Preiß-Daimler and Henrich, submitted) accompanied by low sand fraction contents (Shackelton and Crowhurst, 1997). The comparison of this record with Caribbean Site 999 shows similarity in MAR_{calc} and sand fraction suggesting dissolution and/or productivity pattern in phase (Preiß-Daimler and Henrich, 2011, submitted for publication). The general trend in preservation based on interpretation of sand fraction contents shows increasing preservation from 11.5 Ma on. The preservation minima are associated with Mi events 5 and 6 suggesting a causal relation to influx of corrosive SCW acting as the dominant deep water source during pulsed cooling. The relation to NCW% estimates by Miller and Wright (1996) and Poore et al. (2006) shows that the preservation record is roughly in phase until 10.1 Ma when the increasing preservation is not reflected in increasing NCW %. The interpretation of carbon isotopes are the basis

of NCW % estimates through mixing calculations (Oppo and Fairbanks, 1987). The estimates might be confused by the overall low productivity during this time interval (EP, Peterson et al., 1992; Mix et al., 2003), which might prevent formation of reliable benthic $d^{13}C$ gradients among ocean basins. Furthermore a recent modeling study suggests that the carbon isotope pattern in the Atlantic is not related to the variations in sill depth of the Greenland Scotland Ridge, questioning a major tectonic influence on circulation patterns (Butzin et al., 2011).
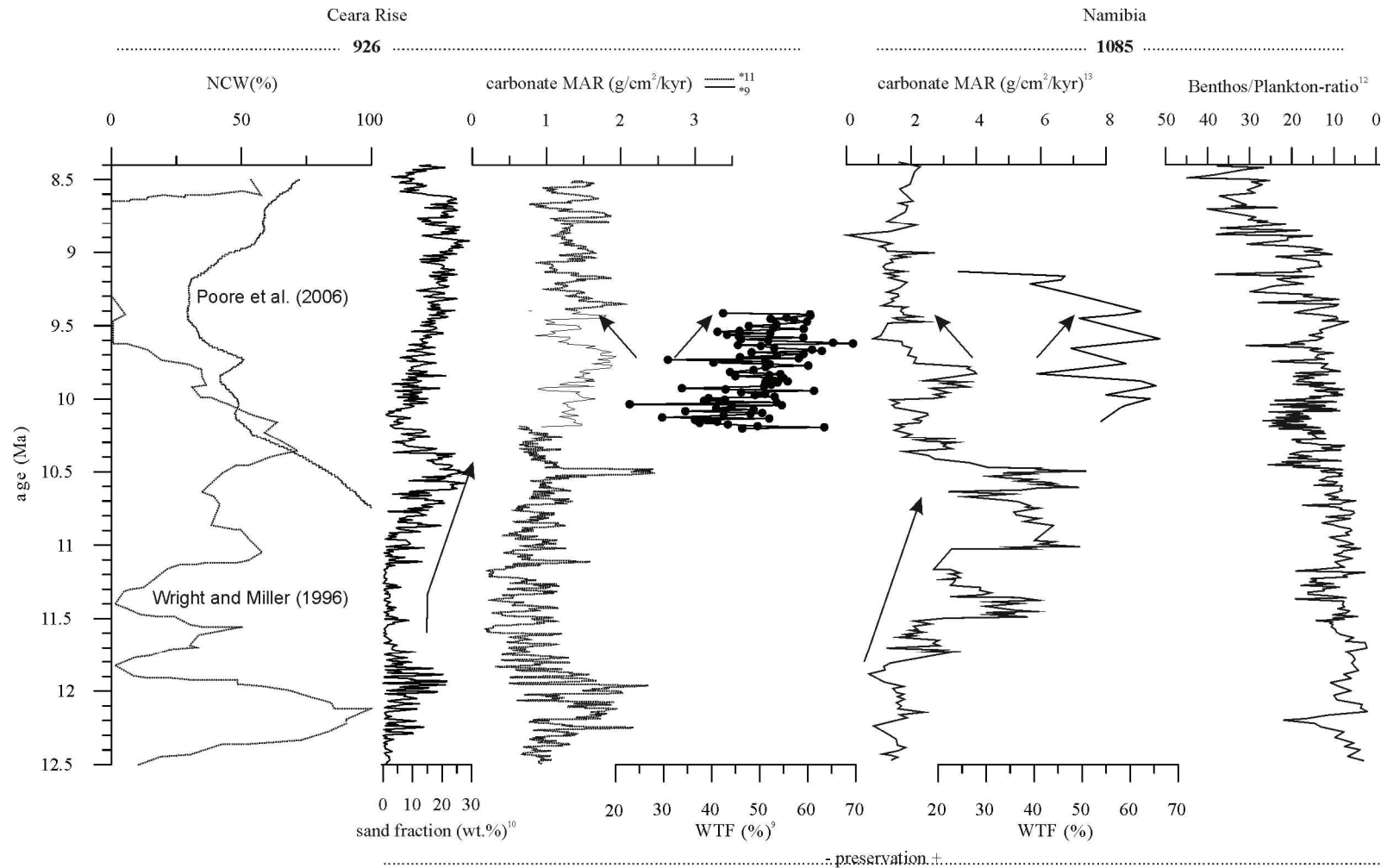
Fig. 4.6: The Atlantic shows in general a preservation pattern in accordance with NCW formation, but the decreasing NCW % estimate (centered at about 9.25 Ma) is not accompanied by a decreasing but increasing preservation in the deep Atlantic. Site 1085 preservation is decreasing at about 9.5 Ma – showing a different preservation pattern to the deep Atlantic, but possibly both sites suffered from productivity decreases of calcareous nannoplankton (in these phases preservation increases and MAR decreased (Preiß-Daimler and Henrich, submitted).

4.4.4. The Indian Ocean

The modern Indian Ocean can be divided into a northern high productivity region (Arabian Sea and the pelagic ocean north of 10°N), which is influenced by the monsoonal gyre system and the lower productive region of the subtropical gyre to the south. The Indian Ocean was drilled through early ODP Legs 115, 117, 121 and 122 and recovered cores mostly shallower 2500 m water depth with the exception of Leg 115 which offers a depth transect. Peterson et al (1992) noted that despite the completely different regional settings the carbonate sedimentation and gradients among sites were low
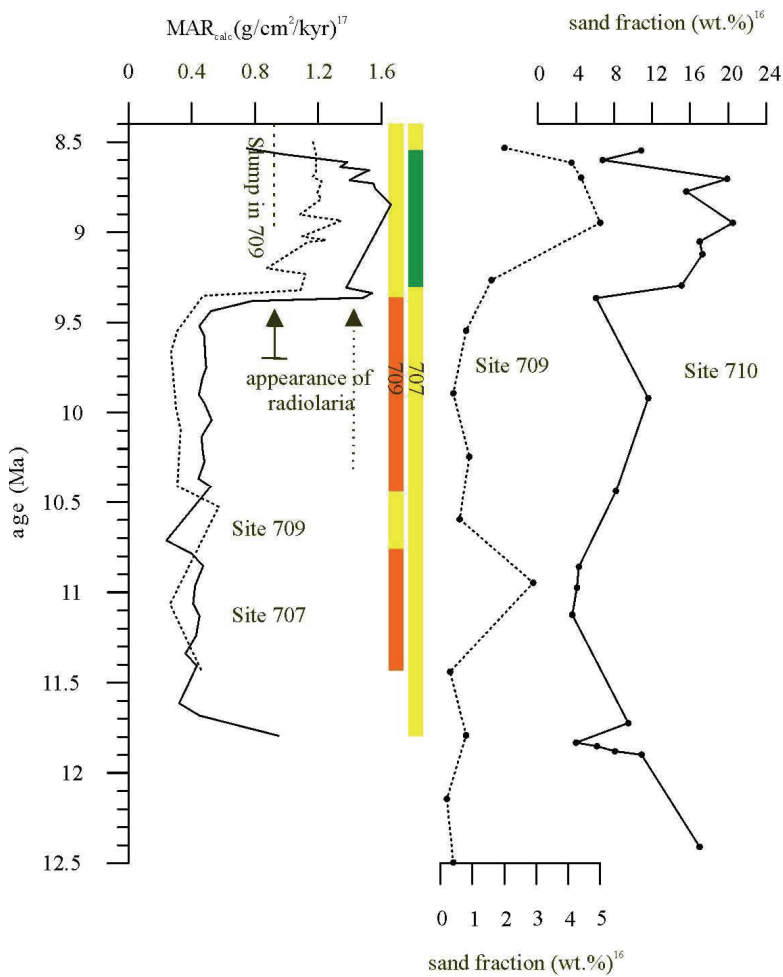

Fig. 4.7: The Indian Ocean, represented by the Mascarene Plateau ODP sites 707, 709 and 710. The carbonate crash interval is characterized by very low carbonate MAR and low MAR gradients among different depths. The opal reappears in form of radiolaria at about 10 Ma. Coarse fraction contents point to better preservation from about 9.4 Ma on.

during most of the Miocene followed by a marked step in the late Miocene accompanied by reappearing opal components in the sediment.

The initiation or intensification of the monsoon in connection to the uplift of the Himalaya and Tibetian Plateau as a major cause of pronounced oceanic productivity has been rejected (e.g. Gupta et al., 2004) as well as the hypothesis of Tethyan outflow water dominating at intermediate depth during the middle to late Miocene (Woodruff et al., 1989; Smart et al., 2007). The overall similarity suggests a global pattern assigned to sea level fluctuations and shelf-basin fractionation rather than a regional influence like the monsoon (Peterson et al., 1992). The increase in accumulation was named biogenic bloom and reported as well in the Pacific and Atlantic with different timing (Dickens and Owen 1999, Diester-Haass et al.2004). In the Indian Ocean it was accompanied by reappearing opal components and benthic foraminifera indicative of high productivity (Smart et al., 2007; Gupta et al., 2004) in the
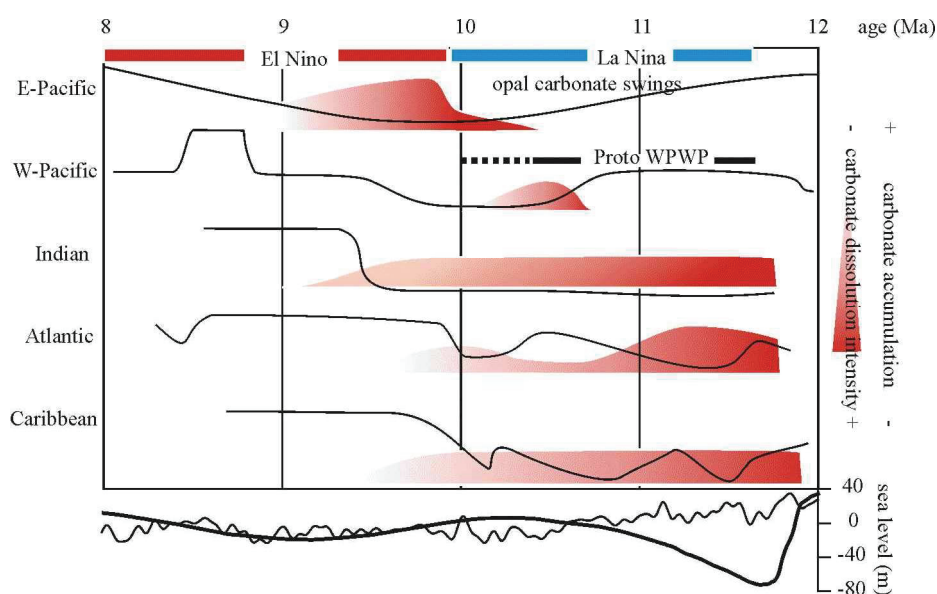

Fig. 4.8: With the CC the pattern of deep preservation changed in all ocean basins. The CCD rises in the EP and deepened probably first in the deep Atlantic, afterwards in the Caribbean and Indian Ocean. There is no clue to sea level, as a first order control on CC-events.

sediment as indicator for high productivity. However, the shift in depth gradients in the Late Miocene implies changes in circulation as well (Peterson et al., 1992). Unfortunately winnowing gives a strong imprint in shallow sediments (Site 707) causing foraminiferal sand contributions of about 50%. In comparison to Site 707 the deeper Site 710 (3812 m) shows about the same MAR_{calc} in accordance with aforementioned overall reduced gradients along the depth transect from 12 to 9.4 Ma right above the LO datum of *D. hamatus.*

The age model of Site 710 bases on magenetostratigraphy which resulted e. g. in a much earlier placement of the FO datum of *D. hamatus* than usual. However the reduced depth gradient might be because of redepositional events in the deeper records but is not purely an artefact of the age model differences and evident among the other sites as described by Peterson et al. (1992). In the deep sites the comparison of sand fraction contents leads to interesting results: At sites 710 and 709 the records of coarse fraction suggest a change to better preservation at 9.5 Ma as well as the abundance and preservation data on planktonic foraminifera (Vincent and Tourmarkine, 1990). The winnowed coarse fraction record of 707 is not shown but despite high coarse fraction contents the preservation of

foraminifera here is changing from moderate to good (Backmann et al., 1988). The reappearance of opal in form of radiolaria date back to 9.7 at Site 707 and to 10.3 Ma at Site 709.

The proportion of the sand fraction might be controlled by other processes besides dissolution. A size change in foraminifera became evident from 10 Ma on (Schmidt et al., 2006). This trend in low latitudes could have had an effect in the records shown. Winnowing could enhance the coarse fraction or dilution by finer grain sizes (nannofossils, terrigenous fraction) could decrease the coarse fraction. However the investigation of multiple proxies or the observation of increasing sand fraction along with better preservation and higher abundance of planktonic foraminifera might confirm the interpretation as dissolution index.

4.5 Conclusions and outlook

In conclusion, the middle to late Miocene carbonate crash events mark a period of major perturbations in the marine carbonate system, which obviously were associated with several steps in reorganisation of global deep and intermediate water circulation affecting various parts of the global ocean basins differently in time and space. A review and comparison of the eastern equatorial records seem to strengthen the hypothesis of alternating El Niño/La Niña – like states, that influenced both opal and carbonate accumulation in the EEP, on the California margin, and off Peru. The emergence of IS probably allowed for the development of a temporary WPWP during a La Niña-like state associated with the sedimentation of diatom mats. The alternating productivity in opaline and calcareous plankton were the main cause rather than dissolution at least in the early phase of the carbonate crash events. The deep water corrosiveness in the Pacific was pronounced at 10.5 to 9.4 Ma and losing influence afterwards. The shallow water record of Site 1241 in the EEP showed severe supralysoclinal dissolution through phases of high productivity.

In the deep Atlantic the preservation change can be recognized at 10.5 to 10.1 Ma already. Thus 10.5 Ma might be the starting point of prolonged basin to basin fractionation through onset of deep convection in the North Atlantic.

Sand fraction contents and preservation of planktonic foraminifera from the deeper Caribbean and the Indian Ocean and Pacific show an increase at 9.3 to 9.5 Ma, which we interpret as the first widespread signal of better preservation indicating a lysocline turning point possibly related to CCD deepening (Fig. 4.8). The Caribbean CC-events end at the same time based on reinterpreted coarse fraction contents, $\delta^{13}C$ signal and Neodymium isotope evidence as well as nannofossil indicators independent from the step to higher carbonate accumulation at 10 Ma, which was as well recognized at Ceará Rise. The similarity of coarse fraction records and mass accumulation records of Ceará Rise and the Caribbean, with however worse preservation in the Caribbean leads to the conclusion that the influence of corrosive Pacific sourced waters in the Caribbean was dampened by NCW formation and

not enhanced as previously assumed. The shoaling of the CAS might have contributed at 9.4 Ma to the Atlantic type preservation pattern in the Caribbean.

Phases of reduced calcareous nannoplankton productivity were evident at least in the Atlantic (Benguela upwelling site 1085) and Pacific and were probably related to reorganizations of the upper water column and surface circulation changes.

While the mass of carbonate in all studies is constituted by coccoliths and other nannoliths, the use of the better known foraminifera dominates the scientific output. However, changes in fine fraction stable isotopes in the Atlantic, Caribbean and Pacific show drastic decreases from 11.5Ma to 10.5 Ma (Mutti, 2000; Shackelton and Hall,1995; Shackleton and Hall, 1997) that are still hardly understood and interpretations are contrasting. Understanding these patterns and the further development of high resolution age models would help to find better insight into the CC-events regarding the timing and budget considerations.

Acknowledgment:

Chapter 5 - Carbonate budget mass estimates for Neogene Discoaster from the Equatorial Atlantic (Ceara Rise - ODP Site 927)

Authors: Inga Preiß-Daimler, Karl-Heinz Baumann, Rüdiger Henrich
Status: in review at Journal of Micropaleontology

Abstract

Mass estimates for extinct Neogene *Discoaster* nannoflora and *Sphenolithus* from samples of the equatorial Atlantic (Ceará Rise ODP Site 927) ranging from 8.6 to 3.25 Ma are presented in this paper. Based on morphometric measurements on 9 *Discoaster* groups models were established and their volumes transferred into mass estimates. Our suggestion for using mass estimates of disoaster nannoliths is to use a shape factors similar to application of extant coccolith flora in sediment traps or cores. The mass estimates for discoaster carbonate range from 10 to 40 % of the total nannofossil carbonate with a decreasing trend in the investigated interval. The general trend in discoaster shape in Late Miocene to Pliocene sediments shows a tendency to lower calcification preceding the well known Pliocene development prior to final extinction of *Discoaster*. A comparison of total nannofossil carbonate from calculation with size corrected abundance data to grain size measurement reveals underestimation by the first method ranging from 10 -20 wt.%.

5.1. Introduction

Estimates for coccolith masses are established for some species and groups of nannofossils deduced from morphometric measurements. The first approaches to infer to the mass were to measure the surface multiplied by a value of thickness and density of a coccolith (Honjo,1976; Samtleben and Bickert, 1990, Knappertsbusch and Brummer, 1995, Beaufort and Heussner, 1999). Subsequently, a more sophisticated volume of rotation approach was applied by Young and Ziveri (2000) for coccolith forms with rotational symmetry. These mass estimates were applied to sediment trap data and sediment cores to convert count data to carbonate flux estimates. This work intends to fill the gap for estimating nannolith carbonate budgets by presenting an approach for discoasters, which contribute significantly to pelagic Neogene sediments. Discoaster nannoliths have a dazzling appearance under the microscope, however they often remain unstudied because of their uncertain position within calcareous nannoplankton. Regarding their abundance, size and worldwide distribution it is reasonable to give them a place next to coccoliths as cell cover of marine phytoplankton (Bown, 1976). Specimens of *Discoaster* exist in the sedimentary record since approximately 60 Ma and became extinct at the end of the Pliocene (Bukry, 1971). It has been noted that there is a secular trend in Discoaster morphology, with progressive evolution from massive skeletal elements to more delicate forms, with a parallel reduction in ray number (Bramlette & Riedel, 1954; Bukry, 1971). The

discoaster nannoliths are relatively dissolution resistant and therefore used as a dissolution proxy (Ramsay et al., 1972; Flores et al., 1995; Gibbs et al., 2004a). The size variations of the early massive *Discoaster multiradiatus* across the Paleocene/Eocene-Thermal maximum had been attributed to temperature changes, rather than being a diagenetic artifact (Tremolada et al., 2008). The ecology of Discoaster has been traditionally attributed mostly to warm oligotrophic low latitude surface waters (Haq & Lohmann, 1976), supported by geochemical evidence (Minoletti et al., 2001). However, some variance could not be explained by temperature changes but was probably modified through productivity controls or abiotic factors (Chepstow-Lusty et al., 1991, Gibbs et al. 2004b).

Changing size phenomena are not only documented in morphometric studies but in integrating granulometric size measurements with laser, coulter or sedigraph devices, measuring either directly size, volume or equivalent spherical diameters according to sinking velocities of sediment grains. A shift to bigger coccolith volumes measured with a Coulter counter in the North Atlantic at sediments from the beginning of the 20th century, was attributed to a shift in calcification response to rising atmospheric CO_2 levels rather than assemblage changes or primary productivity variations (Halloran, 2008). However, integrating methods cannot discriminate between species directly. This work presents 3D models based on morphometric measurements on SEM images from sediments of western equatorial Atlantic ODP Site 927. The Ceará Rise record offers a well dated continuous sedimentary succession to test our results in a time slice from 8.6 to 3.25 Ma. This interval includes significant size changes in coccoliths as the low latitude Reticulofenestra-event and variations in *C. leptoporus* as well as the more general major Pliocene coccolith turnover (Aubry, 2007), which is regarded as a precursor of the subsequent Pleistocene morphologic strategy in nannofossil lineages favoring small sizes e.g. leading to the successive disappearance of Discoasters at the end of the Pliocene (e.g. Chapman & Chepstow-Lusty, 1997).

5.2. Location

The Ceará Rise (CR) is an aseismic ridge located 700 km to the north-east of the mouth of the Amazon River, below the oligotrophic subtropical West Atlantic gyre (Fig. 5.1). Its sediments are composed of terrigenous clay supplied by fluvial discharge and carbonates from nannofossils and foraminifers. ODP Site 927 sediments are composed of 70 to 80 % Carbonate, from which 60 to 90 % is constituted of coccoliths and other nannoliths. Site 927 is located at water depth of 3300m well above the lysocline.

5.3. Methods and Material

13 samples from ODP Site 927 were taken in an interval from 8.60 to 3.25 Ma. Bulk sediments were split into one portion for carbonate measurements and scanning electron microscope (SEM) sample preparation and the other portion was wet-sieved at 63μm. Bulk samples were analyzed for total

Carbon (TC), and after removal of carbonate for total organic Carbon (TOC) using a LECO infrared combustion analyzer. Carbonate contents were calculated after:

(Eq. 5.1) $CaCO_3$ [wt.%] = (TC [wt.%] - TOC [wt.%]) * 8,33

For SEM samples approximately 70mg of bulk sediments were disaggregated in Ammonia buffered water and treated for 3 seconds in an ultrasonic bath. Samples were splitted using a wet splitter and final splits were filtered on polycarbonate membranes (for method details see Andruleit, 1996). Filters were dried and cut to an area of ca $0.5cm^2$ and affixed to SEM stubs, and given a gold palladium coating prior to analysis.

Additionally, on six samples grain size measurements on the silt fraction (2-63µm) were conducted using a Sedigraph 5100 (sample procedure according to Frenz et al., 2005) after removal of clay (<2µm) through repeated settling (up to 30 times) in Atterberg tubes. The Sedigraph assigns settling diameters (Equivalent spherical diameter - ESD) to the
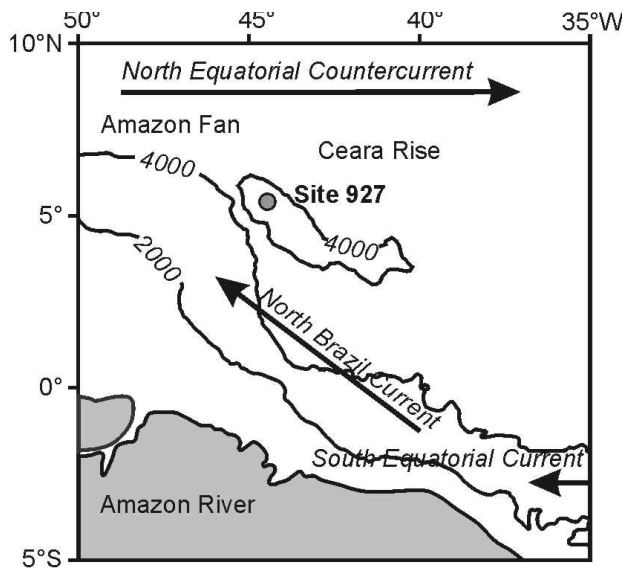

Fig. 5.1: Location of the study area, ODP Site 927 in the Western Equatorial Atlantic at the southwestern edge of the South Atlantic subtropical gyre system.

grains and overrates small particles, especially where they are formed platy in comparison to other methods (e.g. Laser particle sizer). This means that the ESD is smaller than the measured diameter from SEM images. It has been shown from accurately performed settling procedures removing the clay at 2µm ESD that the remaining calcareous placoliths show minimum diameters of about 4-5µm on SEM images.

Morphometry data were taken from a mixture of all 13 Ceará Rise (in the Results Chapter delineated as 'CRmix') bulk samples with the preparation technique described above. Images were taken at magnification of 1000 – 5000 times. For the morphometric measurements, the modeling and the calculation of 3D-geometric parameters a suite of open source software was applied:

For Image analysis and morphometric measurements ImageJ (http://rsbweb.nih.gov/ij/) was used. 3D modeling and editing was carried out with Blender (www.blender.org/) and for model simplification and geometric calculations Meshlab was used (http://meshlab.sourceforge.net/).

5.4. Results

The goal of the modeling is to relate a linear dimension (e.g. ray length-r_1) which can be easily obtained from microscopic analysis to a volume, which can then be transferred to mass. The volume (V) will be represented by the cube of this measure and a shape factor k_s:

(Eq. 5.2) $V = k_s * r_1^3$

This approach of calculating size-independent shape factors (k_s) for different species has previously been used for determination of coccolith mass with rotational symmetry (Young and Ziveri, 1990).
The work path from SEM images to mass estimates of the models was carried out in two steps:
1. Morphometric measurements on SEM images using ImageJ and basic grouping of Discoasters. Establishing statistic relationships between ray length and surface area within groups.
2. 3 D modeling on established groups based on morphometric data with the open source software Blender and subsequent volume calculation using Meshlab geometric filters.

5.4.1 Groups and Morphometry of discoasters from SEM images

Using the SEM for species recognition introduces some differences to the procedure at the light microscope. With the SEM it is possible to investigate the ultra structure and to draw exact outlines of specimens, but it is not possible to observe both sides of the same specimen, which is possible with variable focusing at the light microscope. However, the following species offered enough features making a taxonomic assignment possible from either distal or proximal views. However, the occurrence of morphological groups despite close relation to species concepts do not contain strict stratigraphic information.

The most abundant recognized *Discoaster* taxa within the studied interval were divided into 9 categories, including 5 polyspecific groups and 4 monospecific groups as follows:

Polyspecific groups:

1. *Discoaster-variabilis-group*: Six rayed *D. variabilis, D.   challengeri, D. loeblichi* and more massive forms like *D deflandrei*. Bifurcation of ray tips are always evident and distal and proximal bosses are common but weak and large bosses typical for *D. bolli* or *D. petaliformis* were very rarely observed. Some specimens of this group are similar to *D.surculus*, however these contain solely bifurcations while *D. surculus* shows three ray tip extensions.

2*. Discoaster-bellus-group:* Five rayed discoasters with straight shaped rays and almost undifferentiated central area.

3. *Discoaster-brouweri-group*: Six rayed discoasters with plane central area and deflected rays and a distal knob. *D. brouweri, D. braruudi, D altus*

4. *Discoaster-pentaradiatus-group*: Five rayed *D. prepentaradiatus* intergrading with More delicate *D. pentaradiatus* showing V-shaped bifurcations.

6. *Discoaster-quinqueramus-group:* Five rayed *Discoaster quinqueramus*
almost monospecific due to absence *D. bergenii* and *D. berggrenii in CR-Mix.*

Monospecific groups:

4. *Discoaster-surculus-group*

5. *Discoaster-hamatus-group*

8. *Discoaster-calcaris-group*

9. *Discoaster-exilis-group*

Additionally models of *D. bergenii* and *D. bergrenni* were constructed changing the ray length of D. *quinqueramus* to 0.8 and 1.5 times the central area radius, respectively. Also a model for *Sphenolithus* was created. Some Discoaster specimens occasionally observed were 3-5rayed or asymmetric variants of *D. brouweri*, *D. pentaradiatus*, *D variabilis* and *D. calcaris*. These are not explicitly included in the groups but might be estimated from them.

After sorting morphological groups, image analysis was carried out on size calibrated SEM images. The following parameters (see Fig. 5.2) were measured on e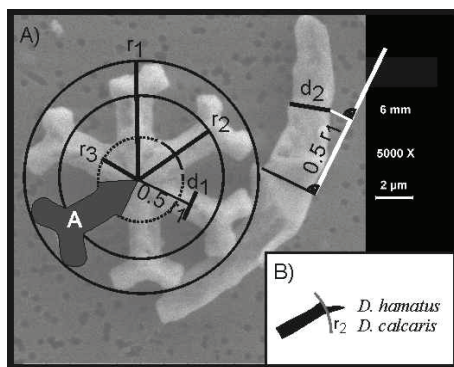ach ray: Ray length (r_1), area (A), central area width (r_3), half ray width (d_1) and if present also the base of the ray tip extension (r_2) (*D. hamatus* group, *D. surculus group*, *D. variabilis* group, *D. calcaris* group, *D. pentaradiatus* group). The base of the ray tip extension was defined differently for *D. hamatus* and *D. calcaris* (see Fig. 5.2 B) compared to the other groups (see Fig. 5.2 A). The ray thickness (d_2) could be determined in some rare cross-sectional debris of single rays or in upright positioned specimens; the thickness was then measured at half of the ray length. Area calculations required thresholded images delineating the borders of the particle outline. Some low contrast images of the SEM prevent an automatic confining of outlines, thus this has been done by redrawing outlines.

Fig. 5.2: A) Parameters measured on each ray in plane view and crossectional view: r1-ray length, A-area, r2_ ray tip base, r3-central area radius, d1-half ray width, d2-half ray thickness. B) Definition of the ray tip base in specimen of *D. hamatus* and *D. calcaris*.

5.4.2. Obtaining statistic relationships from distal and proximal views of specimens

We theorized that the area (A) as two dimensional parameter would represent the closest relationship to the volume, thus the area was fitted to all other linear parameters with linear regression (see Fig. 5.2) (except thickness –d2- see section 5.3) assuming that the underlying relationship generally is:

(Eq.3) $A = k_a * (parameter)^2$, with k_a being a constant shape factor for each parameter.

If the shape is scale invariant then the value of the exponent will be 2. The factor k_a is a first hint to the degree of calcification. Increasing k_a points to heavy calcification independent from size. However, getting size data might reduce errors in mass estimates especially for the highly calcified forms like discoaster nannoliths (see discussion). The ablated k-values and coefficients of determination are reported in Tab. 5.1.

Group	n	r1-A		d1-A		r2-A		r3-A	
		k	r^2	k	r^2	k	r^2	k	r^2
D. bellus	51	0.19	0.93	3.27	0.25			3.16	0.70
D. brouweri	54	0.14	0.71	4.76	0.10			1.62	0.44
D. calcaris	48	0.11	0.57	7.33	-1.51	0.15	-0.36	2.83	0.29
D. exilis	32	0.13	0.79	8.60	-0.07	0.27	0.57	2.61	0.57
D. hamatus	58	0.13	0.73	5.56	0.39	0.19	0.72	4.54	0.71
D. pentaradiatus	55	0.11	0.68	7.29	-1.09	0.19	-0.45	3.26	0.75
D. quinqueramus	47	0.13	0.62	7.71	0.20			2.28	0.66
D. surculus	50	0.18	0.68	5.79	-0.54	0.41	-0.17	2.27	0.28
D. variabilis	44	0.26	0.80	5.06	0.08	0.56	0.44	2.84	0.14

Tab. 5.1: Statistic relations in discoaster specimens of 'CR-mix' sample

Group	n	r1-d2
		c
D. bellus	9	0.266
D. brouweri	11	0.199
D. calcaris	4	0.149
D. exilis	7	0.161
D. hamatus	6	0.182
D. pentaradiatus	12	0.104
D. quinqueramus	6	0.168
D. surculus	14	0.257
D. variabilis	30	0.235

Tab. 5.1: relation of thickness and ray length

5.4.3. Cross sectional views and thickness of specimens

Having established the fit relation between the surface and surface parallel measures, the third dimension was added to the model. Unfortunately, it is not possible to measure the thickness, the area and the other parameters on the same specimen from SEM pictures. Thus we had to find broken rays or upright oriented *Discoaster* for cross-sectional views. These pictures gave thickness (d2) and ray length (r1) for which the underlying relationship is supposed to be:

(Eq. 4) $r1 = d2 * c$ (with c being a constant between 0 and 1).

Estimates for this relationship are based on low numbers of measurements as reported in Tab. 5.2.

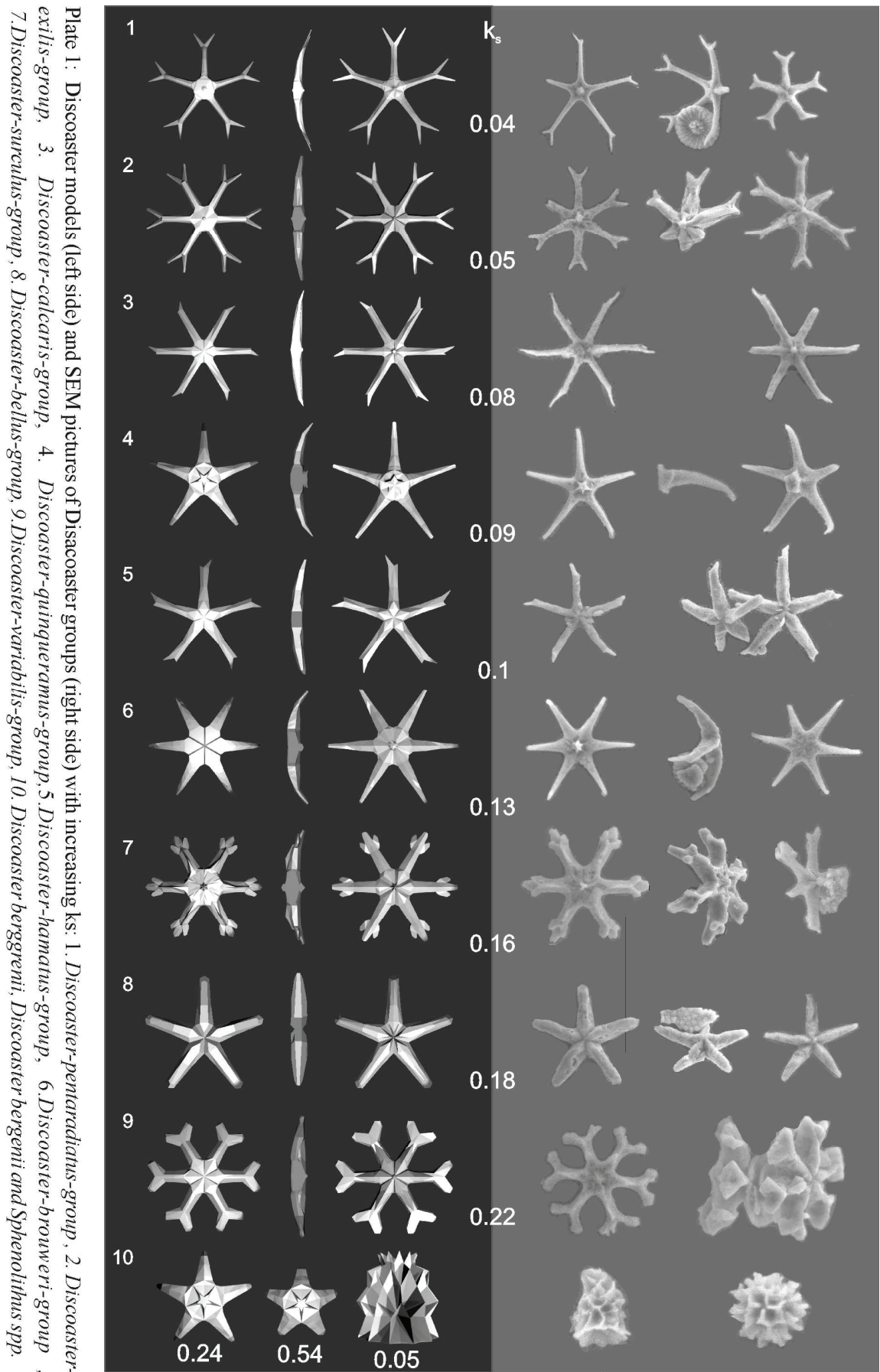## 5.4.4 From morphometric measures to model

For merging the knowledge of morphometry to a 3-D model we choose the area for the model as being the mean of the surfaces measured. From this mean area subsequently all other parameters (r1, r2, r3, d1, d2) were calculated for the model measures according to fit statistics reported in tables 1 and 2. Models were edited as polygonal objects in Blender (see Plate 1). The model volumes were calculated with Meshlab using the inbuilt algorithm based on finite element method. The length of one branch was than related to Volume, thus it is represented by the cube of the length (r1) and a factor similar to that of Young and Ziveri (2000), which we now report as shape factors k_s:

(Eq. 5.5) $V_{model} = r1^3 * k_s$.

5.4.5. Assemblage counts and estimation of Ceará Rise Site 927 nannofossil mass distribution

In the following we applied our ks estimates and ks values from the literature (Beaufort & Heussner, 1999; Young and Ziveri, 2000 see Tab. 5.3) for carbonate budgeting purpose to assemblage counts on 13 samples of Ceará Rise Site 927. In order to avoid errors, size corrections were introduced. During assemblage counting size assignments were already made for *Reticulofenestra* (see Tab. 5.3) and *Calcidiscus leptoporus* for further size correction about 30 specimens were measured (nannolith size, that is placolith diameter, spine length or discoaster ray length). This mean size is calculated as mean volume following the suggestion of Young and Ziveri (2000), in order to avoid underestimation due to deviations from normally distributed sizes.

The bulk number of specimens throughout the record is dominated by the smallest specimens like *Reticulofenestra spp.*, *Floriphaera profunda* and *Umbilicosphaera spp.*, however, some parts of the record, especially the older half contains up to 15 % discoaster nannoliths (see Fig. 5.3 A). The nannofossil content comprises about 10-30% of the total sediment and can preferably be regarded as a minimum content (see discussion). The mass is dominated by discoaster nannoliths contribution that sums up to 11-42 wt. % of the total nannofossil carbonate and accounts for 2-11 wt% of the total sediment. Discoaster nannoliths show a decreasing trend over the interval in both abundance and mass. Together with Discoaster, Reticulofenestra, Helicosphaera and Calcidiscus form already 70-80% of the total nannofossil carbonate. Most mass within Discoaster carbonate is contributed by the D. variabilis-group, D.brouweri-group, D. quinqueramus-group, D. pentaradiatus and D-surculus –group.

Plate 1: Discoaster models (left side) and SEM pictures of Disacoaster groups (right side) with increasing ks: 1.Discoaster-pentaradiatus-group, 2.Discoaster-exilis-group, 3. Discoaster-calcaris-group, 4. Discoaster-quinqueramus-group, 5.Discoaster-hamatus-group, 6.Discoaster-brouweri-group, 7.Discoaster-surculus-group, 8.Discoaster-bellus-group, 9.Discoaster-variabilis-group, 10. Discoaster berggreni, Discoaster bergenii and Sphenolithus spp.

Species	k_s	mass this study range (pg)	mean	Mean mass (k_s (pg)	Source of k_s
D. pentaradiatus	0.04	15-221	63.3	-	this study
D. exilis	0.05	7-21	16.5	-	this study
D. calcaris	0.08	34-155	80.7	-	this study
D. quinqueramus	0.09	4-363	44	-	this study
D. hamatus	0.1	23-48	35.2	-	this study
D. brouweri	0.13	7-343	58	-	this study
D. surculus	0.16	55-562	219.5	-	this study
D. bellus	0.18	57-178	116.5	-	this study
D. variabilis	0.22	20-548	113.1	-	this study
D. berggrenii	0.24	32-94	55	-	this study
D. bergenii	0.54	18-46	33.4	-	this study
Sphenolithus sp.	0.05	2-28	10.6	-	this study
C. leptoporus big	0.08	104-289	146	164.2	Beaufort & Heussner (1999)
C. leptoporus med	0.08	25-115	52	74.1	Young and Ziveri (2000)
C. leptoporus small	0.09	7-20	10	22.6	Beaufort & Heussner (1999)
C. pelagicus	0.06	86-210	67	99.5	Young and Ziveri (2000)
Gephyrocapsa. sp. (small)	0.05	0.2-5	1.1		estimate – this study
R. minuta (open <3μm)	0.05	0.4-4	2.1	-	estimate – this study
R. minutula/haquii (open	0.05	4-17	7.4	-	estimate – this study
R. productella (closed	0.05	-	8.64	-	estimate – this study
R. perplexa (closed	0.06	-	20.3	-	estimate – this study
R. pseudoumbilicus (open	0.06	20-65	32.62	-	estimate – this study
F. profunda	0.03	0.3-6	1.82	1.3	Young and Ziveri (2000)
H. carteri	0.06	83-353	190.7	135.0	Average Y&Z (2000) and B & H (1999)
Helicosphaera spp.	0.06	40-131	96.8		like H. carteri
P. lacunosa	0.04	1.8-13	4.8		estimate – this study
Pontosphaera spp.	0.05	133-168	150.1	65.9	P. discopora B & H (1999)
Syracosphaera spp.	0.03	16-196	96	13.5	Young and Ziveri (2000)
Rhabdosphaera spp.	0.025	5-87	47	67.5	Young and Ziveri (2000)
Oolithotus spp.	0.0	8-88	28.1	96.8	Young and Ziveri (2000)
U. jafari (sibogae)	0.0	2-9	4.5	18.6	Young and Ziveri (2000)
U. rotula (foliosa)	0.0	9-62	19.9	35.0	Young and Ziveri (2000)

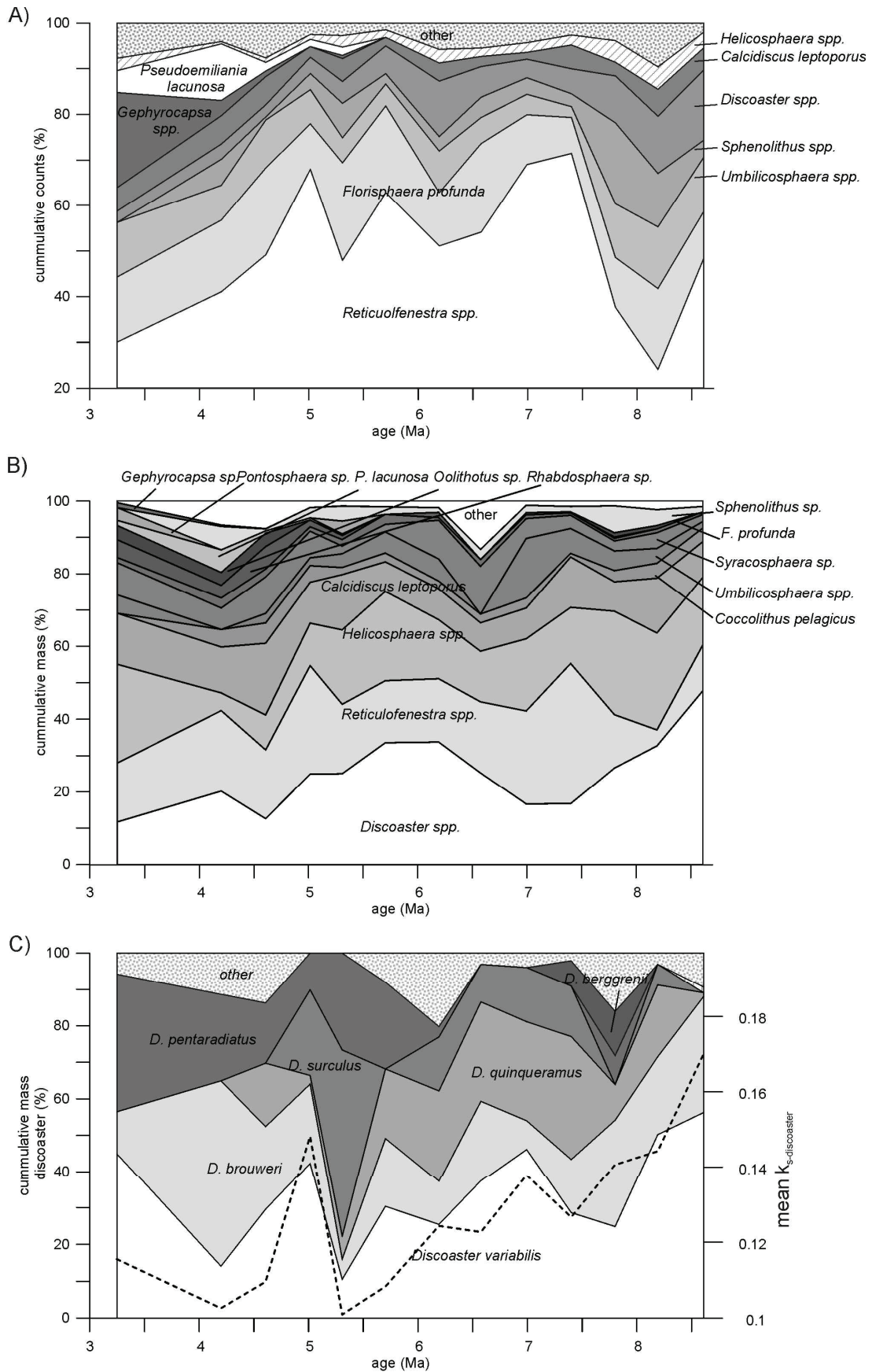Tab. 5.4: k_s estimates and sources used in this study, mass ranges and means.

Fig. 5.3: Nannofossil assemblage data of Site 927 from 8.6 to 3.25 Ma. A) Cumulative counts on nannofossil B) Cumulative mass of the assemblage C) Cumulative discoaster mass and mean ks of *Discoaster* (dashed line) see explanation in discussion 5.1.

5.5. Discussion

In the first part the results of the application of k_s-values to Ceará Rise Site 927 sediments and possible implications will be discussed. Followed by considerations, regarding errors in the group concept, described exemplarily for Discoaster-pentaradiatus-group and possible errors in the basic data of the modeling approach. Afterwards the nannofossil carbonate budget will be evaluated with respect to grain size based budget estimates. However, it might be stressed here, that the main uncertainty in mass estimates is up to the choice of size.

5.5.1 Ecologic implications and the significance of Discoaster carbonate contribution in low latitudes of the late Miocene to Pliocene

The time interval chosen for the application of new shape factors is part of the subtle cooling period, accompanying the beginning of early bipolar glaciation and situated right before the successive disappearance of discoaster (at about 3-2Ma), which is recorded in well known stratigraphic events and decreasing ray numbers, which means decreasing degree of calcification in discoaster nannoliths. Due to carbonate budget results, discoaster contribute significant amounts of nannofossil carbonate in the order of 10-40 %, which can be related to relative abundance counts as low as 2-15%. The low resolution of the data prevents explicit interpretation, however, some general statements and considerations can be made. Abundance and mass estimates show a long term decrease. A change in shape is accompanying this trend with respect to a mean $k_{s\text{-}discoaster}$, which was calculated according to the proportion of morphological groups:

(Eq 5.6) mean $k_{s\text{-}discoaster} = \Sigma ks_{group} * proportion_{group.}$

The trend (Fig. 5.3 C) is caused by the progressive dominance of more slender nannoliths, recorded as increasing abundance of D. pentaradiatus and D. brouweri at the expense of D. varabilis and D. surculus. A study of the late Miocene incipient Benguela upwelling (ODP Site 1085) shows, that contributions of discoaster and sphenoltihus are half that of Ceará Rise during peaks of occurrence (Krammer et al., 2005). Despite low numbers the contribution to the carbonate might be estimated with 5-20 percent and rises preferably during times of low total nannofossil carbonate accumulation at that site supporting the argument of productivity controls similar to Site 662 off North Africa (Chepstow-Lusty et al., 1991). Nannofossil abundance data from Pliocene sediments of the equatorial Pacific (ODP sites 852 and 849) shows similar fluxes of discoaster in the upwelling and convergence zone, but higher relative contributions in the more oligotrophic site suggesting as well control by dilution rather than nutrient availability (Flores et al., 1995). Furthermore the discoaster abundance pattern show a direct imprint of orbital cyclicity in the deeper Site 926 between 4 to 3.5 Ma besides *F. profunda* and *Sphenolithus sp.* (Gibbs et al., 2004b), while other contributors lack obvious response to fluctuations of orbital parameters (Gibbs et al., 2004b). This might emphasize the suitability of extinct

nannofossils as paleoenvironmental indicators, reacting to abiotic forcing with pronounced sensibility throughout a phase of subtle changes.

A comparison of abundance data from low latitudes shows the fade of discoaster nannoliths in the Caribbean, the Eastern Equatorial Pacifc (EEP) and Western Equatorial Pacific (WEP) at about the same time as in the record of Ceará Rise associated with the paracme interval of *R. pseudoumbilicus* in the late Miocene (beginning at 8.85 Ma – see Fig. 5.4). A similar pattern is shown by low resolution data of Rio et al. (1990) from ODP Site 707 in the Indian Ocean. The abundance of discoasters is decreasing here from about 40% in the late Miocene to 20 % and lower at about the time of first occurrence of *D. berggrenii,* indicating the top of nannofossil zone CN8 in the early Pliocene. Following the argumentation that dissolution is a minor factor in the data and that productivity control through species, that are able to thrive, suppress the abundance of discoaster nannoliths, the late Miocene to early Pliocene might represent a "threshold interval" in success of ecologic strategies in the low latitude plankton community as assumed earlier (Aubry, 2007). The interval immediately
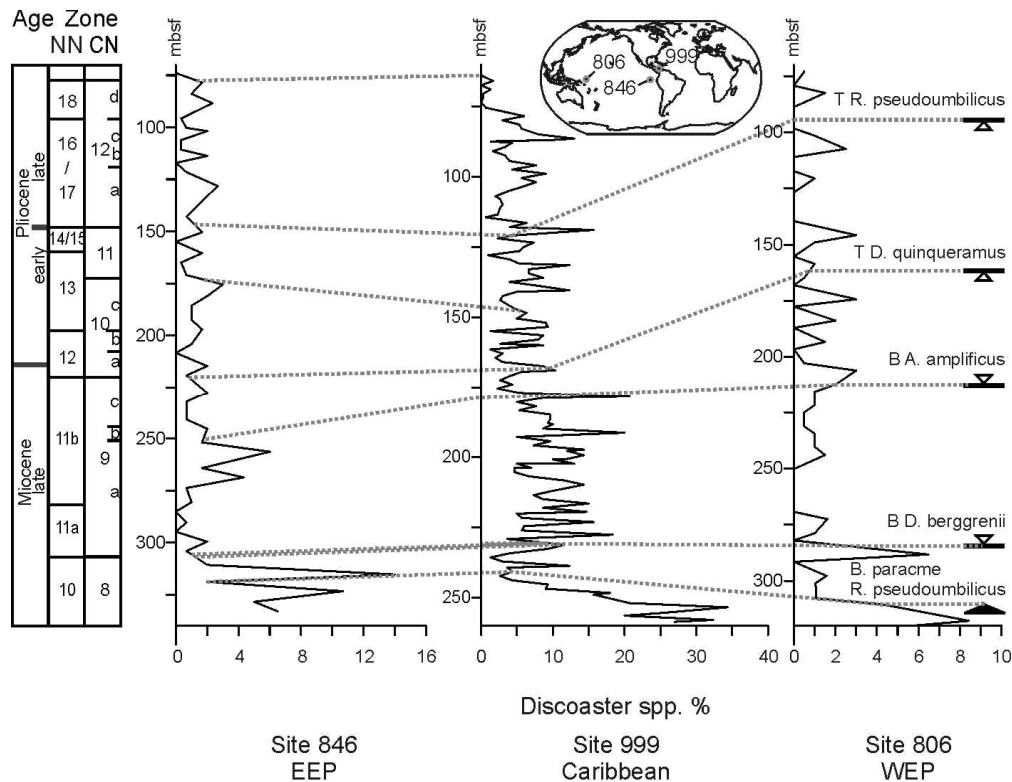

Fig. 5.4:Abundance data of Discoaster spp. from other low latitude locations. From left to right: ODP Site 846 in the EEP (Data from Kameo and Sato 2000, Nannofossil datums according to Raffi and Flores, 1995) and ODP Site 999 in the Caribbean (Data from Kameo and Sato, Nannofossil datums according to Kameo and Bralower, 2000). ODP Site 806 in the WEP (Data and position of Nannofossil datums from Takayama, 1992). Note the similar timing of strong reductions in the Discoaster abundance record associated with the B. paracme of *R. pseudoumbilicus*.

following the decrease in abundance of discoaster is known as the "biogenic bloom" and found in the low latitudes of the Indian and Pacific Ocean and was associated with high levels of carbonate mass

accumulation rates and reorganization of nutrient cycling (Dickens & Owen, 1999). However, there has been evidence that carbonate productivity rises as well far away from typical upwelling regions in the Atlantic, and this was attributed mainly to increasing fluxes of nannofossil carbonate (Diester-Haass et al., 2005). Regarding the timing of changes the reorganization of calcareous plankton communities might have been a prerequisite for the biogenic bloom. This speculation, however, needs further confirmation.

The importance of discoaster nannoliths for Neogene carbonate budgets in low to mid latitudes cannot be dismissed. The sudden abundance reduction of this dissolution resistant form is worth further investigation. It might even draw severe consequences for Carbonate compensation depth reconstructions in the view of dissolution kinetics.

5.5.2 Error sources in mass estimates

Group concept and possible errors in model setup

The hypothesis behind volume and mass estimates is, that the form is scale invariant. However, our mixed sample includes about 6 million years of *Discoaster* evolution, that certainly underwent changes in genotypes and phenotypic expressi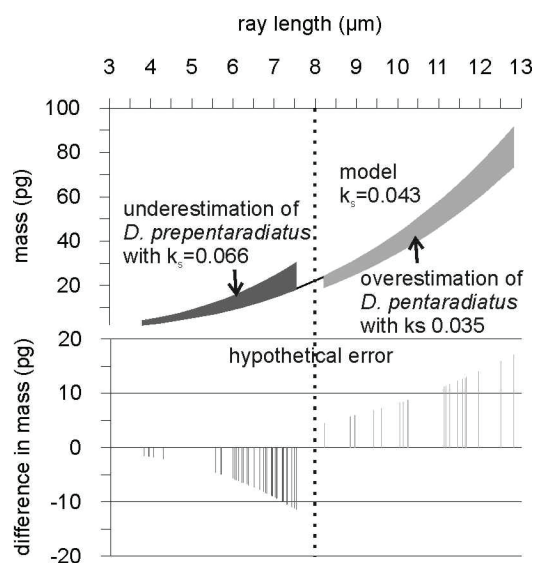on and morphometric groups contain more than one species. Thus some of the observed data variance can probably be assigned to the group concept, allowing for some differences in the morphology. An example for this is given by the D. pentaradiatus group, containing specimens of *D. prepentaradiatus,* which are a more robust precursor of the occasionally delicate shape of *D. pentaradiatus* (see Plate 1 – right side of first row). Here our ks estimate does underrate the smaller but more massive shape of *D. prepentaradiatus* and overrate *D. pentaradiatus* values (see Fig. 5). The interspecific allometry (change in size relations between the two closely related pentaradiate forms) can lead here for example to a 38 % underestimation of *D. prepentaradiatus* and a 19 % overestimation of *D. pentaradiatus*. In the given example the underestimation and overestimation

Fig. 5: The assignment of one shape factor to specimens of the delicate *D. pentaradiatus* and compact *D. prepentaradiatus.* results in over- and underestimation, respectively.

balance each other resulting in a very small absolute error. Some parts of the variance in the other data might be explained by similar less obvious changes regarding allometric tendencies.

Evolutionary trends in the pentaradiate lineages of *D. berggrenii* and *D. quinqueramus* were investigated at Site 926 throughout the Late Miocene (Raffi et al., 1998), leaving the question, whether *D bellus* or *D. berggrenii* is the ancestor of *D. quinqueramus*. Anyway, here as well morphology follows the same concept as in *D. prepentaradiatus-D. pentaradiatus* and showed the transition between a heavily calcified form towards less calcification. Following these observations, the consequence in application of shape factors is, that a fixed shape factor leads to overestimations of discoaster masses towards the younger ages. However, again this will hardly exceed the importance of size for mass estimates.
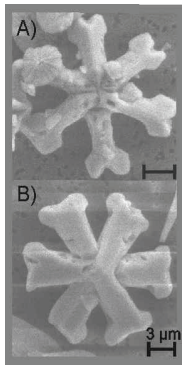
Fig. 5.6: A) Beginning diagenetic over-growth on specimen of *D. variabilis*. B) Late stage of over-growth on D.*variabilis* with complete calcitic veneer (sample 'CR-mix').

Other errors can be induced by minor diagenetic overgrowth, slight dissolution or slight tilting of specimens with respect to the observation plane as well as undetected breakage of parts. Following the latter more delicate forms (lower ks) could be more influenced by this form of error. This might be assumed with suspicion by the fact, that the r^2 follows a loose positive correlation with ks values (see Tab. 5.1).

It has been shown in an experimental setup, that during diagenesis *D. brouweri* first showed etching of the central area and slight thickening of rays leading further to carbonate overgrowth preceding from the inner to the outer (Adelseck et al., 1973). This was observed as well for all the other discoaster morphologies, and in measurements of discoaster in 'CR mix' for model setup, we avoided obvious secondary overgrowth. An example of diagenitic overprint in accordance with these observations shows beginning overgrowth (Fig. 5.6 A) and (Fig. 5.6 B) and at a late stage crystal faces with constant interfacial angles, covering specimens of *D. variabilis*.

Underestimation in mass estimates – a comparison to nannofossil carbonate estimate from granulometry

If we assume, that the splitting of the samples was accurate, we should have distributed a certain mass of the sample on the filter that represents the bulk sample. However, one foraminiferal test can even exceed the weight of the fraction used for investigations, thus the sand fraction will not be represented by the sample. If we further on assume, that the fine fraction smaller 63µm is distributed evenly on the filter we will find juvenile foraminfera and fragments from the silt fraction in the samples. In order to estimate this foraminiferal carbonate we applied bulk silt measurements on six samples,
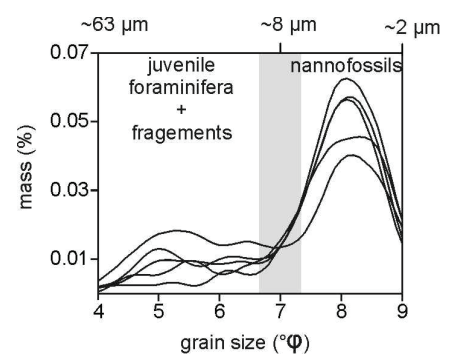

Fig. 5.7: Sedigraph measurements on silt distributions of six samples, showing characteristic polymodal distributions, which can roughly be divided into nannofossil and foraminifera and fragments at about 8um.

using a Sedigraph 5100 (sample procedure as described in Frenz et al. 2005 – see Fig. 5.5). It has been shown from grain size measurements, that the calcareous silt fraction of open ocean pelagic sediments often shows an almost bimodal distribution, from which the coarser part is constituted of foraminifera and their fragments, divided by a minimum from coccoliths and other nannoliths from the fine silt and clay fraction. This minimum ranges depending on the technique and sample features from about 8 to 10 µm (see Fig. 5.7).

According to own results (Preiß-Daimler & Henrich, submitted) and Frenz et al. (2006) the terrigenous fraction (owing to the lack of opal) in the Miocene and Pliocene samples of Site 927 can almost exclusively be assigned to the fine silt and clay fraction with low proportions of terrigenous silt

Sample No. 927-	NC - SEM method (wt.%)	NC -<63µm Sedigraph (wt.%)
C 15-2 125.5 cm	14.7	24.0
A 19-5 29 cm	18.3	31.0
B 21-3 32 cm	15.0	33.2
B 22-5 12 cm	21.5	32.8
B 23-5 26 cm	22.5	44.3
C 23-5 93.5 cm	17.5	36.6

Tab. 5.4 Comparison of nannofossil carbonate content (NC) by two methods.

0.8-2% in the Pliocene coarse silt and a tendency to lower values in the Miocene. For simplicity we therefore allocate the terrigenous fraction to the fine silt <8µm (equivalent spherical diameter-ESD) and clay fraction <2µm (ESD). According to this, the nannofossil carbonate (NC) fraction <63µm is

(Eq. 5.7) NC (wt.%)=(fine fraction < 63µm (g) – coarse silt (g) – terrigenous fraction (g))/(fine fraction (g))*100

The results (see Tab. 5.4) suggest a constantly higher proportion of NC due to grain size measurements than the carbonate mass estimates from assemblage counts. The difference between results is even bigger for the older samples. The most obvious explanation for the constantly lower values is given by the occurrence of aggregates and broken nannofossils on the filters, which cannot be totally avoided and are not part of the budget estimate. Another suggestion is that the fraction on the filters could be represented by a smaller size fraction than <63µm which would raise the terrigenous proportion relatively. However, it has been shown from sediment trap data that flux estimates results in underestimations compared to the fraction <32µm CaCO3 wt.% as well (Boerse et al., 2000). A cause for the rising difference in NC estimates with age might be due to underestimation

of discoaster carbonate, because of conventional counting technique (see e.g. Okada (1992) for recommendation of countings in different size classes) or aforementioned error sources.

5. 6. Conclusions

1. Shape factors of discoaster models range from 0.04 up to 0.54.

2. The size corrected estimate of carbonate mass from discoaster nannoliths comprises about 10 to 40 wt.% of the total calculated nannofossil carbonate and is the most important group in terms of mass followed by the carbonate contribution of the most abundant genus *Reticulofenestra*.

3. The abundances and mass estimates of discoaster contribution follow a decreasing trend from 8.6 to 3.25 Ma, associated with a general trend to more slender forms, dominating the discoaster assemblage. The trend in decreasing abundance of discoaster nannoliths was as well observed in low latitudes of the Caribbean, Indian and Pacific Ocean, and is associated with the small Reticulofenestra interval.

4. Compared to nannofossil content estimates from granulometric measurements (sedigraph) the nannofossil content calculated with shape factors is constantly lower and might be referred to as a minimum content.

Acknowledgment

Appendix:

Taxonomic list:

Following the decriptions of Perch-Nielsen (1985) and References theirin

Discoaster bellus (Bukry and Percival, 1971)

Discoaster bergenii (Knuttel, Russell and Firth, 1989)

Discoaster *berggrenii* (Bukry, 1971)

Discoaster brouweri (Tan, 1927)

Discoaster braarudii (Bukry, 1971)

Discoaster bollii (Martini and Bramlette, 1963)

Discoaster calcaris (Gartner, 1967)

Discoaster challengeri (Bramlette and Riedel, 1954)

Discoaster deflandrei (Bramlette and Riedel, 1954)

Discoaster hamatus (Martini and Bramlette, 1963)

Discoaster loeblichii (Bramlette and Riedel, 1954)

Discoaster pentaradiatus (Tan, 1927)

Discoaster petaliformis (Moshkovitz and Ehrlich, 1980)

Discoaster prepentaradiatus (Bukry and Percival, 1971)

Discoaster quinqueramus (Gartner, 1969)

Discoaster surculus (Martini and Bramlette, 1963)

Discoaster variabilis (Martini and Bramlette, 1963)

Chapter 6 - Summary and Perspective

The Ceará Rise depth transect offered insight into the late Miocene dissolution state of the western equatorial Atlantic, which is quite different from today's. The rather sharp boundary of NADW and AABW today, which accounts for the sharp dissolution gradients in the mixing zone, is not evident in Miocene records. Here a broad zone of dissolution is governing the depth transect above the carbonate compensation depth (CCD) at about 4000 m water depth. However the preservation proxy records indicate decreasing influence of carbonate dissolution over the interval, which has been attributed to initiating deep water formation in the North Atlantic. The use of calcareous silt as a preservation proxy might be most useful in application to modern surface sediments avoiding evolutionary trends in plankton size, diagenetic overprints and productivity changes that could influence the calcareous silt size distributions of a time interval.

Future research might give hints to dissolution intensities and the amount of carbonate dissolved. Especially the transition from lysoclinal (weak) dissolution to heavy dissolution close to the CCD could be investigated by comparing and combining dissolution proxies of varying sensitivity, e.g. nannofossil based dissolution indices at heavier dissolution stages and foraminifer based proxies for less severe carbonate dissolution. Carbonate budget calculations at a depth transect with detailed mass loss calculations could than complement the dissolution indices and relate them to a certain amount carbonate dissolved. Therefore excellent age models have to available.

The overall lowered carbonate accumulation in the period from 12-9 Ma surely has multiple causes, but all investigated sediments below 3000m water depth show signs of dissolution.

Atlantic and Caribbean preservation records were in phase, rather than showing antithetic patterns. Due to our model the Caribbean sediments were likely dissolved by a Pacific sourced water mass entering the Caribbean. The comparison of NCW% estimates with the preservation record suggests furthermore better preservation during NCW formation, thus it can be assumed that the waters entering the Caribbean were diluted through NCW.

However, the comparison of low latitude preservation proxies leads to the conclusion that in the Pacific, the Caribbean and the Indian Ocean basins the preservation is increasing simultaneously since about 9.5 Ma. The preservation proxies and the mass accumulation rates of carbonate are clearly out of phase in the Caribbean and partly in the Atlantic suggesting that productivity changes are controlling accumulation rates. However productivity decreases are hard to trace but might be responsible for the discrepancies among the NCW% reconstructions and dissolution proxies, by weakening $\delta^{13}C$ gradients. Future research should address these discrepancies.

During the CC-events mainly coccoliths and other nannoliths constitute the carbonate sediments. Especially discoaster nannoltihs form an important part. Thus these nannoliths are the only surface water representatives in sediments barren of foraminifera. As also pointed out in this thesis the discoaster are a dissolution index but also an indicator of low productivity conditions. Their

contribution seem to be dominating during the CC Crash events in the Caribbean, but is decreasing in the late Miocene simultaneously in the Indian, Caribbean and Pacific Ocean. Their ecologic preferences and geochemical fingerprints shall be understood better in the future in order to gain understanding of surface water processes. As fine fraction stable isotope signals during CC-events showed drastic decreases in low latitude sites (Mutti, 2000; Shackelton and Hall,1995; Shackleton and Hall, 1997). The key to the interpretation might be given by combined analyses of foraminifera and coccolith/nannolith assemblages as well as a carbonate budget of these contributors in combination with stable isotope measurements. These data sets would allow to track changes in ecologic developments in surface waters (surface water stratification) and to unmix the combined geochemical signals (fine fraction stable isotopes).

Own data from foraminifera assemblage counts points to a drastic change in faunal assemblage at Site 926 from a mixed layer species domination to a thermocline species dominated assemblage (Preiß-Daimler et al., unpublished data, according to the concept of Chaisson and Ravelo (1997) expanded into the Miocene) which might point to profound surface water stratification changes.

A central issue in the perspective of future research will be the development and prosecution of an orbitally tuned time scales in the Cenozoic. This is the foundation of all comparisons, correlations and estimations of mass accumulations. These efforts are invaluable and shall be applied to the ODP and DSDP cores in order to use an archive already established.

In conclusion the application of carbonate budget calculations along with dissolution and productivity proxies is indispensable in the interpretation of dissolution phases like the CC-events.

Chapter 7 - References

Adelseck, C. G., Jr., Geehan, G. W., and Roth, P. H., (1973). Experimental evidence for the selective dissolution and overgrowth of the calcareous nannofossils during diagenesis, Geological Society of America Bulletin, 84, p. 2755.

Andersson, C., Jansen, E., (2003). A Miocene (8-12 Ma) intermediate water benthic stable isotope record from the northeastern Atlantic, ODP Site 982. Paleoceanography, 18, 1.

Andruleit, H., (1996). A filtration technique for quantitative studies of coccoliths. Micropaleontology, 42, pp. 403–406.

Aubry, M.-P (2007) A major Pliocene coccolithophore turnover: Change in morphological strategy in the photic zone. In: Large Ecosystem Perturbations: Causes and Consequences (S. Monechi, R. Coccioni, and M.R. Rampino, eds.) Geological Society of America Special Papers 2007, 424, pp. 25-51.

Archer, D. E. (1991). Equatorial Pacific calcite preservation cycles: Production or dissolution?, Paleoceanography, 6, pp. 561–572.

Archer, D., A. Winguth, D. Lea, and N. Mahowald, (2000) What caused the glacial/interglacial atmospheric pCO2 cycles?, Reviews of Geophysics, 38, pp. 159-189.

Backman, J., Duncan, R.A., et al., (1988). Proc. ODP, Init. Repts., 115: College Station, TX (Ocean Drilling Program).

Backman, J., Raffi, I., (1997). Calibration of Miocene Nannofossil Events to Orbitally Tuned Cyclostratigraphies from Ceará Rise, in: N.J. Shackleton, N.J., Curry, W.B., Richter, C., Bralower, T.J. (Eds.), Proceedings of the Ocean Drilling Program, Scientific Results, 154, pp. 83-99.

Bacon, M. P. (1984). Glacial to interglacial changes in carbonate and clay sedimentation in the Atlantic Ocean estimated from Th-230 measurements, Isot. Geosci., 2(2), pp. 97–111.

Bainbridge, A.E., (1981). GEOSECS Atlantic Expedition, Hydrographic Data, 1972-1973. National Science Foundation, US Printing O⁄ce, Washington, DC, p. 121.

Beaufort, L., Heussner, S., (1999). Coccolithophorids on the continental slope of the Bay of Biscay. Production, transport and contribution to mass fluxes. Deep-Sea Research II, 46, pp. 2147-2174.

Benjamin, M., Johnson, N.M. and Naeser, C.W. (1987). Recent rapid uplift in the Bolivian Andes: evidence from fission-track dating. Geology, 15, pp. 680-683.

Berger W. H. (1970). Biogenous deep-sea sediments: fractionation by deep circululation, Geol. Soc. Am. Bull., 81, pp. 1385-1402.

Berger, W.H., (1972). Deep sea carbonate: dissolution facies and age depth constancy, Nature 236, pp. 392-395.

Berger, W.H., (1975). Deep-sea carbonates: dissolution profiles from foraminiferal preservation. Cushman Foundation for Foraminiferal Research, Special Publication 13, 82–86.

Berger, W.H. (1991). Produktivität des Ozeans aus geologischer Sicht: Denkmodelle und Beispiele.- Z. dt. geol. Ges., 142, 149-178, Hannover.

Berger, W.H., Leckie, R.M., Janecek, T.R., Stax, R., and Takayama, T., (1993). Neogene carbonate sedimentation on Ontong Java Plateau: highlights and open questions. In Berger, W.H., Kroenke, L.W., Mayer, L.A., et al., Proc. ODP, Sci. Results, 130: College Station, TX (Ocean Drilling Program), pp. 711–744.

Berger, W.H., Wefer, G., (1996). Expeditions into the past: Paleoceanographic studies in the South Atlantic, in: Wefer, G., Berger, W. H., Siedler, G., Webb, D. J. (Eds.), The South Atlantic: Present and Past Circulation, pp. 363 – 410.

Berggren, W.A., Kent, D.V., Swisher, C.C., Aubury, M.P., (1995). A revised Cenozoic geochronology and chronostratigraphy, in: Berggren, W.A., Kent, D.V., Aubury, M.P., Hardenbol, J. (Eds.), Geochronology, Time Scales and Global Stratigraphic Correlation, SEPM Special Publication, pp. 129–212.

Berner, R. A., and K. Caldeira (1997). The need for mass balance and feedback in the geochemical carbon cycle, Geology 25, pp. 955-956.

Bickert, T., Haug, G. H., Tiedemann, R. (2004). Late Neogene benthic stable isotope record of Ocean Drilling Program Site 999: Implications for Caribbean paleoceanography, organic carbon burial, and the Messinian Salinity Crisis, Paleoceanography, 19.

Billups, K., (2002). Late Miocene through early Pliocene deep water circulation and climate change viewed from the sub-Antarctic South Atlantic, Paleogeography Paleoclimatology Paleoecology, 185, pp. 287-307.

Boerse, A., Ziveri P., Hinte J.E., van, Honjo, S., (2000). Coccolithophore export production, species composition and coccolith-CaCO3 fluxes in the NE Atlantic (343N 213Wand 483N 213W) In: Ganssen, G.M, Wefer, G. (Eds.), Particle Flux and its Preservation in Deep Sea Sediments. Deep-Sea Research II, 47, pp. 1877-1905.

Bramlette, M. N., Riedel, W. R. (1954). Stratigraphic Value of Discoasters and Some Other Microfossils Related to Recent Coccolithophores. Journal of Paleontology. 28-4, pp. 385-403.

Bramlette, M. N. (1961). Pelagic sediments. In: M. Sears(ed.), Oceanography. Publ. Amer. Ass. Advanc. Sci, 67, pp 345-366.

Broecker, W. S. and Peng, T. H. (1987). The role of $CaCO_3$ compensation in the glacial to interglacial atmospheric CO_2 change. Global Biogeochemical Cycles, 1, pp. 15-29.

Buitenhuis, E., Bleijswijk, J.V., Bakker, D. and Veldhuis, M. (1996). Trends in inorganic and organic carbon in a bloom of Emiliania huxleyi in the North Sea. Mar. Ecol. Prog. Ser.,143, pp.271–282.

Bukry, D. (1971). Discoaster Evolutionary Trends. Micropaleontology 17- 1, pp. 43-52.

Butzin, M., Lohmann, G., and Bickert, T.(2011). Miocene ocean circulation inferred from marine carbon cycle modeling combined with benthic isotope records, Paleoceanography, 26.

Caldeira, K., and R. Berner (1999). Seawater pH and Atmospheric Carbon Dioxide, Science 286, pp. 2043a.

Cande, S., Kent, D. (1995). Revised calibration of the geomagnetic polarity timescale for the Late Cretaceous and Cenozoic, J. Geophys. Res., 111, pp. 6093–6095.

Cerling, T. E., Harris, J. M., MacFadden, B. J., Leakey, M. G., Quade, J., Eisemann, V., Ehleringer, J. R. (1997) Global vegetation change through the Miocene-Pliocene boundary. Nature, 389, pp. 153-158.

Chaisson, W.P., and Ravelo, A.C., (1997). Changes in upper water-column structure at Site 925, late Miocene–Pleistocene: planktonic foraminifer assemblage and isotopic evidence. *In* Shackleton, N.J., Curry, W.B., Richter, C., and Bralower, T.J. (Eds.), *Proc. ODP, Sci. Results,* 154: College Station, TX (Ocean Drilling Program), pp. 255–268.

Chapman, M. R., Chepstow-Lusty, A. J. (1997). Late Pliocene climatic change and the global extinction of the discoasters: an independent assessment using oxygen isotope records. Palaeogeography, Palaeoclimatology, Palaeoecology. 134, Issues 1-4, pp. 109-125.

Chavez, F. P., Pennington, J. T., Castro, C. G., Ryan, J. P., Michisaki, R. P, Schlining, B. Walz, P, Buck, K. R., McFadyen, A., and. Collins, C. A (2002). Biological and chemical consequences of the 1997–1998 El Niño in central California waters. Progress in Oceanography, Volume 54 (1-4), pp. 205-232.

Chepstow-Lusty, A., Backmann, J., Shackleton, N. J. (1991). Palaeoclimatic control of Upper Pliocene Discoaster assemblages in the North Atlantic. Journal of Micropalaeontology 1991; 9; pp. 133-143.

Chung, S. N., Lee, K., Feely, R. A., Sabine, C. L., Millero, F. J. (2003). Calcium carbonate budget in the Atlantic Ocean based on water column inorganic carbon chemistry. Glob. Biogeochem. Cycles 17, pp.1093.

Coakley, J.P and Syvitski, J.P.M. (1991). Sedigraph technique. In: Syvitski, J.P.M. (Eds.), Principles and Methods of Geological Particle Size Analysis.. University Press, Cambridge, pp. 129-142.

Coates, A.G.,Laurel, C.S., Aubry,M.P., Berggren, W.A, (2004). The Geology of the Darien, Panama, and the Late Miocene-Pliocene collision of the Panama arc with northwestern South America. Geological Society of America Bulletin, 116, 11-12, pp. 1327-1344.

Collins, L. S., Coates, A. G., Berggren, W. A., Aubry, M.-P. & Zhang, J. (1996). The late Miocene Panama isthmian strait. Geology 24, pp. 687–690.

Conan, S.M.-H., Ivanova, E.M., Brummer, G.-J.A., (2002). Quantifying carbonate dissolution and calibration of foraminiferal dissolution indices in the Somali Basin. Marine Geology 182, 325–349.

Cortese, G., Gersonde, R., Hillenbrand, C.-D., Kuhn, G. (2004). Opal sedimentation shifts in theWorld Ocean over the last 15 Myr. Earth. Planet. Sci. Lett. 224, pp. 509–527.

Curry, W.B., Cullen, J.L., (1997). Carbonate production and dissolution in the western equatorial Atlantic during the last 1 M.Y., in: N.J. Shackleton, N.J., Curry, W.B., Richter, C., Bralower, T.J. (Eds.), Proceedings of the Ocean Drilling Program, Scientific Results, 154, pp. 189–199.

Curry, W.B., Shackelton, N.J., Richter, C., et al. (1995). Leg 154 Synthesis. Proceedings of the Ocean Drilling Program, Initial Reptorts, 154, pp. 421-442.

Delaney, M. L. (1990). Miocene benthic foraminiferal Cd/Ca records: South Atlantic and western equatorial Pacific. Paleoceanography, 5, pp. 743-760.

de Menocal, P.B., Oppo, D.W., Fairbanks, R.G., Prell, W.L., (1992). Pleistocene N13C variability of North Atlantic Intermediate Water. Paleoceanography, 7,pp. 229-250.

de Villiers, S., (2005). Foraminiferal shell-weight evidence for sedimentary calcite dissolution above the lysocline. Deep-Sea Research I, 52, pp. 671–680.

Dickens, G. R., and R. M. Owen (1999). The latest Miocene-early Pliocene biogenic bloom: A revised Indian Ocean perspective, Marine Geology, 161, pp. 75– 91.

Diester-Haas, L., Meyers, P.A., Bickert T., (2004). Carbonate crash and biogenic bloom in the late Miocene: evidence from ODP Sites 1085, 1086 and 1087 in the Cape Basin, southeast Atlantic Ocean. Paleoceanography, 19.

Diester-Haass, L., and Nees, S. (2004). Late Neogene history of paleoproductivity and ice rafting South of Tasmania, in The Cenozoic Southern Ocean: Tectonics, Sedimentation, and Climate Change Between Australia and Antarctica, Geophysical Monograph Series, 148, edited by N. F. Exon, J. P. Kennett, and M. J. Malone, pp. 253–272.

Diester-Haass, L., K. Billups, and K. C. Emeis (2005). In search of the late Miocene–early Pliocene "biogenic bloom" in the Atlantic Ocean (Ocean Drilling Program Sites 982, 925, and 1088), Paleoceanography, 20.

Dittert, N., Baumann, K.-H., Bickert, T., Henrich, R., Huber, R., Kinkel, H., Meggers, H., (1999). Carbonate dissolution in the deep-sea: methods, quantification and paleoceanographic application. In: Fischer, G., Wefer, G. (Eds.), Use of Proxies in Paleoceanography: Examples from the South Atlantic. Springer-Verlag, Berlin, pp. 255-284.

Dugdale, R. C., Wischmeyer, A. G.. Wilkerson, F. P., Barber, R. T, Chai, F., Jiang, M. S. and. Peng, T. H. (2002). Meridional asymmetry of source nutrients to the equatorial Pacific upwelling ecosystem and its potential impact on ocean atmosphere CO_2 flux: A data and modeling approach, Deep Sea Research., Part II, 49, pp. 2513–2531.

Duque-Caro, H., (1990). Neogene stratigraphy, paleoceanography and paleobiogeography in northwest South America and the evolution of the Panama seaway. Paleogeography Paleoclimatology Paleoecology, 77, pp. 203-234.

Eberli, G.P., (2000). The Record of neogene sea-level changes in the prograding carbonates along the Bahamas transect- Leg 166 Synthesis, in: Swart, P.K., Eberli, G.P., Malone, M.J., Sarg, J.F. (Eds.), Proceedings of the Ocean Drilling Program, Scientific Results, 166, pp. 167-177.

Farrell, J. W. and W. L. Prell, (1991). Pacific CaCO$_3$ preservation and d^{18}O since 4 Ma: Paleoceanic and paleoclimatic implications. Paleoceanography, 6, pp. 485-498.

Farrell, J.W., Raffi, I., Janecek, T.R., Murray, D.W., Levitan, M., Dadey, K.A., Emeis, K.-C., Lyle, M., Flores, J.-A., and Hovan, S. (1995). Late Neogene sedimentation patterns in the eastern equatorial Pacific. Proc. Ocean Drill. Program Sci. Results, 138: pp. 717-756

Flores, J.-A., Sierro, F.J., and Raffi, I., (1995). Evolution of the calcareous nannofossil assemblage as a response to the paleoceanographic changes in the eastern equatorial Pacific Ocean from 4 to 2 Ma (Leg 138, Sites 849 and 852). In Pisias, N.G., Mayer, L.A., Janecek, T.R., Palmer-Julson, A., and van Andel, T.H. (Eds.), Proceedings of ODP, Scientific Results, 138: College Station, TX (Ocean Drilling Program), pp. 163–176.

Flower, B.P. and J.P. Kennett (1994). The middle Miocene climatic transition: East Antarctic ice sheet development, deep ocean circulation and global carbon cycling. Palaeogeography, Palaeoclimatology, Palaeoecology, 108, pp. 537-555.

Fornaciari, E., 2000. Calcareous nannofossil biostratigraphy of the California margin. In Lyle, M., Koizumi, I., Richter, C., and Moore, T.C., Jr. (Eds.), Proc. ODP, Sci. Results, 167: College Station, TX (Ocean Drilling Program), pp. 3–40.

Francois, R.,M., Frank, M.M., R. van der Loeff, and M. P. Bacon (2004). 23OTh normalization: An essential tool for interpreting sedimentary fluxes during the late Quaternary, Paleoceanography, 19.

Frenz, M., Baumann, K.-H., Boeckel, B., Hoppner, R. And Henrich, R. (2005) Quantification of foraminifer and coccolith carbonate in South Atlantic surface sediments by means of carbonate grain-size distributions. Journal of Sedimentary Research, 75, pp. 468–479.

Frenz, M., R. Henrich, and B. Zychla (2006), Carbonate preservation patterns at the Ceará Rise—Evidence for the Pliocene super conveyor, Marine Geology, 232, pp. 173–180.

Frenz, M., Henrich, R., (2007). Carbonate dissolution revealed by silt grain-size distribution: comparison of Holocene and Last Glacial Maximum sediments from the pelagic South Atlantic. Sedimentology, 54, pp. 391-404.

Fronval, T., Jansen, E., (1996). Late Neogene paleoclimates and paleoceanography in the Iceland Norwegian Sea: Evidence from the Iceland and Vøring Plateaus. Proceedings of the Ocean Drilling Program, Scientific Results, 151, pp. 455-468.

Gardner, J. V., Hays, J. D., (1976). Responses of sea-surface temperature and circulation to global climate changes during the past 200,000 years in the eastern equatorial Atlantic. Geological Society of America, Memoires, 145, pp. 221-245.

Gibbs, R. J., Matthews, M. D., Link, D.A (1971). The relationship between sphere size and settling velocity. Journal of Sedimentary Research, 41, pp. 7-18.

Gibbs, S., Shackleton, N. J., Young, J. (2004a) Identification of dissolution patterns in nannofossil assemblages: A high resolution comparison of synchronous records from Ceará Rise, ODP Leg 154. Paleoceanography, 19.

Gibbs, S., Shackleton, N. J., Young, J. (2004b): Orbitally forced climate signals in mid-Pliocene nannofossil assemblages. Marine Micropaleontology, 51, pp. 39-56.

Goodman, P.J.,Haxeleger,W., de Vries, P.,Cane,M., 2005. Pathways into the Pacific Equatorial Undercurrent: a trajectory analysis. Journal of Physical Oceanography, 35, pp. 2134–2151.

Gröger, M., Bickert, T., Henrich, R., (2003). Variabilitiy of silt grain size and planktonic foraminiferal preservation in Plio/Pleistocene sediments from the western equatorial Atlantic and Caribbean. Marine Geology, 201, 4, pp. 307-320.

Gupta, A.K., Singh, R.K., Joseph, S., Thomas, E., (2004). Indian Ocean high-productivity event (10–8 Ma): linked to global cooling or to the initiation of the Indian monsoons? Geology 32, pp 753–756.

Haddad, G.A., and Droxler, A.W. (1996). Metastable CaCO3 dissolution at intermediate water depths of the Caribbean and western North Atlantic: implications for intermediate water circulation during the past 200,000years. Paleoceanography, 11, pp. 701–716.

Hagelberg, T., Shackleton, N., Pisias, N., and Shipboard Scientific Party, (1992). Development of composite depth sections for Sites 844 through 854. In Mayer, L., Pisias, N., Janecek, T., et al., Proc. ODP, Init. Repts., 138 (Pt. 1): College Station, TX (Ocean Drilling Program), pp. 79-85.

Halloran, P. R., Hall, I.R., Colmenero-Hidalgo, E., Rickaby, R.E.M. (2008). Evidence for a multi-species coccolith volume change over the past two centuries: understanding a potential ocean acidification response. Biogeosciences, 5, pp. 1651–1655.

Haq, B.U., and Lohmann, G.P., (1976). Early Cenozoic calcareous nannoplankton biogeography of the Atlantic Ocean. Marine Micropaleontology, 1, pp. 119-194.

Haug, G. H., and R.Tiedemann (1998). Effect of the formation of the Isthmus of Panama on Atlantic Ocean thermohaline circulation. Nature, 393, pp 673-676.

Haug, G.H., Tiedemann, R., Zahn, R., Ravelo, A.C. (2001). Role of Panama uplift on oceanic freshwater balance, Geology, 29, pp- 207-210.

Hay, W.W. (1970) Calcareous nannofossils from cores recovered on Leg 4. Initial Reports of the Deep Sea Drilling Project, 4, pp. 455–501.

Heinze, C. and T. J. Crowley (1997). Sedimentary response to ocean gateway circulation changes. Paleoceanography, 12, pp. 742-754.

Holbourn, A . ,Kuhnt, W., Schulz , M., Erlenkeuser, H. (2005). Impacts of orbital forcing and atmospheric carbon dioxide on Miocene ice-sheet expansion, Nature, 438, pp. 483-487.

Honjo, S., (1976). Coccoliths: production, transportation, and sedimentation. Marine Micropaleontology, 1, pp. 65-79.

Honjo, S., Erez, J., (1978). Dissolution rates of calcium carbonate; an in situ experiment in the North Atlantic Ocean. Earth and Planetary Science Letters, 40, pp. 287-300.

Hoorn, C., (1994). An environmental reconstruction of the palaeo-Amazon Riversystem (Middle-Late Miocene, NW Amazonia). Paleogeography Paleoclimatology Paleoecology, 112, pp.187-238.Hoorn, C., Guerreo, J., Sarmiento, G.A. and M.A. Lorente (1995). Andean tectonics as a cause for changing drainage patterns in the Miocene northern South America. Geology, 23, pp. 237-240.

Hovan, S.A. (1995). Late Cenozoic atmospheric circulation intensity and climatic history recorded by eolian deposition in the eastern equatorial Pacific Ocean, Leg 138. In Pisias, N.G., Mayer, L.A., Janecek, T.R., Palmer-Julson, A., and van Andel, T.H. (Eds.), Proc. ODP, Sci. Results, 138: College Station, TX (Ocean Drilling Program), pp. 615–625.

Hsü, K. J., Wright, R., (1985). History of calcite dissolution of the South Atlantic Ocean, in: Hsü, K. J., and Weissert, H. (Eds.), South Atlantic Paleoceanography: Cambridge (Cambridge University Press), pp 149-196.

Imbrie, J., et al., (1993). On the structure and origin of major glaciations cycles 2. The 100,000-year cycle. Paleoceanography 8, pp. 699-735.

Jansen, E., Raymo, M.E., Blum, P., et al., (1996). Proceedings of the Ocean Drilling Program, Initital Reports, 162, pp.

Jiang, S., Wise Jr., S.W., Wang, J., 2007. Cause of the middle/late Miocene carbonate crash: Dissolution or low productivity? In: Teagle, D.A.H., Wilson, D.S., Acton, G.D., Vanko, D.A. (Eds.), Proceedings of the Ocean Drilling Program. Scientific Results, vol. 206. Ocean Drilling Program, College Station, TX.

Kameo, K., Bralower, T.J., (2000). Neogene calcareous nannofossil biostratigraphy of Sites 998, 999, and 1000, Caribbean Sea. In Leckie, R.M., Sigurdsson, H., Acton, G.D., Draper, G. (Eds.), Proceedings of the Ocean Drilling Program, Scientific Results, 165, pp. 3–17.

Kastanja, M.-M, Diekman, B., Henrich, R., (2006). Controls on carbonate versus terrigenous deposition in the incipient Benguela upwelling system during the Middle to Late Miocene (ODP Sites 1085 and 1087). Paleogeography Paleoclimatology Paleoecology, 241, pp. 515-530.

Kastanja, M.-M., Henrich, R., (2007). Grain size variations in pelagic carbonate oozes from the Walvis Ridge- SE Atlantic (ODP Site 1265): a Miocene record of carbonate sedimentation and preservation. Marine Geology, 237, pp. 97-108.

Keller, G. and J. A. Barron (1983). Paleoceanographic implications of Miocene deep-sea hiatuses, Geol. Soc. Of Am. Bull., 94/5, pp. 590-613

Kemp, A.E.S., Baldauf, J.G., and Pearce, R.B., (1995). Origins and paleoceanographic significance of laminated diatom ooze from the eastern equatorial Pacific Ocean. In Pisias, N.G., Mayer, L.A.,

Janecek, T.R., Palmer-Julson, A., and van Andel, T.H. (Eds.), Proc. ODP, Sci. Results, 138: College Station, TX (Ocean Drilling Program), pp. 641–645.

Kennett, J.P, Keller, G., Srinivasan, M.S., (1985). Miocene planktonic foraminiferal biogeography and paleoceanographic development of the Indo-Pacific region. In: Kennett, J.P. (Ed.), The Miocene Ocean. GSA Mem., vol. 163, pp. 197–236.

Kienast, S. S., M. Kienast, A. C. Mix, S. E. Calvert, and R. Francois (2007). Thorium-230 normalized particle flux and sediment focusing in the Panama Basin region during the last 30,000 years, Paleoceanography, 22, pp. 1-19

King, T.A., Ellis, W.G., Murray, D.W., Shackleton, N.J., Harris, S., (1997). Miocene evolution of carbonate sedimentation at the Ceará Rise: a multivariate data/proxy approach. Proceedings of the Ocean Drilling Program, Scientific Results, 154, pp. 349-365.

Knappertsbusch, M., Brummer, G.-J.A., (1995) A sediment trap investigation of sinking coccolithophorids in: The North Atlantic. Deep-Sea Research I, 42, pp. 1083-1109.

Knappertsbusch, M., (2000). Morphologic evolution of the coccolithophorid Calcidiscus leptoporus from the Early Miocene to Recent. Journal of Paleontology, 74, 3, pp. 712-730.

Krammer, R., Baumann. K.-H. Henrich, R., (2006). Middle to Late Miocene fluctuations in the incipient Benguela Upwelling system revealed by coccolith assemblages. Paleogeography Paleoclimatology Paleoecology, 230, pp. 319-334.

Kroopnick, P.M., (1985). The distribution of 13C and PCO2 in the world oceans. Deep-Sea Res., 32, pp. 57–84.

Krumbein, W.C., (1936). Application of logarithmic moments to size frequency distributions of sediments. Journal of Sedimentary Petrology, 6, pp. 35–47.

Kuhnt, W., Holbourn, A., Hall, R., Zuvela, M., Käse, R., (2004). Neogene history of the Indonesian throughflow. In: Clift, P., Wang, P., Kuhnt, W., Hayes, D. (Eds.), Continent–Ocean Interactions within East Asian Marginal Seas. Geophysical Monograph 149. American Geophysical Union, Washington, DC, pp. 299–320.

Larsen, H.C. et al. (1994). Seven million years of glaciation on Greenland. Science, 264, pp. 952-955.

Lear, C. H., Y. Rosenthal, and J. D. Wright (2003), The closing of a seaway: Ocean water masses and global climate change, Earth Planet. Sci. Lett. , 210, pp. 425-436.

Ledbetter, M.T. (1984). Bottom-current speed in the Vema channel recorded by particle size of sediment fine-fraction. Marine Geology 58, pp. 137–149.

Lee, T.Y. and L.A. Lawer (1995). Cenozoic plate tectonic reconstruction of Southeast Asia. In: T.W.C. Hilde and M.F.J. Flower (Eds.) Southeast Asia Structure and Tectonics. Tectonophysics, pp. 85-138.

Li, Q., Li, B., Zhong, G., McGowran, B., Zhou, Z., Wang, J., Wang, P., (2006). Late Miocene development of theWestern PacificWarm Pool: Planktonic foraminifer and oxygen isotopic evidence. Palaeogeography, Palaeoclimatology, Palaeoecology 237, pp. 465–482.

Lyle, M., Dadey, K.A., J.W. Farrell, (1995). The late Miocene (11-8 Ma) eastern Pacific carbonate crash: evidence for reorganisation of deep water circulation by the closure of the Panama gateway. Proceedings of the Ocean Drilling Program, Scientific Results, 138, pp.821-838.

Lyle, M., Koizumi, I., Richter, C., et al., (1997). Proc. ODP, Inititial Reports., 167: College Station, TX (Ocean Drilling Program).

Marcantonio, F., R. R. Anderson, M. Stute N. Kumar, P. Schlosser, and A. C. Mix (1996). Extraterrestrial ^{3}He as a tracer of marine sediment transport and accumulation, Nature, 383, pp. 705–707.

Marshall, L. G. Land mammals and the Great American Interchange (1988). Am. Sci. 76, pp. 380–388.

Maslin, M.A.. Ridgwell, A. (2005). Mid-Pleistocene Revolution and the 'eccentricity myth', Special Publication of the Geological Society of London, 247, pp. 19–34.

McCave, I.N., Manighetti, B., Robinson, S.G., (1995). Sortable silt and fine sediment size composition slicing: parameters for palaeocurrent speed and palaeoceanography. Paleoceanography 10, pp. 593-610.

McCave, I. N., Hall, I. R. (2006). Size sorting in marine muds: Processes, pitfalls and prospects for paleoflow-speed proxies, Geochemistry, Geophysics, Geosystems., 7.

Miller, K.G., Fairbanks, R.G. and G.S. Mountain (1987). Tertiary oxygen isotope synthesis, sea level history, and continental Margin erosion. Paleoceanography, 2, pp. 1-19.

Miller, K.G., Feigenson, M.D., (1991). Miocene isotope reference section, deep sea drilling project site 608: an evaluation of isotope and biostratigraphic resolution. Paleoceanography 6 (1), pp. 33–52.

Milliman, J.D. (1993). Production and accumulation of calcium carbonate in the ocean—budget of a nonsteady state. Glob. Biogeochem. Cycles, 7, pp. 927–57

Milliman, J.D., Troy, P.J., Balch, W.M., Adams, A.K., Li, Y.H., Mackenzie, F.T. (1999). Biologically mediated dissolution ofcalcium carbonate above the chemical lysocline? Deep-Sea Research I 46, pp. 1653–1669.

Minoletti, F., Gardin, S., Nicot, E., Renard, M., Spezzaferri, S., (2001). Mise au point d'un protocole experimental de separation granulometrique d'assemblages de nannofossiles calcaires; applications paleoecologiques et geochimiques. Bulletin de la Societe Geologique de France, 172 (4); pp. 437-446.

Mix, A.C., Morey, A. E., (1996). Climate feedback and Pleistocene variations in the Atlantic South Equatorial current, in: Wefer, G., Berger, W. H., Siedler, G., Webb, D. J. (Eds.), The South Atlantic: Present and Past Circulation, pp. 503-563.

Mix, A.C., Tiedemann, R., Blum, P., et al., (2003). Proc. ODP, Init. Repts., 202: College Station, TX (Ocean Drilling Program).

Moran, K., (1997). Elastic property corrections applied to Leg 154 sediment, Ceará Rise. In Shackleton, N.J., Curry, W.B., Richter, C., and Bralower, T.J. (Eds.), Proc. ODP, Sci. Results, 154: College Station, TX (Ocean Drilling Program), pp. 151-155.

Molnar, P., Cane, M..A. (2002). El Niño's tropical climate and teleconnections as a blueprint for pre-Ice Age climates. Paleoceanography. 17, pp. 10–21.

Molnar, P., Cane, M..A. (2007). Early Pliocene (pre-Ice Age) El Niño-like global climate: which El Niño?. Geosphere. 3, pp. 337–365.

Muiños, S.B., Frank, M., Maden, C., Hein, J.R., van de Flierdt, T., Lebreiro, S.M., Gaspar, L., Monteiro, J.H., Halliday, A.N., (2008). New constraints on the Pb and Nd isotopic evolution of NE Atlantic water masses. Geochem. Geophys. Geosyst. 9 (2).

Murray, D.W. and L.C. Peterson (1997). Biogenic carbonate production and preservation changes between 5 and 10 Ma at Ceará Rise, western equatorial Atlantic. Proc. Ocean Drill. Program Sci. Results, 154, pp. 375-388.

Mutti, M., (2000). Bulk δ^{18}O and δ^{13}C records from Site 999, Colombian Basin, and Site 1000, Nicaraguan Rise (latest Oligocene to middle Miocene): diagenesis, link to sediment parameters, and paleoceanography. In Leckie, R.M., Sigurdsson, H., Acton, G.D., and Draper, G. (Eds.), Proc. ODP, Sci. Results, 165: College Station, TX (Ocean Drilling Program), pp. 275–283.

Nathan, S., and R. M. Leckie (2009). Early history of the western Pacific warm pool during the middle to late Miocene (~13.2–5.8Ma): Role of sea-level change and implications for equatorial circulation, Palaeogeogr. Palaeoclimatol. Palaeoecol., 274, pp. 140–159.

Newkirk, D.R., Martin, E.E., (2009). Circulation through the Central American Seawayduring the Miocene carbonate crash. Geology 37, 1, pp. 87–90.

Nisancioglu, K.H., Raymo, M.E., Stone, P.H., (2003). Reorganization of Miocene deep water circulation in response to the shoaling of the Central American Seaway. Paleoceanography, 18, 1.

Okada, H., (1992). Biogeographic control of modern nannofossil assemblages in surface sediments of Ise Bay, Mikawa Bay and Kumano-Nada, off coast of central Japan. In: Proto Decima, F., Monechi, S., Rio, D. (Eds.), Proceedings INA Conference, Firenze. Memorie di Scienze Geologiche, 4(3), pp. 431-449.

Oppo, D. W., Fairbanks, R. G. (1987). Variability in the deep and intermediate water circulation of the Atlantic Ocean during the past 25,000 years: Northern hemisphere modulation of the Southern Ocean, Earth Planet. Sci. Lett., 86, pp 1–15.

Pagani, M., Arthur, M.A., Freeman, K.H. (1999). Miocene evolution of atmospheric carbon dioxide. Paleoceanography 14, 3, pp. 273-292.

Paull, C.K., Hills, S.J., Thierstein, H.R., 1988. Progressive dissolution of fine carbonate particles in pelagic sediments. Marine Geology 81, pp. 27–40.

Pearce, R.B., Kemp, A.E.S., Baldauf, J.G., and King, S.C. (1995). High-resolution sedimentology and micropaleontology of laminated diatomaceous sediments from the eastern equatorial Pacific Ocean. In Pisias, N.G., Mayer, L.A., Janecek, T.R., Palmer-Julson, A., and van Andel, T.H. (Eds.), Proc. ODP, Sci. Results, 138: College Station, TX (Ocean Drilling Program), pp. 647–663.

Pearson, P. N., and M. R. Palmer (2000), Atmospheric carbon dioxide concentrations over the past 60 million years, Nature, 406, pp. 695-699.

Peterson, L.C., Prell, W.L., (1985). Carbonate dissolution in recent sediments of the eastern equatorial Indian Ocean: preservation patterns and carbonate loss above the lysocline. Mar. Geol. 64, pp. 259-290.

Peterson, L.C., Murray, D.W., Ehrmann, W.U. and P. Hempel (1992). Cenozoic carbonate accumulation and compensation depth changes in the Indian Ocean. In. R.A. Duncan et al. (eds) Synthesis of Results from Scientific Ocean drilling in the Indian Ocean. Geophysical Monograph Series, 70, pp. 311-333.

Perch-Nielsen, K., (1985). Cenozoic calcareous nannofossils. In Bolli, H.M., Saunders, J.B., and Perch-Nielsen, K. (Eds.), Plankton Stratigraphy: Cambridge (Cambridge University Press), pp. 427-554.

Poore, H.R., Samworth, R., White, N.J., Jones, S.M., McCave, I.N., (2006). Neogene overflow of Northern Component Water at the Greenland-Scotland Ridge. Geochemistry Geophysics Geosystems, 7.

Raffi, I., and Flores, J.-A., (1995). Pleistocene through Miocene calcareous nannofossils from eastern equatorial Pacific Ocean (Leg 138). In Pisias, N.G., Mayer, L.A., Janecek, T.R., Palmer-Julson, A., and van Andel, T.H. (Eds.), Proceedings of ODP, Scientific Results, 138: College Station, TX (Ocean Drilling Program), pp. 233–286.

Raffi, I., Backman, J., Rio, D. (1998). Evolutionary trends of tropical calcareous nannofossils in the late Neogene. Marine Micropaleontology, 35, pp. 17–41.

Rahmstorf, S. (2006). Thermohaline Ocean Circulation. In: Encyclopedia of Quaternary Sciences, Edited by S. A. Elias. Elsevier, Amsterdam.

Ramsay, A.T.S., (1972). Aspects of the distribution of fossil species of calcareous nannoplankton in North Atlantic and Caribbean sediments. Nature, 236, pp. 67-70.

Ravelo, A.C., Dekens, P.S., McCarthy, M.,(2006). Evidence for El Niño-like conditions during the Pliocene. GSA Today 16, pp. 4–11.

Rea, D. K., (1994). The paleoclimatic record provided by eolian deposition in the deep sea: The geologic history of wind, Rev. Geophys., 32, pp. 159–195.

Ridgwell, A. and Zeebe, R. E.(2005). The role of the global carbonate cycle in the regulation and evolution of the Earth system, Earth Planet. Sci. Lett., 234, pp. 299–315.

Rio, D., Fornaciari, E., and Raffi, I., (1990). Late Oligocene through early Pleistocene calcareous nannofossils from western equatorial Indian Ocean (Leg 115). In Duncan, R.A., Backman, J., Peterson, L.C., et al., Proceedings of ODP, Scientific Results, 115: College Station, TX (Ocean Drilling Program), pp. 175–235.

Roters, B., Henrich, R. (2010). The middle to late Miocene climatic development of Southwest Africa derived from the sedimentological record of ODP Site 1085A. International Journal of Earth Sciences, 99(2), pp. 459-471.

Roth, M. J., Droxler, A. W., Kameo, K., (2000). The Caribbean Carbonate Crash at the Middle to Late Miocene Transition: linkage to the establishment of the Modern Global Ocean Conveyor, in: Leckie, R. M., Sigurdsson, H., Acton, G. D., Draper, G. (Eds.), Proceedings of the Ocean Drilling Program, Scientific Results, 165, pp. 249-273.

Samtleben, C., Bickert, T., (1990). Coccoliths from the Norwegian Sea. Marine Micropaleontology 16, pp 39-64.

Schmidt, D. N., Lazarus, D., Young, J. R., Kucera, M., (2006). Biogeography and evolution of body size in marine plankton. Earth-Science Reviews, 78, pp. 239–266.

Shackleton, N.J., Crowhurst, S., Hagelberg, T., Pisias, N.G., and Schneider, D.A., (1995). A new late Neogene time scale: application to Leg 138 sites. In Pisias, N.G., Mayer, L.A., Janecek, T.R., Palmer-Julson, A., and van Andel, T.H. (Eds.), Proc. ODP, Sci. Results, 138: College Station, TX (Ocean Drilling Program), pp. 73–101.

Shackleton, N.J., and Hall, M.A., (1995). Stable isotope records in bulk sediments (Leg 138). In Pisias, N.G., Mayer, L.A., Janecek, T.R., Palmer-Julson, A., and van Andel, T.H. (Eds.), Proc. ODP, Sci. Results, 138: College Station, TX (Ocean Drilling Program), pp. 797–805.

Shackleton, N.J., Crowhurst, S., (1997). Sediment Fluxes based on an Orbitally Tuned Time Scale 5 to 14 Ma, Site 926, in: N.J. Shackleton, W.B. Curry, C. Richter and T.J. Bralower (Eds), Proceedings of the Ocean Drilling Program, Scientific Results, 154, pp. 69-82.

Shackleton, N.J., Hall, M.A., (1997). The late Miocene stable isotope record, Site 926, in: N.J. Shackleton, W.B. Curry, C. Richter and T.J. Bralower (Eds), Proceedings of the Ocean Drilling Program, Scientific Results, 154, pp. 369-373.

Siesser, W. G. (1980). Late Miocene origin of the Benguela upwelling system off northern Namibia. Science 208, pp. 283–285.

Smart, C.W., Thomas, E., Ramsay, A.T.S., (2007). Middle–late Miocene benthic foraminifera in a western Indian Ocean Depth Transect: paleoceanographic implications. Palaeogeography, Palaeoclimatology, Palaeoecology 247, pp. 402–420.

Stein, R., (1985). Rapid grain-size analysis of clay and silt fraction by Sedigraph 5000D: comparison with Coulter Counter and Atterberg methods. Journal of Sedimentary Petrology 55(5), pp. 590-615.

St. John, K. E. K., and L. A. Krissek (2002). The late Miocene to Pleistocene ice-rafting history of southeast Greenland, Boreas, 31, pp. 28-35.

Takayama, T., (1993). Notes on Neogene calcareous nannofossil biostratigraphy of the Ontong Java Plateau and size variations of Reticulofenestra coccoliths. In Berger, W.H., Kroenke, L.W., Mayer, L.A., et al., Proc. ODP, Sci. Results, 130: College Station, TX (Ocean Drilling Program), pp. 179–229.

Takesue, R. K., van Geen, A., Carriquiry, J. D., Ortiz, E., Godinez-Orta, L., Granados, I.; Saldivar, M., Ortlieb, L., Escribano, R., Guzma´n, N., Castilla, J. C., Varas, M., Salamanca, M., Figueroa, C.(2004). Influence of coastal upwelling and El Nin˜o-Southern Oscillation on nearshore water along Baja California and Chile: Shore-based monitoring during 1997-2000. Journal of Geophysical Research, 109, pp. 3009-3023.

Talley, L. D., (1999). Some aspects of ocean heat transport by the shallow, intermediate and deep overturning circulations, in: Clark, P.U. et al. (Eds), Mechanisms of Global Climate Change at Millenial Time Scales, Geophysical Monograph Series, 112, American Geophysical Union, pp. 1-22.

Thiede, J., Winkler, A., Wolf-Welling, T., Eldholm, O., Myhre, A:M., Baumann, K.-H., Henrich, R. and R. Stein (1998). Late Cenozoic history of the Polar North Atlantic: Results from Ocean Drilling. Quat. Sci. Rev., 17, pp. 185-208.

Thiede, J. and A.M. Myhre (1996). The paleoceangraphic history of the North Atlantic-Arctic gateways: synthesis of the Leg 151 drilling results. Proceedings of the Ocean Drilling Program, Scientific Results, 151, pp. 645-658.

Thomas, D. J., Via, R. K., (2007). Neogene evolution of Atlantic thermohaline circulation: Perspective from Walvis Ridge, southeastern Atlantic Ocean, Paleoceanography, 22, PA2212.

Treguer, P., Nelson, D.M., Van Bennekom, A.J., DeMaster, D.J., Leynaert, A., Queguiner, B. (1995). The balance of silica in the world ocean: a reestimate, Science, 268, pp 375– 379.

Tremolada, F., De Bernardi, B., Erba, E. (2008). Size variations of the calcareous nannofossil taxon Discoaster multiradiatus (Incertae sedis) across the Paleocene–Eocene thermal maximum in ocean drilling program holes 690B and 1209B. Marine Micropaleontology, 67, pp. 239-254.

Tripati, A.K., Roberts, C.D., Eagle, R.A. (2009).Coupling of CO2 and ice sheet stability over major climate transitions of the last 20 million years. Science, 326, pp. 1394–1397.

Turco, E., Bambini, A.M., Foresi, L., Iaccarino, S., Lirer, F., Mazzei, R., Salvatorini, G., (2002). Middle Miocene high-resolution calcareous plankton biostratigraphy at Site 926 (Leg 154, equatorial Atlantic Ocean): palaeoecological and palaeobiological implications. Geobios, 35 (Mémoire spécial nr. 24), pp. 257-276.

Van Andel, T. H., Thiede, J., Sclater, J. G., Hay, W. W., (1977). Depositional history of the outh Atlantic Ocean during the last 125 million years. The Journal of Geology. 85, pp. 651–698.

Vincent, E. (1981). Neogene carbonate stratigraphy of Hess Rise (central North Pacific) and paleoceanographic implications. In Thiede, J., Vallier, T.L., et al., Init. Repts. DSDP, 62: Washington (U.S. Govt. Printing Office), pp. 571–606.

Vincent, E., and Toumarkine, M., (1990). Neogene planktonic foraminifers from the western tropical Indian Ocean, Leg 115. In Duncan, R.A., Backman, J., Peterson, L.C., et al., Proc. ODP, Sci. Results, 115: College Station, TX (Ocean Drilling Program), pp. 795–836.

Vincent, E., and Toumarkine, M., (1995). Data report: miocene planktonic foraminifers from the eastern equatorial Pacific. In Pisias, N.G., Mayer, L.A., Janecek, T.R., Palmer-Julson, A., and van Andel, T.H. (Eds.), Proc. ODP, Sci. Results, 138: College Station, TX (Ocean Drilling Program), pp. 895–907.

Von der Heydt, A. S., Dijkstra, H. A. (2011). The impact of ocean gateways on ENSO variability in the Miocene. Geol. Soc., London, Spec. Pub., 355, pp. 305-318.

Walker, L. J.,Wilkinson, B.H. & Ivany, L.C. 2002. Continental drift and Phanerozoic carbonate accumulation in shallow shelf and deep-marine settings. Journal of Geology, 110, pp. 75–87.

Warnke, D.A., Allen, C.P., Mueller, D.W., Hodell, D.A. and C.A. Brummer (1992). Miocene-Pliocene Antarctic glacial evolution: a synthesis of ice-rafted debris, stable isotope and planktonic foraminiferal indicators, ODP Leg 114. In: J.P. Kennett and D.A. Warnke (eds.) The Antarctic paleoenvironment: A perspective on global change. Antarct. Res. Ser., 56, pp. 311-325.

Weltje, G.J., Prins, M.A., (2003). Muddled of mixed? Inferring palaeoclimate from size distributions of deep-sea clastics. Sedimentary Geology 162, pp. 39-62.

Westerhold, T., Bickert, T. Röhl, U., (2005). Middle to late Miocene oxygen isotope stratigraphy of ODP site 1085 (SE Atlantic): new constrains on Miocene climate variability and sea-level fluctuations. Paleogeography Paleoclimatology Paleoecology, 217, pp. 205-222.

Wise, S.W., (1977). Chalk formation: early diagenesis. In Anderson, N.R., and Malahoff, A. (Eds.), The Fate of Fossil Fuel CO2 in the Oceans: New York (Plenum Press), pp. 717–739.

Woodruff, F., and Savin, S.M (1989). Miocene deepwater oceanography. Paleoceanography, 4, pp. 87–140.

Wright, J.D., Miller, K.G., Fairbanks, R.G., (1992). Miocene stable isotopes: implications for deepwater circulation and climate. Paleoceanography, 7, pp. 357–389.

Wright, J.D., Miller, K.G., (1996). Controls of North Atlantic deep water circulation by the Greenland-Scotland Ridge. Paleoceanography, 11, pp. 157-170.

Young, J.R., (1990). Size variation of Neogene Reticulofenestra coccoliths from Indian Ocean DSDP cores. Journal of Micropaleontology, 9, pp. 71– 85.

Young, J. R. and Ziveri, P. (2000). Calculation of coccolith volume and its use in calibration of carbonate flux estimates, Deep-Sea Research II, 47, pp.1679–1700.

Zachos, J., Pagani, M., Sloan, L., Thomas, E., Billups, K., (2001). Trends, rhythms and aberrations in Global Climate 65 Ma to present. Science, 292, pp. 274-278.

Zachos, J.C., Kroon, D., Blum, P., et al., (2004). Proc. ODP, Init. Repts., 208: College Station, TX (Ocean Drilling Program).

Danksagung